



National Technical University of Athens

School of Applied Mathematical And Physical Science

Department of Mathematics

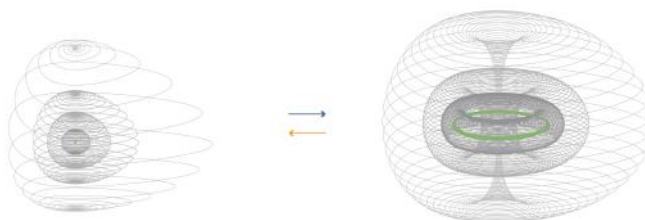
**Mathematical modeling
through topological surgery and applications**

Stathis Antoniou

Ph.D. Thesis

Advisor

Sofia Lambropoulou



Athens, December 2017



National Technical University of Athens
School of Applied Mathematical and Physical Sciences
Department of Mathematics

Mathematical modeling through topological surgery and applications

Stathis Antoniou

Ph.D. Thesis

Advisory Committee: Sofia Lambropoulou
Louis H. Kauffman
Antonios Charalambopoulos

Examining Committee: Sofia Lambropoulou, *Professor, NTUA*
Louis H. Kauffman, *Professor, UIC*
Antonios Charalambopoulos, *Professor, NTUA*
Colin Adams, *Professor, Williams College*
Theocharis Apostolatos, *Associate Professor, UOA*
Cameron Gordon, *Professor, UT Austin*
Dimitrios Kodokostas, *Assistant Professor, NTUA*

Athens, December 2017

We are a way for the cosmos to know itself.

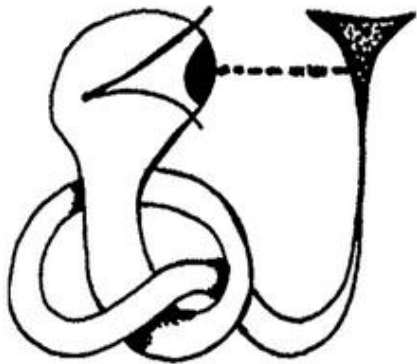
Carl Sagan

La réponse est l'homme, quelle que soit la question.

Louis Aragon

There is a theory which states that if ever anyone discovers exactly what the Universe is for and why it is here, it will instantly disappear and be replaced by something even more bizarre and inexplicable. There is another theory which states that this has already happened.

Douglas Adams



Acknowledgments

I am grateful to my advisor Sofia Lambropoulou who inspired me to change my career to science. She has supported me throughout the whole duration of my thesis in many ways. Her guidance and enthusiasm pushed me towards higher goals, taught me how to properly write in a scientific way and opened up new research directions.

I wish to express my gratitude to Louis H.Kauffman for his commitment to our meetings (real and virtual) which taught me how to tackle difficult problems and gave me the opportunity to expand not only my mathematical knowledge but also the way I am thinking. I would also like to thank Colin Adams, Cameron Gordon and Antonios Charalambopoulos for many insightful discussions and their support during my thesis.

I am grateful to my parents Ioannis and Aggeliki and my aunt Lena who supported me in deciding to change my career to science; this decision which was undoubtedly the right one. Further, I would like to thank Danai, Orfeas, Rea and all my family and friends. All of them supported me, directly or indirectly.

Finally, I am grateful for having the privilege of doing a funded Ph.D. during these unstable economic times for Greece. More precisely, I would like to thank the European Union (European Social Fund - ESF) and the Greek national funds for their funding through the Operational Program "Education and Lifelong Learning" and my teacher Sofia Lambropoulou who coordinated the Research Funding Program Thales. I would also like to thank the Papakyriakopoulos foundation and the Department of Mathematics for the Papakyriakopoulos scholarship.

Abstract

Topological surgery is a mathematical technique used for creating new manifolds out of known ones. We observe that it occurs in natural phenomena where forces are applied and the manifold in which they occur changes type. For example, 1-dimensional surgery happens during chromosomal crossover, DNA recombination and when cosmic magnetic lines reconnect, while 2-dimensional surgery happens in the formation of Falaco solitons, in drop coalescence and in the cell mitosis. Inspired by such phenomena, we enhance topological surgery with the observed *forces* and *dynamics*. We then generalize these low-dimensional cases to a model which extends the formal definition to a continuous process caused by local forces for an arbitrary dimension m . Next, for modeling phenomena which do not happen on arcs, respectively surfaces, but are 2-dimensional, respectively 3-dimensional, we fill in the interior space by defining the notion of *solid topological surgery*. We further present a dynamical system as a model for both natural phenomena exhibiting a ‘hole drilling’ behavior and our enhanced notion of solid 2-dimensional 0-surgery. Moreover, we analyze the ambient space S^3 in order to introduce the notion of *embedded topological surgery* in S^3 . This notion is then used for modeling phenomena which involve more intrinsically the ambient space, such as the appearance of knotting in DNA and phenomena where the causes and effects of the process lie beyond the initial manifold, such as the formation of tornadoes. Moreover, we present a visualization of the 4-dimensional process of 3-dimensional surgery by using the new notion of *decompactified 2-dimensional surgery* and *rotations*. Finally, we propose a model for a phenomenon exhibiting 3-dimensional surgery: the formation of black holes from cosmic strings. We hope that through this study, topology and dynamics of many natural phenomena, as well as topological surgery itself, will be better understood.

Contents

1	Introduction	9
2	Useful mathematical notions	12
2.1	Manifolds	13
2.2	Homeomorphisms	13
2.3	Properties of manifolds	13
2.4	n -spheres and n -balls	14
2.5	The compactification of \mathbb{R}^n	14
2.6	Product spaces	15
2.7	Embeddings	17
3	The formal definition of surgery	18
3.1	1-dimensional 0-surgery	19
3.2	2-dimensional 0-surgery	21
3.3	2-dimensional 1-surgery	22
3.4	3-dimensional 0- and 1-surgery	23
4	Continuity	24
4.1	The continuous definition of surgery	24
4.2	Continuous 2-dimensional 0-surgery	26
5	Dynamics	26
5.1	Dynamic 1-dimensional topological surgery	27
5.2	Modeling phenomena exhibiting 1-dimensional surgery	29
5.3	Dynamic 2-dimensional topological surgery	31
5.4	Modeling phenomena exhibiting 2-dimensional surgery	35

5.5	A model for dynamic m -dimensional n -surgery	36
6	Solid surgery	36
6.1	Solid 1-dimensional topological surgery	38
6.2	Solid 2-dimensional topological surgery	40
6.3	Modeling phenomena exhibiting solid 2-dimensional 0-surgery	45
6.4	Modeling phenomena exhibiting solid 2-dimensional 1-surgery	46
7	A dynamical system modeling solid 2-dimensional 0-surgery	48
7.1	The dynamical system and its steady state points	49
7.2	Local behavior and numerical simulations	50
7.3	Connecting the dynamical system with solid 2-dimensional 0-surgery	56
8	The ambient space S^3	58
8.1	Descriptions of S^3	59
8.1.1	Via \mathbb{R}^3	59
8.1.2	Via two 3-balls	59
8.1.3	Via two solid tori	60
8.2	Connecting the descriptions of S^3	61
8.2.1	Via corking	61
8.2.2	Via surgery	63
8.3	Dynamical systems exhibiting the topology of S^3	63
8.3.1	The 3-dimensional Lotka–Volterra system	63
8.3.2	The pair of linear harmonic oscillators	64
9	Embedded surgery	66
9.1	Embedded 1-dimensional surgery	67
9.2	Embedded 2-dimensional surgery	68
9.3	Modeling phenomena exhibiting embedded solid 2-dimensional surgery	69

	8
9.3.1 A topological model for the density distribution in black hole formation	69
9.3.2 A topological model for the formation of tornadoes	73
9.3.3 Embedded solid 2-dimensional 1-surgery on $M = D^3$	76
10 3-dimensional surgery	78
10.1 Decompactified 2-dimensional surgery	79
10.2 Visualizing 3-dimensional surgery in \mathbb{R}^3	82
10.2.1 Initial and final steps	82
10.2.2 Intermediate steps	84
10.3 The continuity of 3-dimensional surgery	85
10.4 Modeling black hole formation from cosmic strings	89
10.4.1 Terminology	89
10.4.2 Black holes from cosmic strings	90
10.4.3 Black holes from 3-dimensional 1-surgery	91
11 Conclusions	93
A Appendix: Definitions	96

1 Introduction

Topological surgery is a mathematical technique used for changing the homeomorphism type, or simply the shape, of a manifold. For example, all orientable surfaces may arise from the 2-dimensional sphere using surgery. The mathematical notions needed for understanding the definition of surgery can be found in Section 2. The examples of 1, 2- and 3-dimensional surgery are analyzed in Sections 3.1, 3.2, 3.3 and 3.4.

Topological surgery is exhibited in nature in numerous, diverse processes of various scales for ensuring new results. Surgery in nature is usually performed on basic manifolds with or without boundary, that undergo merging and recoupling. For example, in dimension 1 topological surgery can be seen in DNA recombination and during the reconnection of cosmic magnetic lines, while in dimension 2 it happens when genes are transferred in bacteria and during the formation of black holes. Such processes are initiated by attracting forces acting on a sphere of dimension 0 (that is, two points) or 1 (that is, a circle).

A large part of this work is dedicated to defining new theoretical concepts which are better adapted to the phenomena, to modeling such phenomena in dimensions 1,2 and 3 and to presenting a generalized topological model for m -dimensional n -surgery which captures the observed dynamics. With our enhanced definitions and our model of topological surgery in hand, we match surgery patterns with natural phenomena and we study the physical implications of our modeling. Furthermore, we present a dynamical system that performs a specific type of surgery and we pin down its relation with topological surgery. Finally, we propose a new type of surgery, the decompactified 2-dimensional surgery, which allows the visualization of 3-dimensional surgery in \mathbb{R}^3 . More precisely, the new concepts are:

- **Continuity and dynamics:** In Section 4, we start by enhancing the formal definition of

surgery with continuity, whereby an m -dimensional surgery is considered as the continuous local process of passing from an appropriate boundary component of an $m + 1$ -dimensional handle to its complement boundary component. We further notice that surgery in nature is caused by forces. For example, in dimension 1, during meiosis the pairing is caused by mutual attraction of the parts of the chromosomes that are similar or homologous, as detailed and illustrated in Section 5.1. In dimension 2, the creation of tornadoes is caused by attracting forces between the cloud and the earth (as detailed and illustrated in Section 9.3.2), while soap bubble splitting is caused by the surface tension of each bubble which acts as an attracting force (this is discussed in Section 5.4). In Section 5.5 we incorporate these dynamics to our continuous definition and present a model for m -dimensional n -surgery. These dynamics explain the intermediate steps of the formal definition of surgery and extend it to a continuous process caused by local forces. Note that these intermediate steps can also be explained by Morse theory but this approach does not involve the forces.

- **Solid surgery:** The interior of the initial manifold is now filled in. We observe that phenomena like tension on soap films or the merging of oil slicks are undergoing 1-dimensional surgery but they happen on surfaces instead of 1-manifolds. For example, an oil slick is seen as a disc, which is a continuum of concentric circles together with the center. Similarly, moving up one dimension, during the biological process of mitosis and during tornado formation, 2-dimensional surgery is taking place on 3-dimensional manifolds instead of surfaces. For example, during the process of mitosis, the cell is seen as a 3-ball, that is, a continuum of concentric spheres together with the central point (this is discussed in Section 6.4). Thus, in order to fit natural phenomena where the interior of the initial manifold is filled in, in Section 6, we extend the formal definition by introducing the notion of *solid topological surgery* in both dimensions 1 and 2.

- **Connection with a dynamical system:** We establish a connection between these new notions applied on 2-dimensional topological surgery and the dynamical system presented in [30]. In Section 7 we analyze how, with a slight perturbation of parameters, trajectories pass from spherical to toroidal shape through a ‘hole drilling’ process. We show that our new topological notions are verified by both the local behavior of the steady state points of the system and the numerical simulations of its trajectories. This result gives us on the one hand a mathematical model for 2-dimensional surgery and on the other hand a dynamical system that can model natural phenomena exhibiting this type of surgery.

- **Embedded surgery:** We notice that in some phenomena exhibiting topological surgery, the ambient space is also involved. For example in dimension 1, during DNA recombination the initial DNA molecule which is recombined can also be knotted. In other words, the initial 1-manifold can be a knot (an embedding of the circle) instead of an abstract circle (see description and illustration in Section 9.1). Similarly in dimension 2, the processes of tornado and black hole formation are not confined to the initial manifold and topological surgery is causing (or is caused by) a change in the whole space (see Section 9.3 and illustrations therein). We therefore define the notion of *embedded topological surgery* in Section 9 which allows us to model these kind of phenomena but also to view all natural phenomena exhibiting topological surgery as happening in 3-space instead of abstractly. We consider our ambient 3-space to be S^3 and an extensive analysis of its descriptions together with the presentation of dynamical systems exhibiting its topology is done in Section 8.

- **The visualization of 3-dimensional surgery:** Finally, in Section 10, we present a way to visualize the 4-dimensional process of 3-dimensional surgery. In order to do so, we introduce the notion of decompactified 2-dimensional surgery which allows us to

visualize the process of 2-dimensional surgery in \mathbb{R}^2 instead of \mathbb{R}^3 . Using this new notion and rotation, we present a way to visualize 3-dimensional surgery in \mathbb{R}^3 . This is done in Section 10.2. Further, in Section 10.4, we propose a model for a phenomenon exhibiting 3-dimensional surgery: the formation of black holes from cosmic strings.

This thesis gathers, links and completes the results presented in [18], [19], [3], [2] while extending them one dimension higher. The material is organized as follows: In Section 2 we recall the topological notions that will be used and provide specific examples that will be of great help to readers that are not familiar with the topic. In Section 3, we present the formal definition of topological surgery for an arbitrary dimension m . In Section 4, we enhance the formal definition of surgery with continuity. In Section 5, we introduce dynamics to 1 and 2-dimensional surgery and we discuss natural processes exhibiting these types of surgeries. In Section 5.5, we present a generalized model for m -dimensional n -surgery. In Section 6 we define solid 1 and 2-dimensional surgery and discuss related natural processes. We then present the dynamical system connected to these new notions in Section 7. As all natural phenomena exhibiting surgery (1 or 2-dimensional, solid or usual) take place in the ambient 3-space, in Section 8 we present the 3-sphere S^3 and the duality of its descriptions. This allows us to define in Section 9 the notion of embedded surgery. Finally, in Section 10, we use lower dimensional surgeries to visualize 3-dimensional surgery and propose a topological model for black hole formation from cosmic strings.

2 Useful mathematical notions

In this section we introduce basic notions related to topological surgery. Reader that are familiar with the formalism of the topic can directly move to the formal definition in

Section 3.

2.1 Manifolds

- An *n-manifold without boundary* is a ‘nice’ topological space with the property that each point in it has a neighborhood topologically equivalent to the usual n -dimensional Euclidean space \mathbb{R}^n . In other words an n -manifold resembles locally \mathbb{R}^n .
- Similarly, an *n-manifold with boundary* is ‘nice’ topological space with the property that each point in it has a neighborhood topologically equivalent either to \mathbb{R}^n (if the point lies in the interior) or \mathbb{R}_+^n (if the point lies on the boundary).

2.2 Homeomorphisms

In Section 2.1 by ‘topologically equivalent’ we mean the following: two n -manifolds X and Y are *homeomorphic* or *topologically equivalent* if there exists a homeomorphism between them, namely a function $f : X \rightarrow Y$ with the properties that:

- f is continuous
- There exists the inverse function $f^{-1} : Y \rightarrow X$ (equivalently f is 1-1 and onto)
- f^{-1} is also continuous

Intuitively the homeomorphism f is an elastic deformation of the space X to the space Y , not involving any self-intersections or any ‘cutting’ and ‘regluing’ (see also Appendix A).

2.3 Properties of manifolds

An n -manifold, M , is said to be:

- *connected* if it consists of only one piece,
- *compact* if it can be enclosed in some k -dimensional ball,
- *orientable* if any oriented frame that moves along any closed path in M returns to a position that can be transformed to the initial one by a rotation.

The above notions are more rigorously defined in Appendix A.

2.4 n -spheres and n -balls

In each dimension the basic connected, oriented, compact n -manifold without boundary is the n -sphere, S^n . Also, the basic connected, oriented n -manifold with boundary is the n -ball, D^n . The boundary of a n -dimensional ball is a $n - 1$ -dimensional sphere, $\partial D^n = S^{n-1}$, $n \geq 1$. In Fig 1, this relation is shown for $n = 1, 2$ and 3 . As shown in Fig 1 (1), the space S^0 is the disjoint union of two points. By convention, we consider these two one-point spaces to be $\{+1\}$ and $\{-1\}$: $S^0 = \{+1\} \amalg \{-1\}$. Note that, in this analysis, we will follow this convention by considering that n -spheres and n -balls are centered at the origin.

Besides the relation of S^n with D^{n+1} described above, the n -sphere S^n is also intrinsically related to the Euclidian space \mathbb{R}^n via the notion of compactification.

2.5 The compactification of \mathbb{R}^n

Compactification is the process of making a topological space into a compact space. For each dimension n , the space \mathbb{R}^n with all points at infinity compactified to one single point is homeomorphic to S^n . So, S^n is also called the one-point compactification of \mathbb{R}^n . Conversely, a sphere S^n can be decompactified to the space \mathbb{R}^n by the so-called

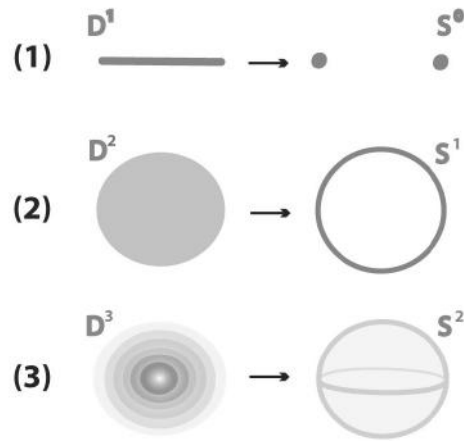


Figure 1. (1) A segment D^1 is bounded by two points S^0 (2) A disc D^2 is bounded by a circle S^1 (3) A 3-ball D^3 is bounded by a sphere S^2 .

stereographic projection. For example, for $n = 1$ we have that the circle S^1 is the one-point compactification of the real line \mathbb{R}^1 , see Fig 2 (1), while for $n = 2$ the sphere S^2 is the one-point compactification of the plane \mathbb{R}^2 , see Fig 2 (2). The compactification of \mathbb{R}^3 is discussed and illustrated in Section 8.1.1 (see Appendix A for details on the one-point compactification of \mathbb{R}^n).

2.6 Product spaces

The *product space* of two manifolds X and Y is the manifold made from their Cartesian product $X \times Y$ (see also Appendix A). If X, Y are manifolds with boundary, the boundary of product space $X \times Y$ is:

$$\partial(X \times Y) = (\partial X \times Y) \cup (X \times \partial Y)(\star)$$

For example the next common connected, oriented, compact 2-manifold without boundary after S^2 is the *torus*, which can be perceived as the boundary of a doughnut,

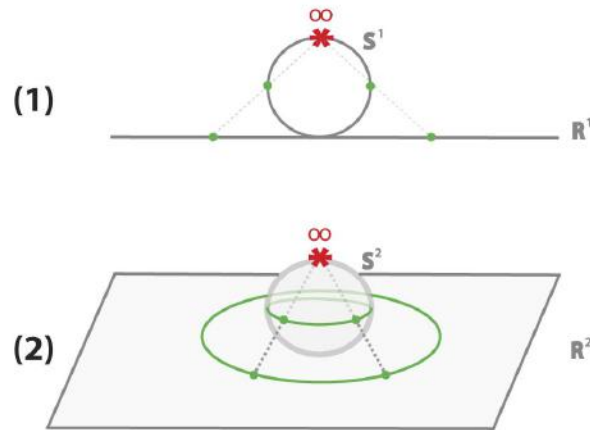


Figure 2. (1) S^1 onto \mathbb{R}^1 (2) S^2 onto \mathbb{R}^2 .

and it is the product space $S^1 \times S^1$. Analogously, a *solid torus*, which can be perceived as a whole doughnut, is the product space $S^1 \times D^2$. A solid torus is a 3-manifold with boundary a torus: $\partial(S^1 \times D^2) = S^1 \times \partial D^2 = S^1 \times S^1$.

Other product spaces that we will be using here are: the *cylinder* $S^1 \times D^1$ or $D^1 \times S^1$ (see Fig 3), the *solid cylinder* $D^2 \times D^1$ which is homeomorphic to the 3-ball and the spaces of the type $S^0 \times D^n$, which are the disjoint unions of two n -balls $D^n \amalg D^n$.

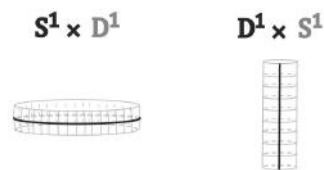


Figure 3. Two ways of viewing a cylinder

All the above examples of product spaces that are of the form $S^p \times D^q$ can be viewed as q -thickenings of the p -sphere. For example the 2-thickening of S^0 comprises two discs, while the 3-thickening of S^0 comprises two 3-balls. It is also worth noting that the product

spaces $S^p \times D^q$ and $D^{p+1} \times S^{q-1}$ have the same boundary:

$$\partial(S^p \times D^q) = \partial(D^{p+1} \times S^{q-1}) = S^p \times S^{q-1}(\star\star).$$

2.7 Embeddings

- An *embedding* of an n -manifold N^n in an m -manifold M^m is a map $f : N \hookrightarrow M$ such that its restriction on the image $f(N)$ is a homeomorphism between N and $f(N)$. The notion of embedding allows to view spaces inside specific manifolds instead of abstractly. Embeddings even of simple manifolds can be very complex. For example, the embeddings of the circle S^1 in the 3-space \mathbb{R}^3 are the well-known knots whose topological classification is still an open problem of low-dimensional topology.
- An embedding of a submanifold $N^n \hookrightarrow M^m$ is *framed* if it extends to an embedding $N^n \times D^{m-n} \hookrightarrow M$.
- A *framed n -embedding in M* is an embedding of the $(m - n)$ -thickening of the n -sphere, $h : S^n \times D^{m-n} \hookrightarrow M$, with core n -embedding $e = h|_ : S^n = S^n \times \{0\} \hookrightarrow M$. For example, the framed 1-embeddings in \mathbb{R}^3 comprise embedded solid tori in the 3-space with core 1-embeddings being knots.
- Let X, Y be two n -manifolds with homeomorphic boundaries ∂X and ∂Y (which are $(n - 1)$ -manifolds). Let also h denote a homeomorphism $h : \partial X \rightarrow \partial Y$. Then, from $X \cup Y$ one can create a new n -manifold without boundary by ‘gluing’ X and Y along their boundaries. The gluing is realized by identifying each point $x \in \partial X$ to the point $h(x) \in \partial Y$. The map h is called *gluing homeomorphism*, see Appendix A. One important example is the gluing of two n -discs along their common boundary which gives rise to the n -sphere, see Fig 4 for $n = 1, 2$. For $n = 3$, the gluing of two

3-balls yielding the 3-sphere S^3 is illustrated and discussed in Section 8.1.2. Another interesting example is the gluing of solid tori which also yield the 3-sphere. This is illustrated and discussed in Section 8.1.3

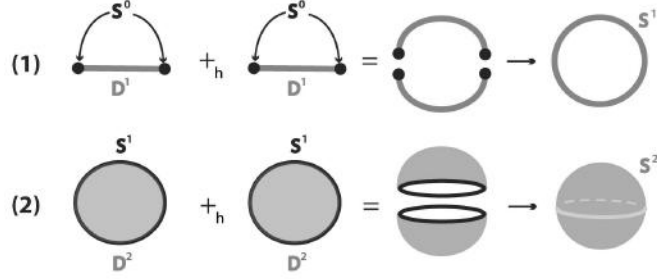


Figure 4. (1) $D^1 \cup_h D^1 = S^1$ (2) $D^2 \cup_h D^2 = S^2$

As we will see in next section, the notions of embedding and gluing homeomorphism together with property $(\star\star)$ described in 2.6 are the key ingredients needed to define topological surgery. It is roughly the procedure of removing an embedding of $S^p \times D^q$ and gluing back $D^{p+1} \times S^{q-1}$ along their common boundary.

3 The formal definition of surgery

We recall the following well-known definition of surgery:

Definition 1. An m -dimensional n -surgery is the topological procedure of creating a new m -manifold M' out of a given m -manifold M by removing a framed n -embedding $h : S^n \times D^{m-n} \hookrightarrow M$, and replacing it with $D^{n+1} \times S^{m-n-1}$, using the ‘gluing’ homeomorphism h along the common boundary $S^n \times S^{m-n-1}$. Namely, and denoting surgery by χ :

$$M' = \chi(M) = \overline{M \setminus h(S^n \times D^{m-n})} \cup_{h|_{S^n \times S^{m-n-1}}} (D^{n+1} \times S^{m-n-1}).$$

The symbol ‘ χ ’ of surgery comes from the Greek word ‘ $\chi\epsilon\iota\rho\upsilon\rho\gamma\iota\kappa\acute{\eta}$ ’ (cheirourgiki) whose term ‘cheir’ means hand. Note that from the definition, we must have $n + 1 \leq m$. Also, the horizontal bar in the above formula indicates the topological closure of the set underneath.

Further, the *dual m -dimensional $(m - n - 1)$ -surgery* on M' removes a dual framed $(m - n - 1)$ -embedding $g : D^{n+1} \times S^{m-n-1} \hookrightarrow M'$ such that $g|_{S^n \times S^{m-n-1}} = h^{-1}|_{S^n \times S^{m-n-1}}$, and replaces it with $S^n \times D^{m-n}$, using the ‘gluing’ homeomorphism g (or h^{-1}) along the common boundary $S^n \times S^{m-n-1}$. That is:

$$M = \chi^{-1}(M') = \overline{M' \setminus g(D^{n+1} \times S^{m-n-1})} \cup_{h^{-1}|_{S^n \times S^{m-n-1}}} (S^n \times D^{m-n}).$$

The resulting manifold $\chi(M)$ may or may not be homeomorphic to M . From the above definition, it follows that $M = \chi^{-1}(\chi(M))$. Preliminary definitions behind the definition of surgery such as topological spaces, homeomorphisms, embeddings and other related notions are provided in Section 2 and Appendix A. For further reading, excellent references on the subject are [26, 28, 29]. We shall now apply the above definition to dimensions 1 and 2.

3.1 1-dimensional 0-surgery

We only have one kind of surgery on a 1-manifold M , the *1-dimensional 0-surgery* where $m = 1$ and $n = 0$:

$$M' = \chi(M) = \overline{M \setminus h(S^0 \times D^1)} \cup_{h|_{S^0 \times S^0}} (D^1 \times S^0).$$

The above definition means that two segments $S^0 \times D^1$ are removed from M and they are replaced by two different segments $D^1 \times S^0$ by reconnecting the four boundary points

$S^0 \times S^0$ in a different way. In Fig. 5 (a) and 6 (a), $S^0 \times S^0 = \{1, 2, 3, 4\}$. As one possibility, if we start with $M = S^1$ and use as h the standard (identity) embedding denoted with h_s , we obtain two circles $S^1 \times S^0$. Namely, denoting by 1 the identity homeomorphism, we have $h_s : S^0 \times D^1 = D^1 \amalg D^1 \xrightarrow{1 \amalg 1} S^0 \times D^1 \hookrightarrow M$, see Fig. 5 (a). However, we can also obtain one circle S^1 if h is an embedding h_t that reverses the orientation of one of the two arcs of $S^0 \times D^1$. Then in the substitution, joining endpoints 1 to 3 and 2 to 4, the two new arcs undergo a half-twist, see Fig. 6 (a). More specifically, if we take $D^1 = [-1, +1]$ and define the homeomorphism $\omega : D^1 \rightarrow D^1; t \rightarrow -t$, the embedding used in Fig. 6 (a) is $h_t : S^0 \times D^1 = D^1 \amalg D^1 \xrightarrow{1 \amalg \omega} S^0 \times D^1 \hookrightarrow M$ which rotates one D^1 by 180° . The difference between the embeddings h_s and h_t of $S^0 \times D^1$ can be clearly seen by comparing the four boundary points 1, 2, 3 and 4 in Fig. 5 (a) and Fig. 6 (a).

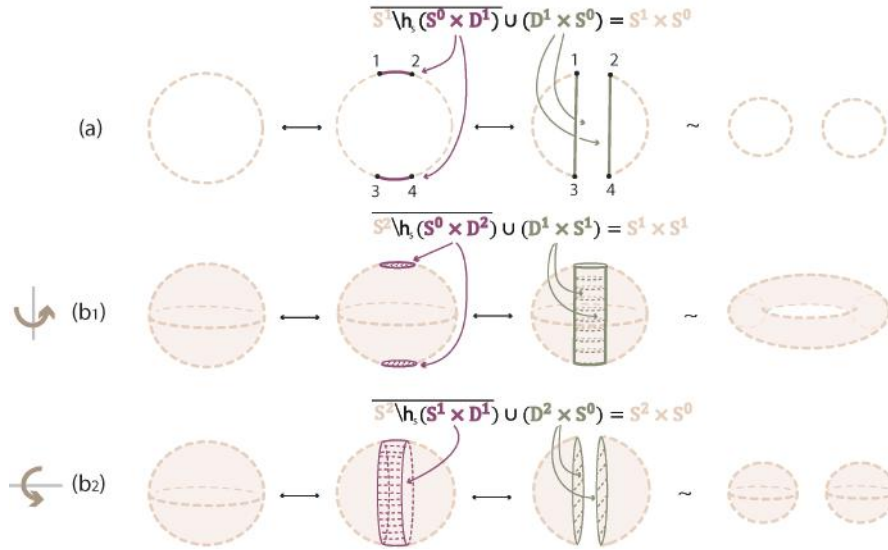


Figure 5. Formal (a) 1-dimensional 0-surgery (b₁) 2-dimensional 0-surgery and (b₂) 2-dimensional 1-surgery using the standard embedding h_s .

Note that in dimension one, the dual case is also an 1-dimensional 0-surgery. For

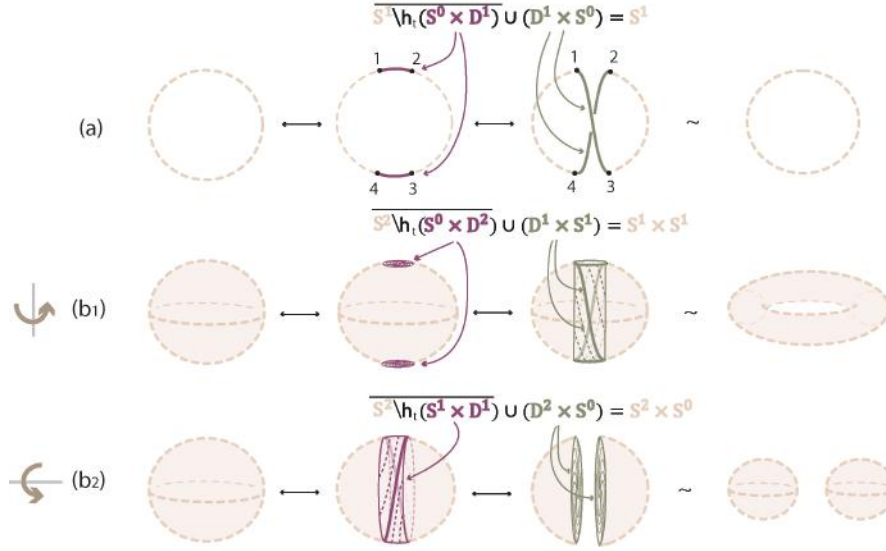


Figure 6. Formal (a) 1-dimensional 0-surgery (b₁) 2-dimensional 0-surgery and (b₂) 2-dimensional 1-surgery using a twisting embedding h_t .

example, looking at the reverse process of Fig. 5 (a), we start with two circles $M' = S^1 \amalg S^1$ and, if each segment of $D^1 \times S^0$ is embedded in a different circle, the result of the (dual) 1-dimensional 0-surgery is one circle: $\chi^{-1}(M') = M = S^1$.

3.2 2-dimensional 0-surgery

Starting with a 2-manifold M , there are two types of surgery. One type is the *2-dimensional 0-surgery*, whereby two discs $S^0 \times D^2$ are removed from M and are replaced in the closure of the remaining manifold by a cylinder $D^1 \times S^1$, which gets attached via a homeomorphism along the common boundary $S^0 \times S^1$ comprising two copies of S^1 . The gluing homeomorphism of the common boundary may twist one or both copies of S^1 . For $M = S^2$ the above operation changes its homeomorphism type from the 2-sphere to that of the torus. View Fig. 5 (b₁) for the standard embedding h_s and Fig. 6 (b₁) for a twisting

embedding h_t . For example, the homeomorphism $\mu : D^2 \rightarrow D^2; (t_1, t_2) \rightarrow (-t_1, -t_2)$ induces the 2-dimensional analogue h_t of the embedding defined in the previous example, namely: $h_t : S^0 \times D^2 = D^2 \amalg D^2 \xrightarrow{\text{III}\mu} S^0 \times D^2 \hookrightarrow M$ which rotates one D^2 by 180° . When, now, the cylinder $D^1 \times S^1$ is glued along the common boundary $S^0 \times S^1$, the twisting of this boundary induces the twisting of the cylinder, see Fig. 6 (b₁).

3.3 2-dimensional 1-surgery

The other possibility of 2-dimensional surgery on M is the *2-dimensional 1-surgery*: here a cylinder (or annulus) $S^1 \times D^1$ is removed from M and is replaced in the closure of the remaining manifold by two discs $D^2 \times S^0$ attached along the common boundary $S^1 \times S^0$. For $M = S^2$ the result is two copies of S^2 , see Fig. 5 (b₂) for the standard embedding h_s . Unlike Fig. 5 (b₁) where the cylinder is illustrated vertically, in Fig. 5 (b₂), the cylinder is illustrated horizontally. This choice was made so that the instances of 1-dimensional surgery can be obtained by crosssections of the instances of both types of 2-dimensional surgeries, see further Remark 1. Fig. 6 (b₂) illustrates a twisting embedding h_t , where a twisted cylinder is being removed. In that case, taking $D^1 = \{h : h \in [-1, 1]\}$ and homeomorphism ζ :

$$\zeta : S^1 \times D^1 \rightarrow S^1 \times D^1;$$

$$\zeta : (t_1, t_2, h) \rightarrow (t_1 \cos \frac{(1-h)\pi}{2} - t_2 \sin \frac{(1-h)\pi}{2}, t_1 \sin \frac{(1-h)\pi}{2} + t_2 \cos \frac{(1-h)\pi}{2}, h)$$

the embedding h_t is defined as: $h_t : S^1 \times D^1 \xrightarrow{\zeta} S^1 \times D^1 \hookrightarrow M$. This operation corresponds to fixing the circle S^1 bounding the right side of the cylinder $S^1 \times D^1$, rotating the circle S^1 bounding the left side of the cylinder by 180° and letting the rotation propagate from left to right. This twisting of the cylinder can be seen by comparing the second instance

of Fig. 5 (b₂) with the second instance of Fig. 6 (b₂), but also by comparing the third instance of Fig. 5 (b₁) with the third instance of Fig. 6 (b₁).

It follows from Definition 1 that a dual 2-dimensional 0-surgery is a 2-dimensional 1-surgery and vice versa. Hence, Fig. 5 (b₁) shows that a 2-dimensional 0-surgery on a sphere is the reverse process of a 2-dimensional 1-surgery on a torus. Similarly, as illustrated in Fig. 5 (b₂), a 2-dimensional 1-surgery on a sphere is the reverse process of a 2-dimensional 0-surgery on two spheres. In the figure the symbol \longleftrightarrow depicts surgeries from left to right and their corresponding dual surgeries from right to left.

Remark 1. The stages of the process of 2-dimensional 0-surgery on S^2 can be obtained by rotating the stages of 1-dimensional 0-surgeries on S^1 by 180° around a vertical axis, see Fig. 5 (b₁). Similarly, the stages of 2-dimensional 1-surgery on S^2 can be obtained by rotating the stages of 1-dimensional 0-surgeries on S^1 by 180° around a horizontal axis, see Fig. 5 (b₂). It follows from the above that 1-dimensional 0-surgery can be obtained as a cross-section of either type of 2-dimensional surgery.

3.4 3-dimensional 0- and 1-surgery

Starting with a 3-manifold M , there are three types of 3-dimensional surgeries. For $m = 3$ and $n = 0$, we have the *3-dimensional 0-surgery* whereby two 3-balls $S^0 \times D^3$ are removed from M and are replaced in the closure of the remaining manifold by $D^1 \times S^2$:

$$\chi(M) = \overline{M \setminus h(S^0 \times D^3)} \cup_h (D^1 \times S^2)$$

Next, for $m = 3$ and $n = 2$, we have the *3-dimensional 2-surgery* but we will not analyze this type of surgery as it is the reverse process of 3-dimensional 0-surgery. Finally, for $m = 3$ and $n = 1$, we have the *3-dimensional 1-surgery* whereby a solid torus $S^1 \times D^2$

is removed from M and is replaced by another solid torus $D^2 \times S^1$:

$$\chi(M) = \overline{M \setminus h(S^1 \times D^2)} \cup_h (D^2 \times S^1)$$

Both processes will be analyzed and visualized in Section 10.

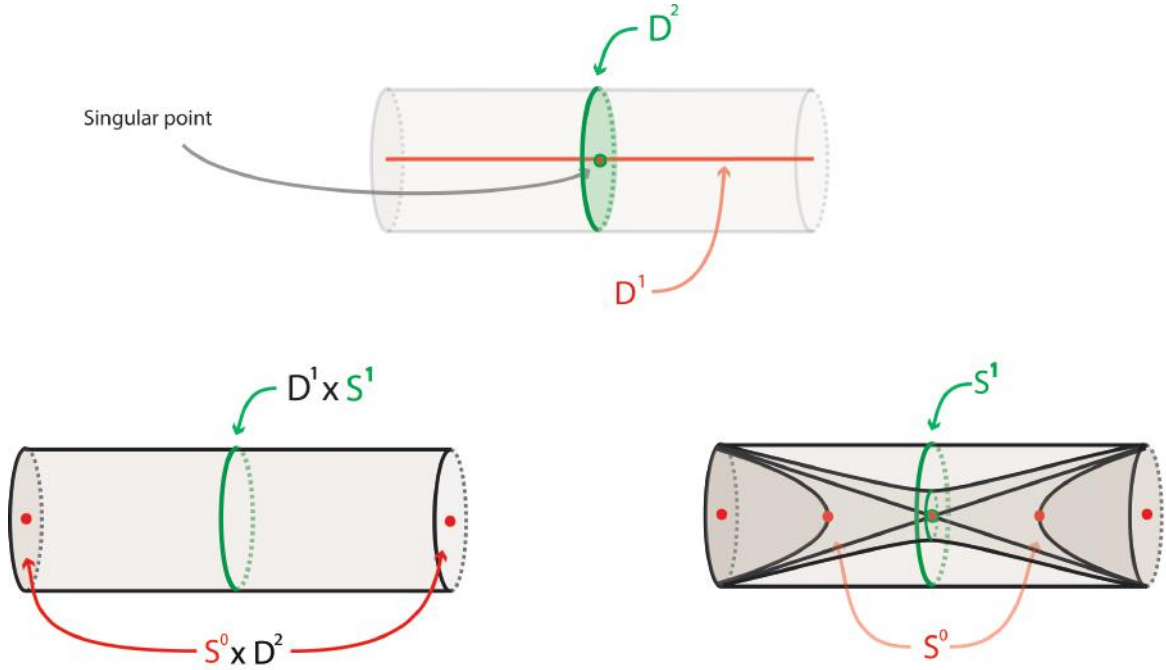
4 Continuity

As we will see in the following sections, topological surgery happens in nature as a continuous process caused by local forces. However, the formal definition of surgery presented in Definition 1 gives only a static description of the initial and the final stage. In this section we define the continuous process of m -dimensional n -surgery as an extension of Definition 1. This new definition, enhanced with the observed dynamics, will become a topological model for natural phenomena exhibiting 1- and 2-dimensional surgery in Section 5 and for 3-dimensional surgery in Section 10.

4.1 The continuous definition of surgery

Let us first notice that if we glue together the two m -manifolds involved in the process of m -dimensional n -surgery along their common boundary we obtain the m -sphere. Namely, from Definition 1 and using property (\star) discussed in Section 2.6, we can see that $(S^n \times D^{m-n}) \cup_h (D^{n+1} \times S^{m-n-1}) = (\partial D^{n+1} \times D^{m-n}) \cup_h (D^{n+1} \times \partial D^{m-n}) = \partial(D^{n+1} \times D^{m-n}) \cong \partial(D^{m+1}) = S^m$. This means that an m -dimensional n -surgery on an m -manifold M can be viewed as the process of cutting out a boundary component of $D^{n+1} \times D^{m-n}$ from M and gluing back the complement boundary component of $D^{n+1} \times D^{m-n}$ to the resulting manifold. Hence, a continuous analogue of Definition 1 is the following:

Definition 2. Given an m -manifold M and an embedding $h : S^n \times D^{m-n} \hookrightarrow M$, we consider the handle $D^{n+1} \times D^{m-n}$ which is bounded by $\partial(D^{n+1} \times D^{m-n}) = (S^n \times D^{m-n}) \cup_h (D^{n+1} \times S^{m-n-1})$. An m -dimensional n -surgery on a m -manifold M is the local process of continuously passing, within $D^{n+1} \times D^{m-n}$, from boundary component $(S^n \times D^{m-n}) \subset \partial(D^{n+1} \times D^{m-n})$ to its complement $(D^{n+1} \times S^{m-n-1}) \subset \partial(D^{n+1} \times D^{m-n})$, by going through the unique intersection point $D^{n+1} \cap D^{m-n}$. We will refer to this point as the *singular point*. Note that each ‘slice’ of the process is an m -dimensional manifold but the whole time evolution of the process requires $m + 1$ dimensions in order to be visualized, as the whole process occurs inside the handle $D^{n+1} \times D^{m-n} \cong D^{m+1}$.



$$S^2 = (S^0 \times D^2) \cup (D^1 \times S^1) = \text{bound}(D^1 \times D^2)$$

Figure 7. Continuous 2-dimensional 0-surgery

Given that the first boundary component $S^n \times D^{m-n}$ of $D^{n+1} \times D^{m-n}$ is a thickening

of the core S^n and the second boundary component $D^{n+1} \times S^{m-n-1}$ is a thickening of the core S^{m-n-1} , both components can be seen as thickenings (or framings) of the cores (or spheres) to dimension m . Hence, the surgery process can be viewed locally as starting with the boundary $S^n = \partial D^{n+1}$ and considering it as the core of thickening $S^n \times D^{m-n}$. We then collapse the core S^n to the singular point from which the thickened S^{m-n-1} emerges, which is also the boundary $S^{m-n-1} = \partial D^{m-n}$. Note that these intermediate steps can also be explained through Morse theory. See Remark 2 for details.

4.2 Continuous 2-dimensional 0-surgery

For example, for $m = 2$ and $n = 0$ we have the case of 2-dimensional 0-surgery, where the boundary component $D^1 \times S^1$ is a cylinder with its two ends closed by the other boundary component $S^0 \times D^2$. The result is homeomorphic to the 2-sphere: $(S^0 \times D^2) \cup_h (D^1 \times S^1) = S^2$, see the left illustration of Fig. 7. The way of continuously passing from $(S^0 \times D^2)$ to $(D^1 \times S^1)$ is shown in the illustration side of Fig. 7, where we see how the core S^0 of $S^0 \times D^2$ (in red) collapses to the unique intersection point (in red/green) from which the core S^1 of $D^1 \times S^1$ emerges (in green). The whole process happens inside the handle $D^1 \times D^2$, see also Fig. 7. This process together with continuous 1-dimensional surgery will be elaborated in much more details in the next section where dynamics are also introduced.

5 Dynamics

In this section we present natural processes exhibiting topological surgery in dimensions 1 and 2 and we incorporate the observed dynamics to Definition 2, thus creating a model which extends surgery to a continuous process caused by local forces. Further, for each dimension, we go back to the phenomena and pin down the forces introduced by our

models.

5.1 Dynamic 1-dimensional topological surgery

We find that 1-dimensional 0-surgery is present in phenomena where 1-dimensional splicing and reconnection occurs. It can be seen for example during meiosis when new combinations of genes are produced, see Fig. 8 (3), during magnetic reconnection, the phenomena whereby cosmic magnetic field lines from different magnetic domains are spliced to one another, changing their pattern of conductivity with respect to the sources, see Fig. 8 (2) from [5] and in site-specific DNA recombination (see Fig 22) whereby nature alters the genetic code of an organism, either by moving a block of DNA to another position on the molecule or by integrating a block of alien DNA into a host genome (see [32]). It is worth mentioning that 1-dimensional 0-surgery is also present during the reconnection of vortex tubes in a viscous fluid and quantized vortex tubes in superfluid helium. As mentioned in [17], these cases have some common qualitative features with the magnetic reconnection shown in Fig. 8 (2).

Since all the above phenomena follow a dynamic process, in Fig. 8 (1), we introduce dynamics to Definition 2 which shows how the intermediate steps of surgery are caused by local forces. The process starts with the two points (in red) specified on any 1-dimensional manifold, on which attracting forces are applied (in blue). We assume that these forces are caused by an attracting center (also in blue). Then, the two segments $S^0 \times D^1$, which are neighborhoods of the two points, get close to one another. When the specified points (or centers) of the two segments reach the attracting center they touch and recoupling takes place, giving rise to the two final segments $D^1 \times S^0$, which split apart. In Fig. 8 (1), case (s) corresponds to the identity embedding h_s described in Section 3.1, while (t) corresponds to the twisting embedding h_t described in Section 3.1.

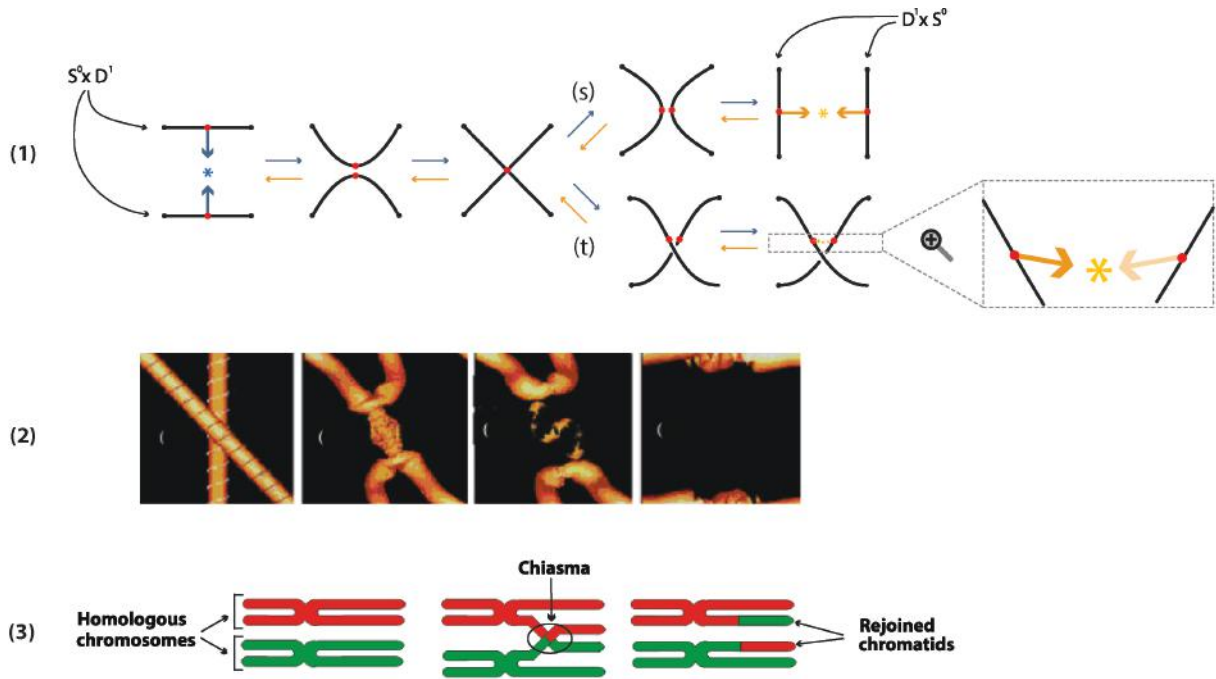


Figure 8. (1) Dynamic 1-dimensional surgery locally (2) The reconnection of cosmic magnetic lines (3) Crossing over of chromosomes during meiosis.

As also mentioned in Section 3.1, the dual case is also a 1-dimensional 0-surgery, as it removes segments $D^1 \times S^0$ and replaces them by segments $S^0 \times D^1$. This is the reverse process which starts from the end and is illustrated in Fig. 8 (1) as a result of the orange forces and attracting center which are applied on the ‘complementary’ points.

Note that these local dynamics produce different manifolds depending on where the initial neighborhoods are embedded. Taking the known case of the standard embedding h_s and $M = S^1$, we obtain $S^1 \times S^0$, see Fig 9 (a). Furthermore, as shown in Fig 9 (b), we also obtain $S^1 \times S^0$ even if the attracting center is outside S^1 . Note that these outcomes are not different than the ones shown in formal surgery (recall Fig 5 (a)) but we can now see the intermediate instances as a result of forces.

Remark 2. It is worth mentioning that the intermediate steps of surgery presented in

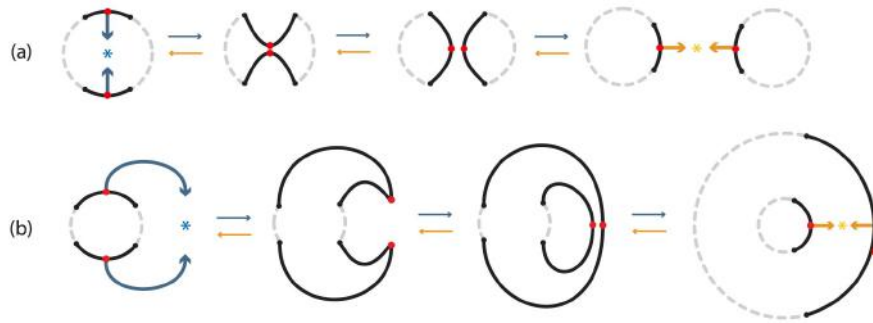


Figure 9. 1-dimensional surgery on one and two circles.

Fig. 8 (1) can also be viewed in the context of Morse theory [24]. By using the local form of a Morse function, we can visualize the process of surgery by varying parameter t of equation $x^2 - y^2 = t$. For $t = -1$ it is the hyperbola shown in the second stage of Fig. 8 (1) where the two segments get close to one another. For $t = 0$ it is the two straight lines where the reconnection takes place as shown in the third stage of Fig. 8 (1) while for $t = 1$ it represents the hyperbola of the two final segments shown in case (s) of the fourth stage of Fig. 8 (1). This sequence can be generalized for higher dimensional surgeries as well. For example, for 2-dimensional surgery, we can visualize the process by varying parameter t of equation $x^2 + y^2 - z^2 = t$. We mention this approach because it gives us an algebraic formulation of surgery's time evolution. However, in this analysis we will not use it as we are focusing on the introduction of forces and the attracting center.

5.2 Modeling phenomena exhibiting 1-dimensional surgery

The aforementioned phenomena are all 1-dimensional in the sense that they involve 1-dimensional surgery happening in a initial 1-dimensional manifold. We will take a closer look at them and show that the described dynamics and attracting forces introduced by our model are present in all cases. Namely, **magnetic reconnection** (Fig. 8 (2)) corresponds

to a dual 1-dimensional 0-surgery (see case (t) of Fig. 8 (1)) where $g : D^1 \times S^0 \hookrightarrow M'$ is a dual embedding of the twisting homeomorphism h_t defined in Section 3.1. The tubes are viewed as segments and correspond to an initial manifold $M = S^0 \times D^1$ (or $M = S^1$ if they are connected) on which the local dynamics act on two smaller segments $S^0 \times D^1$. Namely, the two magnetic flux tubes have a nonzero parallel net current through them, which leads to attraction of the tubes (cf. [16]). Between them, a localized diffusion region develops where magnetic field lines may decouple. Reconnection is accompanied with a sudden release of energy and the magnetic field lines break and rejoin in a lower energy state.

In the case of chromosomal crossover during **meiosis** (Fig. 8 (3)), we have the same dual 1-dimensional 0-surgery as magnetic reconnection (see case (t) of Fig. 8 (1)). During this process, the homologous (maternal and paternal) chromosomes come together and pair, or synapse, during prophase. The pairing is remarkably precise and is caused by mutual attraction of the parts of the chromosomes that are similar or homologous. Further, each paired chromosomes divide into two chromatids. The point where two homologous non-sister chromatids touch and exchange genetic material is called chiasma. At each chiasma, two of the chromatids have become broken and then rejoined (cf. [27]). In this process, we consider the initial manifold to be one chromatid from each chromosome, hence the initial manifold is $M = S^0 \times D^1$ on which the local dynamics act on two smaller segments $S^0 \times D^1$.

For **site-specific DNA recombination** (see Fig 22), we have a 1-dimensional 0-surgery (see case (t) of Fig. 8 (1)). Here the initial manifold is a knot which is an embedding of $M = S^1$ in 3-space but this will be detailed in Section 9.1. As mentioned in [11], enzymes break and rejoin the DNA strands, hence in this case the seeming attraction of the two specified points is realized by the enzyme. Note that, while both

are genetic recombinations, there is a difference between chromosomal crossover and site-specific DNA recombination. Namely, chromosomal crossover involves the homologous recombination between two similar or identical molecules of DNA and we view the process at the chromosome level regardless of the knotting of DNA molecules.

Finally, **vortices reconnect** following the steps of 1-dimensional 0-surgery with a standard embedding shown in (see case (s) of Fig. 8 (1)). The initial manifold is again $M = S^0 \times D^1$. As mentioned in [13], the interaction of the anti-parallel vortices goes from attraction before reconnection, to repulsion after reconnection.

5.3 Dynamic 2-dimensional topological surgery

Both types of 2-dimensional surgeries are present in nature, in various scales, in phenomena where 2-dimensional merging and recoupling occurs. For example, *2-dimensional 0-surgery* can be seen during the formation of tornadoes, see Fig. 10 (2) (this phenomenon will be detailed in Section 9.3.2). Further, it can be seen in the formation of Falaco solitons, see Fig. 10 (3) (note that each Falaco soliton consists of a pair of locally unstable but globally stabilized contra-rotating indentations in the water-air discontinuity surface of a swimming pool, see [14] for details). It can also be seen in gene transfer in bacteria where the donor cell produces a connecting tube called a ‘pilus’ which attaches to the recipient cell, see Fig. 10 (4); in drop coalescence, the phenomenon where two dispersed drops merge into one, and in the formation of black holes (this phenomena will be discussed in Section 9.3.1), see Fig. 23 (2) (Source: www.black-holes.org).

On the other hand, *2-dimensional 1-surgery* can be seen during soap bubble splitting, where a soap bubble splits into two smaller bubbles, see Fig. 10 (5) (Source: soapbubble.dk); when the tension applied on metal specimens by tensile forces results in the phenomena of necking and then fracture, see Fig. 10 (6) and in the biological process of mitosis, where a

cell splits into two new cells, see Fig. 10 (7).

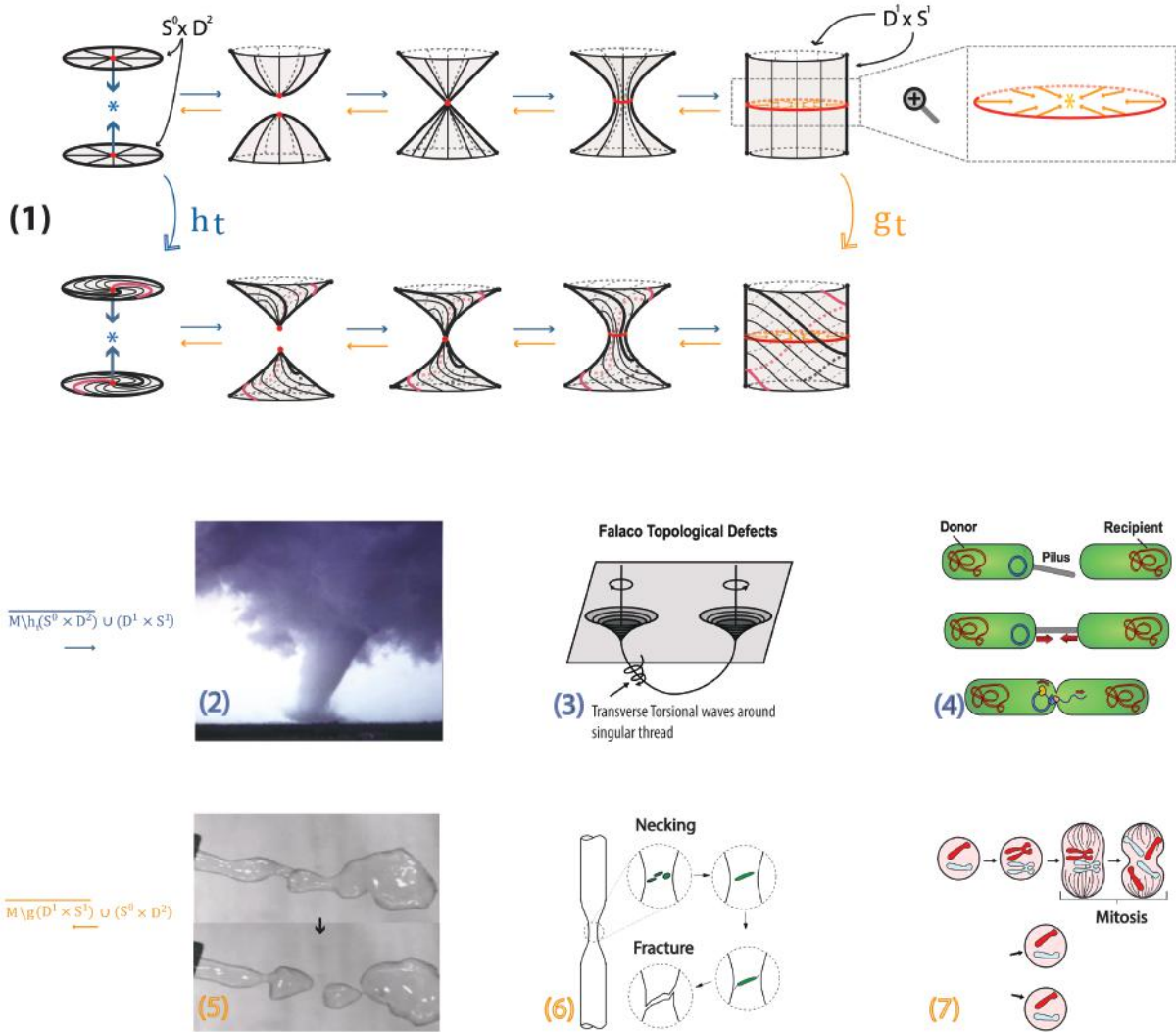


Figure 10. (1) Dynamic 2-dimensional surgery locally (2) Tornadoes (3) Falaco solitons (4) Gene transfer in bacteria (5) Soap bubble splitting (6) Fracture (7) Mitosis

Phenomena exhibiting 2-dimensional 0-surgery are the results of *two colinear attracting forces which ‘create’ a cylinder*. These phenomena have similar dynamics and are characterized by their continuity and the attracting forces causing them. In order to model them topologically and understand 2-dimensional surgery through continuity and dynamics we

introduce the model of Fig. 10 (1) which shows the instances of dynamic 2-dimensional 0-surgery from left to right.

In Fig. 10 (1), below the instances of the standard embedding, we also show the instances of these processes when a non-trivial embedding are used (recall Section 3.2). Note that these embeddings are more appropriate for natural processes involving twisting, such as tornadoes and Falaco solitons. In this example of *twisted 2-dimensional 0-surgery*, the two discs $S^0 \times D^2$ are embedded via a twisted homomorphism h_t while, in the dual case, the cylinder $D^1 \times S^1$ is embedded via a twisted homomorphism g_t . Here h_t rotates the two initial discs in opposite directions by an angle of $3\pi/4$ and we can see how this rotation induces the twisting of angle $3\pi/2$ of the final cylinder (which corresponds to homomorphism g_t rotating the top and bottom of the cylinder by $3\pi/4$ and $-3\pi/4$ respectively). More specifically, if we define the homeomorphism $\omega_1, \omega_2 : D^2 \rightarrow D^2$ to be rotations by $3\pi/4$ and $-3\pi/4$ respectively, then h_t is defined as the composition $h_t : S^0 \times D^2 \xrightarrow{\omega_1 \amalg \omega_2} S^0 \times D^2 \xrightarrow{h} M$. The homeomorphism $g_t : D^1 \times S^1 \rightarrow M$ is defined analogously.

The process of *dynamic 2-dimensional 0-surgery* starts with two points, or poles, specified on the manifold (in red) on which attracting forces caused by an attracting center are applied (in blue). Then, the two discs $S^0 \times D^2$, neighbourhoods of the two poles, approach each other. When the centers of the two discs touch, recoupling takes place and the discs get transformed into the final cylinder $D^1 \times S^1$, see Fig. 10 (1). The cylinder created during 2-dimensional 0-surgery can take various forms. For example, it is a tubular vortex of air in the case of tornadoes, a transverse torsional wave in the case of Falaco solitons and a pilus joining the genes in gene transfer in bacteria.

On the other hand, phenomena exhibiting 2-dimensional 1-surgery are the result of *an infinitum of coplanar attracting forces which ‘collapse’ a cylinder*, see Fig. 10 (1) from

the end. As mentioned in Section 3.3, the dual case of 2-dimensional 0-surgery is the 2-dimensional 1-surgery and vice versa. This is illustrated in Fig. 10 (1) where the reverse process is the *2-dimensional 1-surgery* which starts with the cylinder and a specified circular region (in red) on which attracting forces caused by an attracting center are applied (in orange). A ‘necking’ occurs in the middle which degenerates into a point and finally tears apart creating two discs $S^0 \times D^2$. This cylinder can be embedded, for example, in the region of the bubble’s surface where splitting occurs, on the region of metal specimens where necking and fracture occurs or on the equator of the cell which is about to undergo a mitotic process.

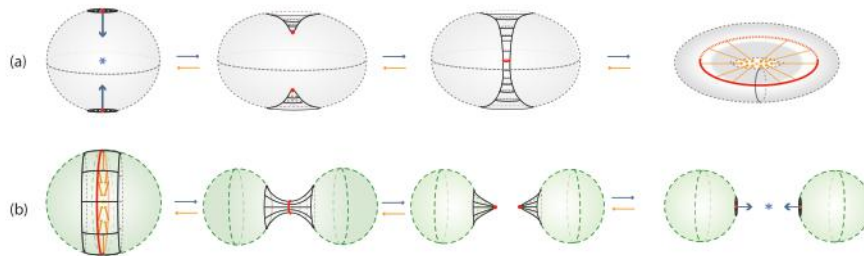


Figure 11. (a) 2-dimensional 0-surgery on $M = S^2$ and 2-dimensional 1-surgery on $M' = S^0 \times S^2$ (b) 2-dimensional 1-surgery on $M = S^2$ and 2-dimensional 0-surgery on $M' = S^0 \times S^2$.

In Fig 11 (a) and (b), we apply the local dynamics of Fig. 10 (1) to the initial manifold $M = S^2$ and produce the same manifolds seen in formal 2-dimensional surgery (recall Fig. 5 (b₁)(b₂)) through a continuous process resulting of forces. Note that, as also seen in 1-dimensional surgery (Fig 9 (b)), if the blue attracting center in Fig 11 (a) was outside the sphere and the cylinder was attached on S^2 externally, the result would still be a torus.

Finally, it is worth pointing out that these local dynamics produce different manifolds depending on the initial manifold where they act. Taking examples from natural phenomena, 2-dimensional 0-surgery transforms an $M = S^0 \times S^2$ to an S^2 by adding a cylinder during

gene transfer in bacteria (see Fig. 10 (4)) but can also transform an $M = S^2$ to a torus by ‘drilling out’ a cylinder during the formation of Falaco solitons (see Fig. 10 (3)) in which case S^2 is the pool of water and the cylinder is the boundary of the tubular neighborhood around the thread joining the two poles.

Remark 3. Note that Remark 1 is also true here. One can obtain Fig. 10 (1) by rotating Fig. 8 (1) and this extends also to the dynamics and forces. For instance, by rotating the two points, or S^0 , on which the pair of forces of 1-dimensional 0-surgery acts (shown in red in the last instance of Fig. 8 (1)) by 180° around a vertical axis we get the circle, or S^1 , on which the infinitum of coplanar attracting forces of 2-dimensional 1-surgery acts (shown in red in the last instance of Fig. 10 (1)).

5.4 Modeling phenomena exhibiting 2-dimensional surgery

Looking back at the natural phenomena happening on surfaces, an example is **soap bubble splitting** during which a soap bubble splits into two smaller bubbles. This process is the 2-dimensional 1-surgery on $M = S^2$ shown in Fig 11 (b). The orange attracting force in this case is the surface tension of each bubble that pulls molecules into the tightest possible groupings.

If one looks closer at the other phenomena exhibiting 2-dimensional surgery shown in Fig. 10, one can see that these phenomena do not happen on surfaces but on 3-dimensional manifolds, therefore we can’t model them as 2-dimensional surgeries. As we will see in Section 6, these processes are described by the notion of solid surgery. Therefore they will be analyzed after the introduction of this notion. For instance, gene transfer in bacteria, drop coalescence and the formation of Falaco solitons are discussed in Section 6.3 while mitosis and fracture will be discussed in Section 6.4.

Moreover, as we will see in Section 9, the ambient space is also involved in the process of tornado formation, see Fig. 10 (2). Therefore it will be analyzed in Section 9.3.2, after the introduction of the notion of embedded surgery.

5.5 A model for dynamic m -dimensional n -surgery

As mentioned in Section 4.1, surgery can be viewed as collapsing the thickened core S^n to a singular point and then uncollapsing the thickened core S^{m-n-1} . As seen in Fig. 10 (1), in the case of 2-dimensional 0-surgery, forces (in blue) are applied to core S^0 , whose thickening comprises the two discs, while in the case of the 2-dimensional 1-surgery, forces (in orange) are applied on the core S^1 , whose thickening is the cylinder. In other words, the forces that model 2-dimensional n -surgery are always applied to the core n -embedding $e = h|_1 : S^n = S^n \times \{0\} \hookrightarrow M$ of the framed n -embedding $h : S^n \times D^{2-n} \hookrightarrow M$.

This observation can be generalized as follows: The process followed by natural phenomena exhibiting topological surgery is modeled by Definition 2 enhanced with attracting forces acting on the cores S^n and S^{m-n-1} of embeddings $S^n \times D^{m-n}$ and $D^{n+1} \times S^{m-n-1}$. Moreover, we view this continuous passage as a result of forces towards the attracting center, which is identified with the singular point.

The above are shown in Fig. 12 (1) and (2) for dimensions 1 and 2 respectively. This figure completes Fig. 7 with the observed dynamics.

6 Solid surgery

Looking closer at the phenomena exhibiting 2-dimensional surgery shown in Fig. 10, one can see that, with the exception of soap bubble splitting that involves surfaces, all others involve 3-dimensional manifolds. For instance, what really happens during a mitotic

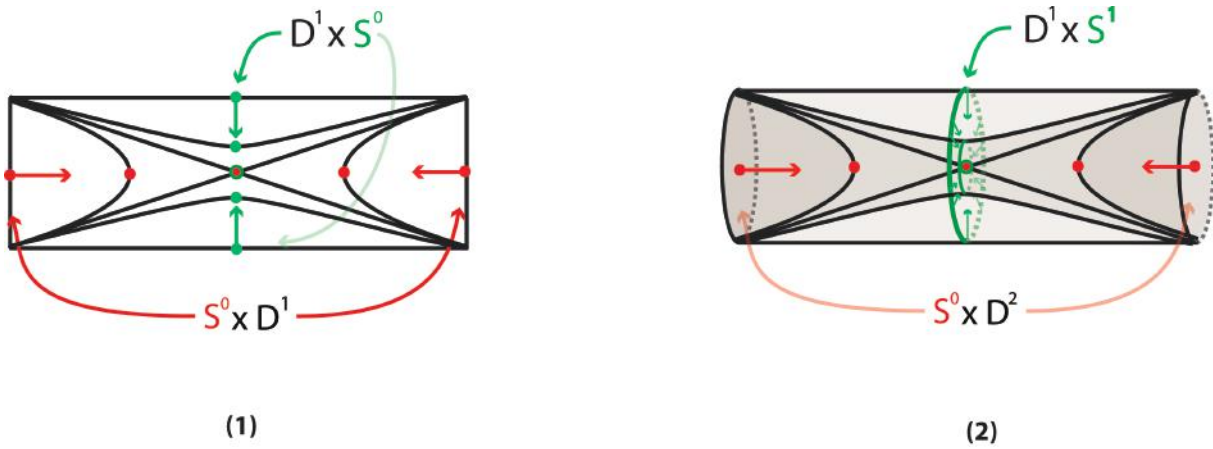


Figure 12. (1) Model for dynamic 1-dimensional 0-surgery (2) Model for dynamic 2-dimensional 0-surgery

process is that a solid cylindrical region located in the center of the cell collapses and a D^3 is transformed into an $S^0 \times D^3$. Similarly, during tornado formation, the created cylinder is not just a cylindrical surface $D^1 \times S^1$ but a solid cylinder $D^2 \times S^1$ containing many layers of air (this phenomena will be detailed in Section 9.3.2). Of course we can say that, for phenomena involving 3-dimensional manifolds, the outer layer of the initial manifold is undergoing 2-dimensional surgery. In this section we will define topologically what happens to the whole manifold.

The need of such a definition is also present in dimension 1 for modeling phenomena such as the merging of oil slicks and tension on membranes (or soap films). These phenomena undergo the process of 1-dimensional 0-surgery but happen on surfaces instead of 1-manifolds.

We will now introduce the notion of solid surgery (in both dimensions 1 and 2) where the interior of the initial manifold is filled in. There is one key difference compared to the dynamic surgeries discussed in the previous section. While the local dynamics described in Fig. 8 and 10 can be embedded in any manifold, here we also have to fix the initial

manifold in order to define solid surgery. For example, as we will see next, we define separately the processes of *solid 1-dimensional 0-surgery on D^2* and *solid 1-dimensional 0-surgery on $D^2 \times S^0$* . However, the underlying features are common in both.

6.1 Solid 1-dimensional topological surgery

Solid 1-dimensional 0-surgery on the 2-disc D^2 is the topological procedure whereby a ribbon $D^1 \times D^1$ is being removed, such that the closure of the remaining manifold comprises two discs $D^2 \times S^0$. The reader is referred to Fig 5 (a) where the interior is now supposed to be filled in. This process is equivalent to performing 1-dimensional 0-surgeries on the whole continuum of concentric circles included in D^2 , see Fig. 13. More precisely, and introducing at the same time dynamics, we define:

Definition 3. *Solid 1-dimensional 0-surgery on D^2* is the following process. We start with the 2-disc of radius 1 with polar layering:

$$D^2 = \cup_{0 < r \leq 1} S_r^1 \cup \{P\},$$

where r the radius of a circle and P the limit point of the circles, which is the center of the disc and also the circle of radius zero. We specify colinear pairs of antipodal points, all on the same diameter, with neighbourhoods of analogous lengths, on which the same colinear attracting forces act. See Fig 13 (1) where these forces and the attracting center are shown in blue. Then, in (2), the antipodal segments get closer to one another or, equivalently, closer to the attracting center. Note that here, the attracting center coincides with the limit point of all concentric circles, which is shown in green from instance (2) and on. Then, as shown from (3) to (9), we perform 1-dimensional 0-surgery on the whole continuum of concentric circles. The natural order of surgeries is as follows: first, the

center of the segments that are closer to the center of attraction touch, see (4). After all other points have also reached the center, see (5), decoupling starts from the central or limit point. We define 1-dimensional 0-surgery on the limit point P to be the two limit points of the resulting surgeries. That is, the effect of *solid 1-dimensional 0-surgery on a point is the creation of two new points*, see (6). Next, the other segments reconnect, from the inner, see (7), to the outer ones, see (8), until we have two copies of D^2 , see (9) and (10). The proposed order of reconnection, from inner to outer, is the same as the one followed by skin healing, namely, the regeneration of the epidermis starts with the deepest part and then migrates upwards.

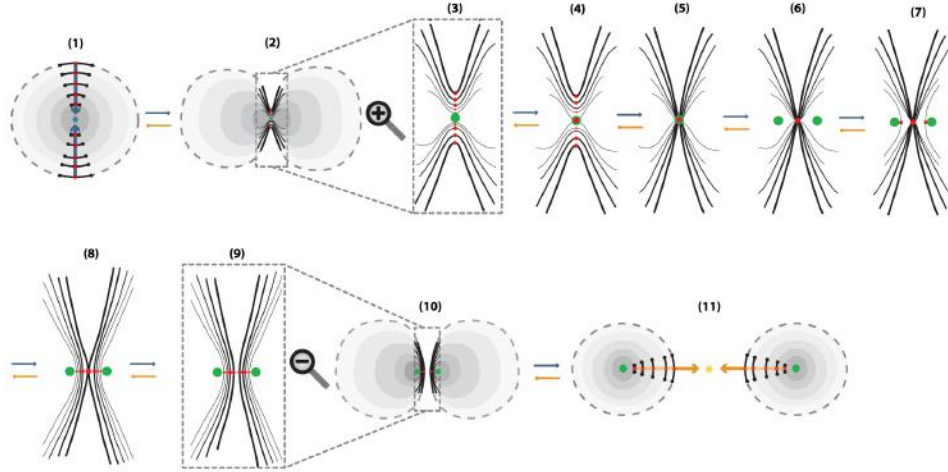


Figure 13. Solid 1-dimensional surgery.

The above process is the same as first removing the center P from D^2 , doing the 1-dimensional 0-surgeries and then taking the closure of the resulting space. The resulting manifold is

$$\chi(D^2) := \cup_{0 < r \leq 1} \chi(S_r^1) \cup \chi(P),$$

which comprises two copies of D^2 .

We also have the reverse process of the above, namely, *solid 1-dimensional 0-surgery on two discs* $D^2 \times S^0$ is the topological procedure whereby a ribbon $D^1 \times D^1$ joining the discs is added, such that the closure of the remaining manifold comprise one disc D^2 . This process is the result of the orange forces and attracting center which are applied on the ‘complementary’ points, see Fig. 13 in reverse order. This operation is equivalent to performing 1-dimensional 0-surgery on the whole continuum of pairs of concentric circles in $D^2 \amalg D^2$. We only need to define solid 1-dimensional 0-surgery on two limit points to be the limit point P of the resulting surgeries. That is, the effect of *solid 1-dimensional 0-surgery on two points is their merging into one point*. The above process is the same as first removing the centers from the $D^2 \times S^0$, doing the 1-dimensional 0-surgeries and then taking the closure of the resulting space. The resulting manifold is

$$\chi^{-1}(D^2 \times S^0) := \cup_{0 < r \leq 1} \chi^{-1}(S_r^1 \times S^0) \cup \chi^{-1}(P \times S^0),$$

which comprises one copy of D^2 .

6.2 Solid 2-dimensional topological surgery

Moving up one dimension, there are two types of solid 2-dimensional surgery on the 3-ball, D^3 , analogous to the two types of 2-dimensional surgery. Both are shown in Fig. 14 (b₁) and (b₂) in relation with solid 1-dimensional surgery, see Fig. 14 (a). The first one is the *solid 2-dimensional 0-surgery* which is the topological procedure of removing a solid cylinder homeomorphic to the product set $D^1 \times D^2$, $h(D^1 \times D^2)$ (such that the part $S^0 \times D^2$ of its boundary lies in the boundary of D^3) and taking the closure of the remaining manifold $D^3 \setminus h(D^1 \times D^2)$, which is a regular (or twisted) solid torus. See Fig 5 (b₁) where the interior is supposed to be filled in. The second type is the *solid*

2-dimensional 1-surgery which is the topological procedure of removing a solid cylinder homeomorphic to the product set $D^2 \times D^1$, $h(D^2 \times D^1)$, (such that the part $S^1 \times D^1$ of its boundary lies in the boundary of D^3) and taking the closure of the remaining manifold $D^3 \setminus h(D^2 \times D^1)$, which is two copies of D^3 . See Fig 5 (b₂) where the interior is supposed to be filled in. Those processes are equivalent to performing 2-dimensional surgeries on the whole continuum of concentric spheres included in D^3 . More precisely we have:

Definition 4. We start with the 3-ball of radius 1 with polar layering:

$$D^3 = \cup_{0 < r \leq 1} S_r^2 \cup \{P\},$$

where r the radius of the 2-sphere S_r^2 and P the limit point of the spheres, that is, their common center and the center of the ball. *Solid 2-dimensional 0-surgery on D^3* is the topological procedure whereby 2-dimensional 0-surgery takes place on each spherical layer that D^3 is made of. More precisely, as illustrated in Fig. 14 (b₁), on all spheres S_r^2 colinear pairs of antipodal points are specified, all on the same diameter, on which the same colinear attracting forces act. The poles have disc neighborhoods of analogous areas. Then, 2-dimensional 0-surgeries are performed on the whole continuum of the concentric spheres using the same embedding h (recall Section 3.2). Moreover, 2-dimensional 0-surgery on the limit point P is defined to be the limit circle of the nested tori resulting from the continuum of 2-dimensional 0-surgeries. That is, the effect of *2-dimensional 0-surgery on a point is defined to be the creation of a circle.*

The process is characterized on one hand by the 1-dimensional core L of the solid cylinder which joins the two selected antipodal points of the outer shell and intersects each spherical layer at its two corresponding antipodal points, and on the other hand by the embedding h . The process results in a continuum of layered tori and can be viewed as

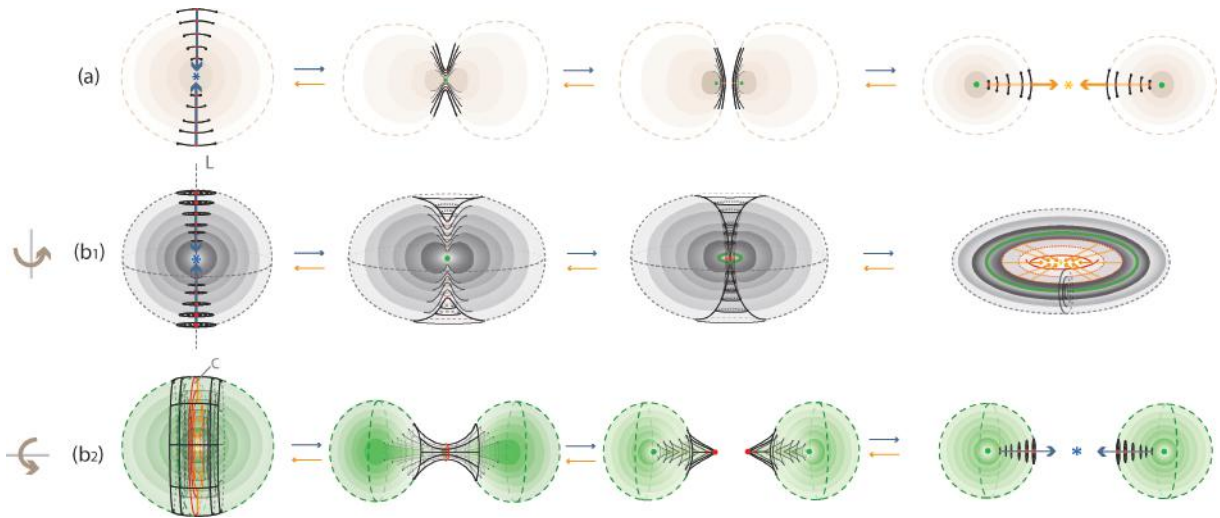


Figure 14. (a) Solid 1-dimensional 0-surgery on D^2 (b₁) Solid 2-dimensional 0-surgery on D^3 (b₂) Solid 2-dimensional 1-surgery on D^3

drilling out a tunnel along L according to h . Note that in Fig. 14, the identity embedding has been used. However, a twisting embedding, which is the case shown in Fig. 10 (1), agrees with our intuition that, for opening a hole, *drilling with twisting* seems to be the easiest way. Examples of these two embeddings can be found in Section 3.2.

Furthermore, *solid 2-dimensional 1-surgery on D^3* is the topological procedure where on all spheres S_r^2 nested cylindrical peels of the solid cylinder of analogous areas are specified and the same coplanar attracting forces act on all spheres, see Fig. 14 (b₂). Then, 2-dimensional 1-surgeries are performed on the whole continuum of the concentric spheres using the same embedding h . Moreover, 2-dimensional 1-surgery on the limit point P is defined to be the two limit points of the nested pairs of 2-spheres resulting from the continuum of 2-dimensional surgeries. That is, the effect of *2-dimensional 1-surgery on a point is the creation of two new points*. The process is characterized by the 2-dimensional central disc of the solid cylinder and the embedding h , and it can be viewed as squeezing the central disc C or, equivalently, as pulling apart the left and right hemispheres with

possible twists, if h is a twisting embedding. This agrees with our intuition that for cutting a solid object apart, *pulling with twisting* seems to be the easiest way. Examples of the identity and the twisting embedding can be found in Section 3.3.

For both types of solid 2-dimensional surgery, the above process is the same as: first removing the center P from D^3 , performing the 2-dimensional surgeries and then taking the closure of the resulting space. Namely we obtain:

$$\chi(D^3) := \cup_{0 < r \leq 1} \chi(S_r^2) \cup \chi(P),$$

which is a solid torus in the case of solid 2-dimensional 0-surgery and two copies of D^3 in the case of solid 2-dimensional 1-surgery.

As seen in Fig. 14, we also have the two dual solid 2-dimensional surgeries, which represent the reverse processes. As already mentioned in Section 3.3, the dual case of 2-dimensional 0-surgery is the 2-dimensional 1-surgery and vice versa. More precisely:

Definition 5. The *dual case of solid 2-dimensional 0-surgery on D^3* is the solid 2-dimensional 1-surgery on a solid torus $D^2 \times S^1$ whereby a solid cylinder $D^1 \times D^2$ filling the hole is added, such that the closure of the resulting manifold comprises one 3-ball D^3 . This is the reverse process shown in Fig. 14 (b₁) which results from the orange forces and attracting center. Given that the solid torus can be written as a union of nested tori together with the core circle: $D^2 \times S^1 = (\cup_{0 < r \leq 1} S_r^1 \cup \{0\}) \times S^1$, solid 2-dimensional 1-surgeries are performed on each toroidal layer starting from specified annular peels of analogous sizes where the same coplanar forces act on the central rings of the annuli. These forces are caused by the same attracting center lying outside the torus. It only remain to define the solid 2-dimensional 1-surgery on the limit circle to be the limit point P of the resulting surgeries. That is, the effect of *solid 2-dimensional 1-surgery on the core*

circle is that it collapses into one point, the attracting center. The above process is the same as first removing the core circle from $D^2 \times S^1$, doing the 2-dimensional 1-surgeries on the layered tori, with the same coplanar acting forces, and then taking the closure of the resulting space. Hence, the resulting manifold is

$$\chi^{-1}(D^2 \times S^1) := \cup_{0 < r \leq 1} \chi^{-1}(S_r^1 \times S^1) \cup \chi^{-1}(\{0\} \times S^1),$$

which comprises one copy of D^3 .

Further, *the dual case of solid 2-dimensional 1-surgery on D^3* is the solid 2-dimensional 0-surgery on two 3-balls D^3 whereby a solid cylinder $D^2 \times D^1$ joining the balls is added, such that the closure of the resulting manifold comprise of one 3-ball D^3 . This is the reverse process shown in Fig. 14 (b₂) which results from the blue forces and attracting center. We only need to define the solid 2-dimensional 0-surgery on two limit points to be the limit point P of the resulting surgeries. That is, as in solid 1-dimensional surgery (see Fig. 14 (a)), the effect of *solid 2-dimensional 0-surgery on two points is their merging into one point*. The above process is the same as first removing the centers from the $D^3 \times S^0$, doing the 2-dimensional 0-surgeries on the nested spheres with the same colinear forces and then taking the closure of the resulting space. The resulting manifold is

$$\chi^{-1}(D^3 \times S^0) := \cup_{0 < r \leq 1} \chi^{-1}(S_r^2 \times S^0) \cup \chi^{-1}(P \times S^0),$$

which comprises one copy of D^3 .

Note that remarks 1 and 3 are also true here. One can obtain the instances of solid 2-dimensional surgeries (Fig. 14 (b₁) and Fig. 14 (b₂)) by rotating the instances of solid 1-dimensional surgery (Fig. 14 (a)) respectively by 180° around a vertical axis and by 180° around a horizontal axis.

Remark 4. The notions of 2-dimensional (resp. solid 2-dimensional) surgery, can be generalized from S^2 (resp. D^3) to a surface (resp. a handlebody) of genus g creating a surface (resp. a handlebody) of genus $g \pm 1$ or a disconnected surface (resp. handlebody).

6.3 Modeling phenomena exhibiting solid 2-dimensional 0-surgery

We will now describe the phenomena mentioned in Section 5.4 which undergo the process of solid 2-dimensional 0-surgery.

For **gene transfer in bacteria**, see Fig. 10 (4) (also, for description and instructive illustrations see [8]), the donor cell produces a connecting tube called a ‘pilus’ which attaches to the recipient cell, brings the two cells together and transfers the donor’s DNA. This process is similar to the one shown earlier in Fig 14 (b₂) as two copies of D^3 merge into one, but here the attracting center is located on the recipient cell. This process is a solid 2-dimensional 0-surgery on two 3-balls $M = D^3 \times S^0$.

Similarly, the process of **drop coalescence** is also a solid 2-dimensional 0-surgery on two 3-balls $M = D^3 \times S^0$, see Fig 14 (b₂). The process of drop coalescence also exhibits the forces of our model. Namely, the surfaces of two drops must be in contact for coalescence to occur. This surface contact is dependent on both the van der Waals attraction and the surface repulsion forces between two drops. When the van der Waals forces cause rupture of the film, the two surface films are able to fuse together, an event more likely to occur in areas where the surface film is weak. The liquid inside each drop is now in direct contact, and the two drops are able to merge into one.

Moreover, as already mentioned in Section 5.3, the formation of Falaco solitons is a natural phenomenon exhibiting solid 2-dimensional 0-surgery, see Fig. 10 (3) (for photos of pairs of Falaco solitons in a swimming pool, see [14]). Note that the term ‘Falaco Soliton’ appears in 2001 in [15]. These pairs of singular surfaces (poles) are connected by means of

a stabilizing thread. The two poles get connected and their rotation propagates below the water surface along the joining thread and the tubular neighborhood around it. This process is a solid 2-dimensional 0-surgery with a twisted homeomorphism (see Fig. 10 (1)) where the initial manifold is the water contained in the volume of the pool where the process happens, which is homeomorphic to a 3-ball, that is $M = D^3$. It is also worth mentioning that the creation of Falaco solitons is immediate and does not allow us to see whether the transitions of solid 2-dimensional 0-surgery shown in Fig. 14 (b₁) are followed or not. However, these dynamics are certainly visible during **the annihilation of Falaco solitons**. Namely, when the topological thread joining the poles is cut, the tube tears apart and slowly degenerates to the poles until they both stop spinning and vanish. Therefore, the continuity of our dynamic model is clearly present during the reverse process which corresponds to a solid 2-dimensional 1-surgery on a pair of Falaco solitons, that is, a solid torus $D^2 \times S^1$ degenerating into a still swimming pool D^3 , see the reverse process of Fig. 14 (b₁).

Note that it is conjectured in [14] that the coherent topological features of the Falaco solitons and, by extension, the process of solid 2-dimensional 0-surgery appear in both macroscopic level (for example in the Wheeler's wormholes) and microscopic level (for example in the spin pairing mechanism in the microscopic Fermi surface). For more details see [14].

6.4 Modeling phenomena exhibiting solid 2-dimensional 1-surgery

We will now describe the phenomena mentioned in Section 5.4 which undergo the process of solid 2-dimensional 1-surgery.

As already mentioned, the collapsing of the central disc of the sphere caused by the orange attracting forces in Fig. 14 (b₂) can also be caused by pulling apart left and right

hemispheres of the 3-ball D^3 , that is, the causal forces can also be repelling. For example, during the fracture of metal specimens under tensile forces, solid 2-dimensional 1-surgery is caused by forces that pull apart each end of the specimen. On the other hand, in the biological process of mitosis, both attracting and repelling forces are present. We will now describe these two processes in details.

When the tension applied on metal specimens by tensile forces results in **necking** and then **fracture**, the process exhibits solid 2-dimensional 1-surgery. More precisely, in experiments in mechanics, tensile forces (or loading) are applied on a cylindrical specimen made of ductile material (steel, aluminium, etc.). Up to some critical value of the force the deformation is homogeneous (the cross-sections have the same area). At the critical value the deformation is localized within a very small area where the cross-section is reduced drastically, while the sections of the remaining portions increase slightly. This is the ‘necking phenomenon’. Shortly after, the specimen is fractured (view [35] for details). In Fig. 10 (6) are the the basic steps of the process: void formation, void coalescence (also known as crack formation), crack propagation, and failure or fracture. Here, the process is not as smooth as our theoretical model and the tensile forces applied on the specimen are equivalent to repelling forces. The specimen of Fig. 10 (6) is homeomorphic to the sphere shown in Fig. 14 (b₂) hence the initial manifold is $M = D^3$.

Solid 2-dimensional 1-surgery on $M = D^3$ also happens in the biological process of **mitosis**, where a cell splits into two new cells. See Fig. 10 (7) (for description and instructive illustrations see for example [12]). We will see that both aforementioned forces are present here. During mitosis, the chromosomes, which have already duplicated, condense and attach to fibers that pull one copy of each chromosome to opposite sides of the cell (this pulling is equivalent to repelling forces). The cell pinches in the middle and then divides by cytokinesis. The structure that accomplishes cytokinesis is the contractile

ring, a dynamic assembly of filaments and proteins which assembles just beneath the plasma membrane and contracts to constrict the cell into two (this contraction is equivalent to attracting forces). In the end, two genetically-identical daughter cells are produced.

7 A dynamical system modeling solid 2-dimensional 0-surgery

So far, inspired by natural processes undergoing surgery, we have extended the formal definition of topological surgery by introducing new notions such as continuity and solid surgery and presented a model showing where the observed forces act. However, in our model, time and dynamics were not introduced by differential equations. In this section we connect topological surgery, enhanced with these notions, with a dynamical system. We will see that, with a small change in parameters, the trajectories of its solutions are performing solid 2-dimensional 0-surgery. Therefore, this dynamical system constitutes a specific set of equations modeling natural phenomena undergoing solid 2-dimensional 0-surgery. More specifically, we will see that the change of parameters of the system affects the eigenvectors and induces a flow along a segment joining two steady state points. The induced flow represents the attracting forces shown in Fig. 14 (b₁). Finally, we will see how our topological definition of solid 2-dimensional 0-surgery presented in Section 6.2 is verified by our numerical simulations and, in particular, that surgery on a steady point creates a limit cycle.

7.1 The dynamical system and its steady state points

In [30], N.Samardzija and L.Greller study the behavior of the following dynamical system (Σ) that generalizes the classical Lotka–Volterra problem [21, 33] into three dimensions:

$$\left. \begin{array}{l} \frac{dX}{dt} = X - XY + CX^2 - AZX^2 \\ \frac{dY}{dt} = -Y + XY \\ \frac{dZ}{dt} = -BZ + AZX^2 \end{array} \right\} A, B, C > 0 \quad (\Sigma)$$

In subsequent work [31], the authors present a slightly different model, provide additional numerical simulations and deepen the qualitative analysis done in [30]. Since both models coincide in the parametric region we are interested in, we will use the original model and notation and will briefly present some key features of the analyses done in [30] and [31].

The system (Σ) is a two-predator and one-prey model, where the predators Y, Z do not interact directly with one another but compete for prey X . As X, Y, Z are populations, only the positive solutions are considered in this analysis. It is worth mentioning that, apart from a population model, (Σ) may also serve as a biological model and a chemical model, for more details see [30].

The parameters A, B, C are analyzed in order to determine the bifurcation properties of the system, that is, to study the changes in the qualitative or topological structure of the family of differential equations (Σ) . As parameters A, B, C affect the dynamics of constituents X, Y, Z , the authors were able to determine conditions for which the ecosystem of the three species results in steady, periodic or chaotic behavior. More precisely, the authors derive five steady state solutions for the system but only the three positive ones are taken into consideration. These points are:

$$S_1 = \begin{pmatrix} 0 \\ 0 \\ 0 \end{pmatrix}, \quad S_2 = \begin{pmatrix} 1 \\ 1+C \\ 0 \end{pmatrix}, \quad S_3 = \begin{pmatrix} \sqrt{B/A} \\ 0 \\ \frac{1+C\sqrt{B/A}}{\sqrt{AB}} \end{pmatrix}$$

It is worth reminding here that a steady state (or singular) point of a dynamical system is a solution that does not change with time.

7.2 Local behavior and numerical simulations

Let, now, $J(S_i)$ be the Jacobian of (Σ) evaluated at S_i for $i = 1, 2, 3$ and let the sets $\Gamma\{J(S_i)\}$ and $W\{J(S_i)\}$ to be, respectively, the eigenvalues and the corresponding associated eigenvectors of $J(S_i)$. These are as follows:

$$\Gamma\{J(S_1)\} = \{1, -1, -B\}; \quad W\{J(S_1)\} = \left\{ \begin{bmatrix} 1 \\ 0 \\ 0 \end{bmatrix}, \begin{bmatrix} 0 \\ 1 \\ 0 \end{bmatrix}, \begin{bmatrix} 0 \\ 0 \\ 1 \end{bmatrix} \right\}$$

$$\Gamma\{J(S_2)\} = \{A - B, (C + \sqrt{(C-2)^2 - 8})/2, (C - \sqrt{(C-2)^2 - 8})/2\}$$

$$W\{J(S_2)\} = \left\{ \begin{bmatrix} 1 \\ (C+1)/(A-B) \\ \frac{B+C-A+(C+1)/(B-A)}{A} \end{bmatrix}, \begin{bmatrix} 1 \\ \frac{C-\sqrt{(C-2)^2-8}}{2} \\ 0 \end{bmatrix}, \begin{bmatrix} 1 \\ \frac{C+\sqrt{(C-2)^2-8}}{2} \\ 0 \end{bmatrix} \right\}$$

$$\Gamma\{J(S_3)\} = \left\{ \sqrt{\frac{B}{A}} - 1, \frac{-1 + \sqrt{1 - 8B(1 + C\sqrt{B/A})}}{2}, \frac{-1 - \sqrt{1 - 8B(1 + C\sqrt{B/A})}}{2} \right\}$$

$$W\{J(S_3)\} = \left\{ \left[\begin{array}{c} 1 \\ -1 - \frac{2\sqrt{AB}(1+C\sqrt{B/A})}{\sqrt{B/A}-1} \\ \frac{2(1+C\sqrt{B/A})}{\sqrt{B/A}-1} \end{array} \right], \left[\begin{array}{c} 1 \\ 0 \\ \frac{-1-\sqrt{1-8B(1+C\sqrt{B/A})}}{2B} \end{array} \right], \left[\begin{array}{c} 1 \\ 0 \\ \frac{-1+\sqrt{1-8B(1+C\sqrt{B/A})}}{2B} \end{array} \right] \right\}$$

Using the sets of eigenvalues and eigenvectors presented above, the authors characterize in [30], [31] the local behavior of the dynamical system around these three points using the Hartman-Grobman (or linearization) Theorem. Since $1 > 0$ and $-1, -B < 0$, S_1 is a saddle point for all values of parameters A, B, C . However, the behavior around S_2 and S_3 changes as parameters A, B, C are varied. The authors show that the various stability conditions can be determined by only two parameters: C and B/A . It is also shown in [30] that stable solutions are generated left of and including the line $B/A = 1$ while chaotic/periodic regions appear on the right of the line $B/A = 1$. We are interested in the behavior of (Σ) as it passes from stable to chaotic/periodic regions. Therefore we will focus and analyze the local behavior around S_2 and S_3 and present numerical simulations for: stable region (a) where $B/A = 1$ and $(1/8B - 1)\sqrt{A/B} < C \leq 2(1 + \sqrt{2})$ and chaotic/periodic region (b) where $B/A > 1$ and $(1/8B - 1)\sqrt{A/B} < C \leq 2(1 + \sqrt{2})$.

- **Region (a)**

Setting $B/A = 1$ and equating the right side of (Σ) to zero, one finds as solution the one-dimensional singular manifold:

$$L = \{(X, Y, Z); X = 1, Z = (1 + C - Y)/A\}$$

that passes through the points S_2 and S_3 . Since all points on L are steady state points,

there is no motion along it. For $(1/8B-1)\sqrt{A/B} < C \leq 2(1+\sqrt{2})$, S_2 is an unstable center while S_3 is a stable center (for a complete analysis of all parametric regions see [30]). This means that if $\lambda_1, \lambda_2, \lambda_3$ denote the eigenvalues of either S_2 or S_3 with $\lambda_1 \in \mathbb{R}$ and $\lambda_2, \lambda_3 \in \mathbb{C}$, then $\lambda_1 = 0$ and $Re(\lambda_2) = Re(\lambda_3) > 0$ for S_2 while $\lambda_1 = 0$ and $Re(\lambda_2) = Re(\lambda_3) < 0$ for S_3 . Moreover, the point $(X, Y, Z) = (1, 1, C/A)$ is the center of L . The line segment $X = 1, 0 < Y < 1$ and $(1 + C)/A < Z < C/A$ supports attracting type singularities (and includes S_3) while the line segment defined by $X = 1, 1 < Y < 1 + C$ and $0 < Z < C/A$ supports unstable singularities (and includes S_2), for details see [31]. More precisely, each attracting point corresponds to an antipodal repelling point, the only exception being the center of L which can be viewed as the spheroid of 0-diameter. The local behavior of (Σ) around S_2 and S_3 in this region together with line L are shown in Fig 15 (a). A trajectory (or solution) initiated near L in the repelling segment expands until it gets trapped by the attracting segment, forming the upper and lower hemisphere of a distinct sphere. Hence, a nest of spherical shells surrounding line L is formed, see Fig 16 (a). Moreover, the nest fills the entire positive space with stable solutions.

• **Region (b)**

For $B/A > 1$ and $(1/8B - 1)\sqrt{A/B} < C \leq 2(1 + \sqrt{2})$, S_2 is an inward unstable vortex and S_3 is an outward stable vortex. This means that in both cases they must satisfy the conditions $\lambda_1 \in \mathbb{R}$ and $\lambda_2, \lambda_3 \in \mathbb{C}$ with $\lambda_3 = \lambda_2^*$, the conjugate of λ_2 . The eigenvalues of S_2 must further satisfy $\lambda_1 < 0$ and $Re(\lambda_2) = Re(\lambda_3) > 0$, while the eigenvalues of S_3 must further satisfy $\lambda_1 > 0$ and $Re(\lambda_2) = Re(\lambda_3) < 0$. The local behaviors around S_2 and S_3 for this parametric region are shown in Fig 15 (b). It is worth mentioning that Fig 15 (b) reproduces Fig 1 of [30] with a change of the axes so that the local behaviors of S_2 and S_3 visually correspond to the local behaviors of the trajectories in Fig 16 (b) around the

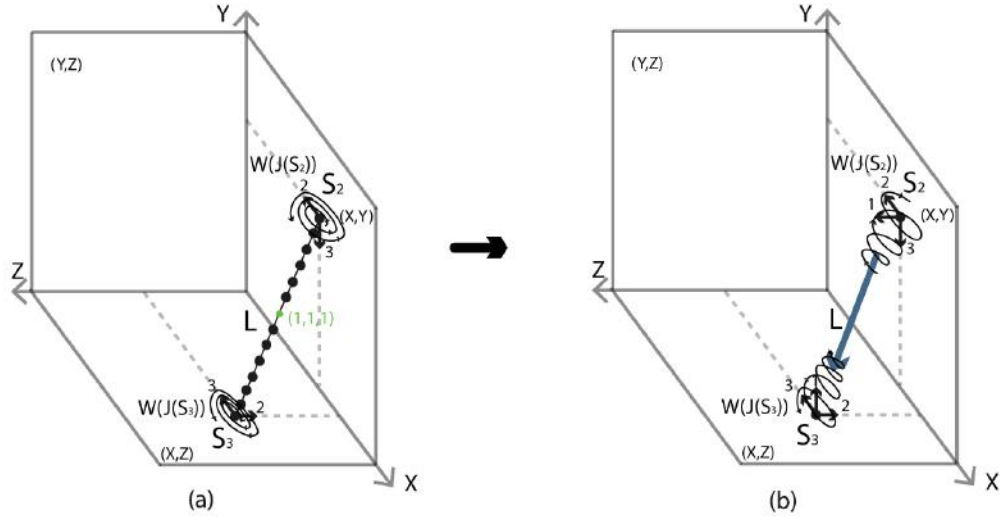


Figure 15. Local behavior. Flow induced along L by changing parameter space from (a) $B/A = 1$ to (b) $B/A > 1$. Indices 1,2 and 3 indicate the first, second and third component in $W(J(S_2))$ and $W(J(S_3))$.

north and the south pole.

Note now that the point S_2 as well as the eigenvectors corresponding to its two complex eigenvalues, all lie in the xy -plane. On the other hand, the point S_3 and also the eigenvectors corresponding to its two complex eigenvalues all lie in the xz -plane. The flow along line L produced by the actions of these eigenvectors forces trajectories initiated near S_2 to wrap around L and move toward S_3 in a motion reminiscent of hole drilling. The connecting manifold L is also called the ‘slow manifold’ in [30] due to the fact that trajectories move slower when passing near it. As trajectories reach S_3 , the eigenvector corresponding to the real eigenvalue of S_3 breaks out of the xz -plane and redirects the flow toward S_2 . As shown in Fig 16 (a) and (b), as $B/A = 1$ moves to $B/A > 1$, this process transforms each spherical shell to a toroidal shell. The solutions scroll down the toroidal surfaces until a limit cycle (shown in green in Fig 16 (b)) is reached. It is worth pointing out that this limit cycle is a torus of 0-diameter and corresponds to the sphere of

0-diameter, namely, the central steady point of L also shown in green in Fig 16 (a).

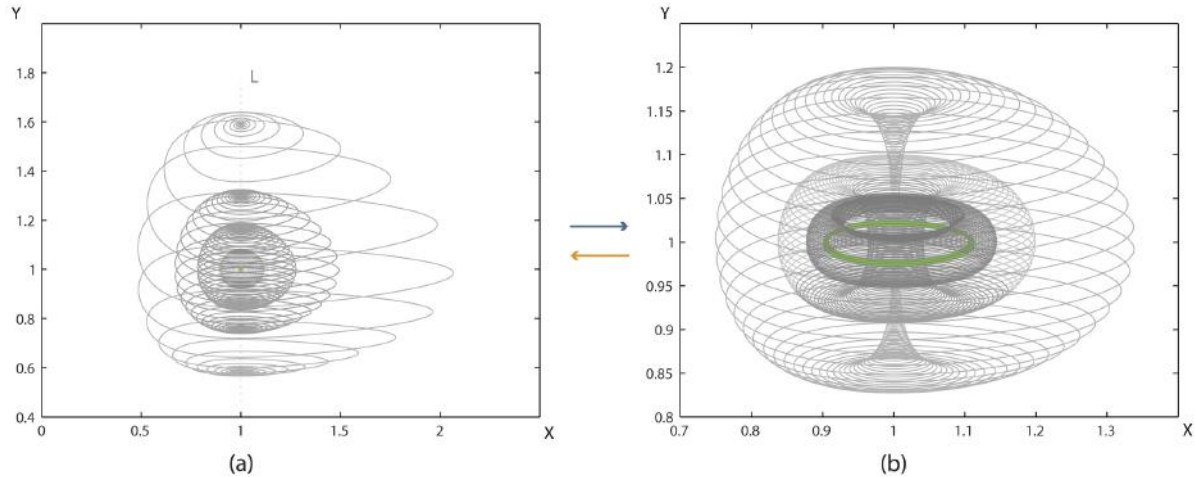


Figure 16. Solid 2-dimensional 0-surgery by changing parameter space from (a) $B/A = 1$ to (b) $B/A > 1$.

However, as the authors elaborate in [31], while for $B/A = 1$ the entire positive space is filled with nested spheres, when $B/A > 1$, only spheres up to a certain volume become tori. More specifically, quoting the authors: “to preserve uniqueness of solutions, the connections through the slow manifold L are made in a way that higher volume shells require slower, or higher resolution, trajectories within the bundle”. As they further explain, to connect all shells through L , (Σ) would need to possess an infinite resolution. As this is never the case, the solutions evolving on shells of higher volume are ‘choked’ by the slow manifold. This generates solution indetermination, which forces higher volume shells to rapidly collapse or dissipate. The behavior stabilizes when trajectories enter the region where the choking becomes weak and weak chaos appears. As shown in both [30] and [31], the outermost shell of the toroidal nesting is a fractal torus. Note that in Fig 16 (b) we do not show the fractal torus because we are interested in the interior of the fractal torus which supports a topology stratified with toroidal surfaces. Hence, all trajectories

are deliberately initiated in its interior where no chaos is present.

It is worth pointing out that Fig 16 reproduces the numerical simulations done in [31]. More precisely, Fig 16 (a) represents solutions of (Σ) for $A = B = C = 3$ and trajectories initiated at points $[1, 1.59, 0.81]$, $[1, 1.3, 0.89]$, $[1, 1.18; 0.95]$, $[1, 1.08, 0.98]$ and $[1, 1, 1]$. Fig 16 (b) represents solutions of (Σ) for $A = 2.9851, B = C = 3$ and trajectories initiated at points $[1.1075, 1, 1]$, $[1, 1, 0.95]$, $[1, 1, 0.9]$ and $[1, 1, 1]$.

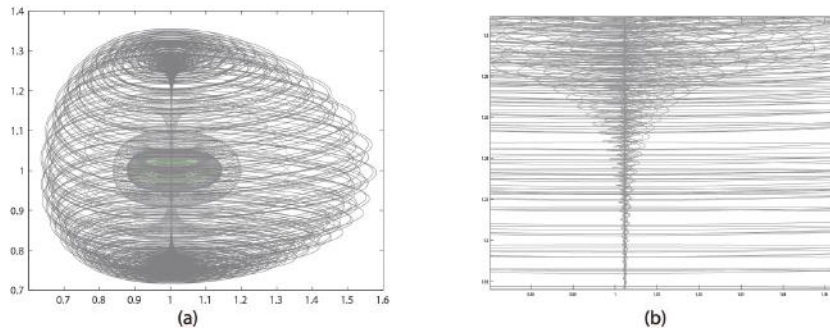


Figure 17. (a) The fractal torus for $B/A > 1$ (b) Zooming on the slow manifold of the fractal torus (*for colored Fig., see online version*)

In Fig. 17 (a), we also present the outermost fractal torus as a trajectory initiated at point $[1.45, 1, 1.45]$ for the same parameters used in Fig. 16, namely $A = 2.9851$ and $B = C = 3$. On the inside of the fractal torus, one can still see the periodic toroidal nesting. By zooming on the slow manifold of the outermost fractal torus shell, in Fig. 17 (b) we can view the ‘hole drilling’ behavior of the trajectories.

As already mentioned, as $B/A = 1$ changes to $B/A > 1$, S_2 changes from an unstable center to an inward unstable vortex and S_3 changes from a stable center to an outward stable vortex. It is worth reminding that this change in local behavior is true not only for the specific parametrical region simulated in Fig. 16 and 17, but applies to all cases satisfying $(1/8B - 1)\sqrt{A/B} < C \leq 2(1 + \sqrt{2})$. For details we refer the reader to Tables

II and III in [30] that recapitulate the extensive diagrammatic analysis done therein.

Finally, it is worth observing the changing of the local behavior around S_2 and S_3 in our numerical simulations. In Fig 16 (a), for $B/A = 1$ we have:

$$\begin{aligned}\Gamma\{J(S_2)\} &= \{\mathbf{0.0000}, 1.500 - 1.3229i, 1.500 + 1.3229i\}, \\ \Gamma\{J(S_3)\} &= \{\mathbf{0.0000}, -1.000 + 4.8780i, -1.000 - 4.878i\}\end{aligned}$$

while in Fig 16 (b), for $B/A > 1$, both centers change to vortices (inward unstable and outward stable) through the birth of the first eigenvalue shown in bold (negative and positive respectively):

$$\begin{aligned}\Gamma\{J(S_2)\} &= \{-\mathbf{0.0149}, 1.500 - 1.3229i, 1.500 + 1.3229i\}, \\ \Gamma\{J(S_3)\} &= \{\mathbf{0.0025}, -1.000 + 4.8780i, -1.000 - 4.878i\}\end{aligned}$$

Remark 5. The use of different numerical methods may affect the shape of the attractor. For example, as mentioned in [31], higher resolution produces a larger fractal torus and a finer connecting manifold. However, the ‘hole drilling’ process and the creation of a toroidal nesting is always a common feature.

7.3 Connecting the dynamical system with solid 2-dimensional 0-surgery

In this section, we will focus on the process of solid 2-dimensional 0-surgery on a 3-ball D^3 viewed as a continuum of concentric spheres together with their common center: $D^3 = \cup_{0 < r \leq 1} S_r^2 \cup \{P\}$. Recall from Section 6.2 that the process is defined as the union of 2-dimensional 0-surgeries on the whole continuum of concentric spheres S_r^2 and on the limit point P . For each spherical layer, the process starts with attracting forces acting

between $S^0 \times D^2$, i.e two points, or poles, centers of two discs.

Having presented the dynamical system (Σ) in Section 7.1 and its local behavior in Section 7.2, its connection with solid 2-dimensional 0-surgery on a 3-ball is now straightforward. To be precise, surgery is performed on the manifold formed by the trajectories of (Σ) . Indeed, as seen in Fig 16 (a) and (b), with a slight perturbation of parameters, trajectories pass from spherical to toroidal shape through a ‘hole drilling’ process along a slow manifold L which pierces all concentric spheres. The spherical and toroidal nestings in Fig. 14 (b₁) and 16 are analogous. The attracting forces acting between the two poles shown in blue in the first instance of Fig. 14 (b₁) are realized by the flow along L (also shown in blue in Fig 15 (b)). When $B/A > 1$, the action of the eigenvectors is an attracting force between S_2 and S_3 acting along L , which drills each spherical shell and transforms it to a toroidal shell.

Furthermore, in order to introduce solid 2-dimensional 0-surgery on D^3 as a new topological notion, we had to define that 2-dimensional 0-surgery on a point is the creation of a circle. This new topological definition also has a meaning in the language of dynamical systems. Namely, the limit point P in the spherical nesting of trajectories shown in green in Fig 16 (a) is a steady state point and the core of the toroidal nesting of trajectories shown in green in in Fig 16 (b) is a limit cycle. In other words, surgery on the limit point P creates the limit cycle. As mentioned in [31], this type of bifurcation is a ‘Hopf bifurcation’, so surgery on the trajectories can be also seen as a Hopf bifurcation.

Hence, instead of viewing surgery as an abstract topological process, we may now view it as a property of a dynamical system. Moreover, natural phenomena exhibiting 2-dimensional topological surgery through a ‘hole-drilling’ process, such as the creation of Falaco solitons, the formation of tornadoes, of whirls, of wormholes, etc, may be modeled mathematically by the dynamical system (Σ) . This system enhances the topological model

presented in Fig. 14 (b₁) with analytical formulation of the underlying dynamics. Indeed, if we link the three time-dependent quantities X, Y, Z to physical parameters of related phenomena undergoing 2-dimensional 0-surgery, system (Σ) can provide time forecasts for these phenomena.

Remark 6. In [14] R.M. Kiehn studies how the Navier-Stokes equations admit bifurcations to Falaco solitons. In other words, the author looks at another dynamical system modeling this natural phenomenon which, as mentioned in Section 5.3, exhibits solid 2-dimensional 0-surgery. To quote the author: “It is a system that is globally stabilized by the presence of the connecting 1-dimensional string” and “The result is extraordinary for it demonstrates a global stabilization is possible for a system with one contracting direction and two expanding directions coupled with rotation”. It is also worth quoting Langford [20] which states that computer simulations indicate that “the trajectories can be confined internally to a sphere-like surface, and that Falaco Soliton minimal surfaces are visually formed at the North and South pole”. One possible future research direction would be to investigate the similarities between this system and (Σ) in relation to surgery.

8 The ambient space S^3

All natural phenomena exhibiting surgery (1- or 2-dimensional, solid or usual) take place in the ambient 3-space. Moreover, as mentioned in Section 5.4, the ambient space can play an important role in the process of surgery. This will be detailed in next section where the notion of embedded surgery in 3-space is introduced. By *3-space* we mean here the compactification of \mathbb{R}^3 which is the 3-sphere S^3 . This choice, as opposed to \mathbb{R}^3 , takes advantage of the duality of the descriptions of S^3 . In this section we present the three most common descriptions of S^3 (see Section 8.1) in which this duality is apparent and which will

set the ground for defining the notion of embedded surgery in S^3 (see Section 9). Beyond that, in Section 8.2, we also demonstrate how these descriptions are interrelated. Finally, in Section 8.3, we pin down how the trajectories of the dynamical system (Σ) presented in Section 7 are related to the descriptions of S^3 and further introduce a Hamiltonian system exhibiting the topology of S^3 .

8.1 Descriptions of S^3

In dimension 3, the simplest c.c.o. 3-manifolds are: the 3-sphere S^3 and the lens spaces $L(p, q)$. In this analysis however, we will focus on S^3 . We start by recalling its three most common descriptions:

8.1.1 Via \mathbb{R}^3

S^3 can be viewed as \mathbb{R}^3 with all points at infinity compactified to one single point: $S^3 = \mathbb{R}^3 \cup \{\infty\}$, see Fig. 18 (a) and (a') where the point at infinity is symbolized with a red star. Given that \mathbb{R}^3 can be viewed as an unbounded continuum of nested 2-spheres centered at the origin together with the point at the origin, see Fig. 18 (a'), S^3 minus the point at the origin and the point at infinity can be viewed as a continuous nesting of 2-spheres.

8.1.2 Via two 3-balls

S^3 can be viewed as the union of two 3-balls: $S^3 = B^3 \cup D^3$, see Fig. 18 (b). This second description of S^3 is clearly related to the first one, since a (closed) neighborhood of the point at infinity can stand for one of the two 3-balls. Note that, when removing the point at infinity, see the passage from Fig. 18 (b) to Fig. 18 (b'), we can see the concentric spheres of the 3-ball B^3 (in red) wrapping around the concentric spheres of the 3-ball D^3 .

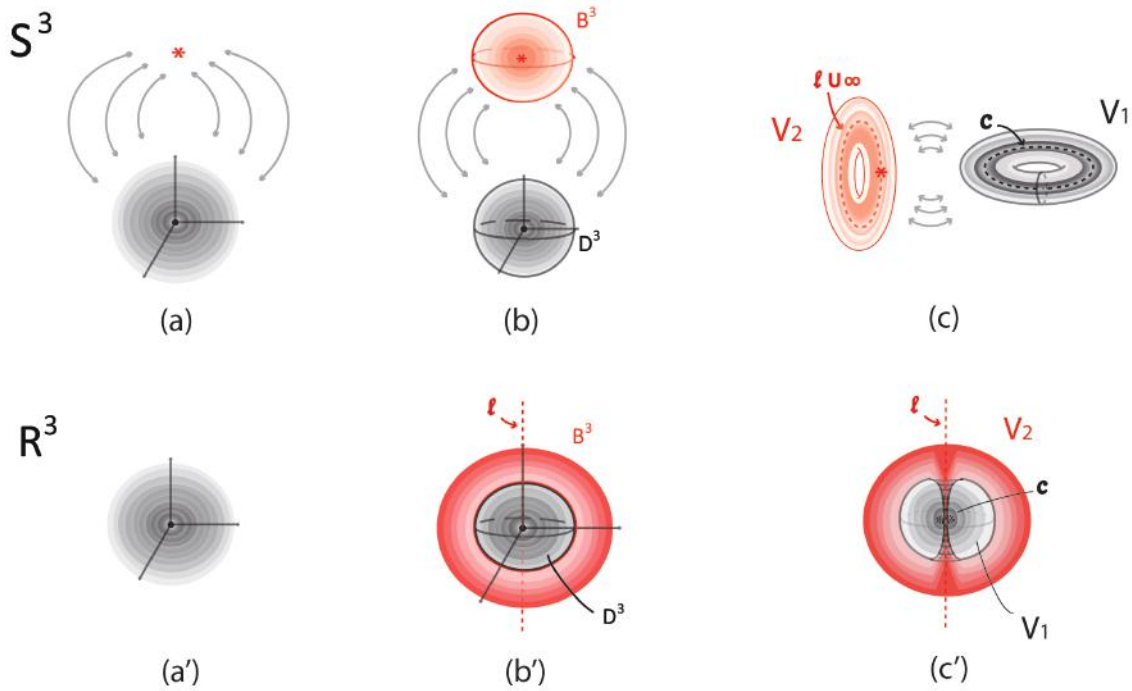


Figure 18. (a) S^3 as the compactification of \mathbb{R}^3 (b) S^3 as the union of two 3-balls (c) S^3 as the union of two solid tori (a') (b') (c') corresponding decompactified views in \mathbb{R}^3

Note that, in both cases B^3 represents the hole space outside D^3 which means that the spherical nesting of B^3 in Fig. 18 (b') extends to infinity, even though only a subset of B^3 is shown. This is another way of viewing \mathbb{R}^3 as the de-compactification of S^3 . This picture is the analogue of the stereographic projection of S^2 on the plane \mathbb{R}^2 (recall Figure 2), whereby the projections of the concentric circles of the south hemisphere together with the projections of the concentric circles of the north hemisphere form the well-known polar description of \mathbb{R}^2 with the unbounded continuum of concentric circles.

8.1.3 Via two solid tori

The third well-known representation of S^3 is as the union of two solid tori along their common boundary: $S^3 = V_1 \cup_{\vartheta} V_2$, via the torus homeomorphism ϑ along the common

boundary, see Fig. 18 (c). ϑ maps a meridian of V_2 to a longitude of V_1 which has linking number zero with the core curve c of V_1 . The illustration in Fig. 18 (c) gives an idea of this splitting of S^3 . In the figure, the core curve c of V_1 is in dashed black. So, the complement of a solid torus V_1 in S^3 is another solid torus V_2 whose core curve l (shown in dashed red) may be assumed to pass by the point at infinity. Note that, S^3 minus the core curves c and l of V_1 and V_2 can be viewed as a continuum of nested tori, see Fig. 18 (c').

When removing the point at infinity in the representation of S^3 as a union of two solid tori, the core of the solid torus V_2 becomes an infinite line l and the nested tori of V_2 can now be seen wrapping around the nested tori of V_1 , see the passage from Fig. 18 (c) to Fig. 18 (c'). Therefore, \mathbb{R}^3 can be viewed as an unbounded continuum of nested tori, together with the core curve c of V_1 and the infinite line l . This line l joins pairs of antipodal points of all concentric spheres of the first description. Note that in the nested spheres description (Fig. 18 (b')) the line l pierces all spheres while in the nested tori description the line l is the 'untouched' limit circle of all tori.

Remark 7. It is also worth mentioning that another way to visualize S^3 as two solid tori is the **Hopf fibration**, which is a map of S^3 into S^2 . The parallels of S^2 correspond to the nested tori of S^3 , the north pole of S^2 correspond to the core curve l of V_2 while the south pole of S^2 corresponds to the core curve c of V_1 . An insightful animation of the Hopf fibration can be found in [10].

8.2 Connecting the descriptions of S^3

8.2.1 Via corking

The connection between the first two descriptions of S^3 was already discussed in previous section. The third description is a bit harder to connect with the first two. We shall do

this here. A way to see this connection is the following. Consider the description of S^3 as the union of two 3-balls, B^3 and D^3 (Fig. 18 (b')). Combining with the third description of S^3 (Fig. 18 (c')) we notice that both 3-balls are pierced by the core curve l of the solid torus V_2 . Therefore, D^3 can be viewed as the solid torus V_1 to which a solid cylinder $D^1 \times D^2$ is attached via the homeomorphism ϑ :

$$D^3 = V_1 \cup_{\vartheta} (D^1 \times D^2).$$

This solid cylinder is part of the solid torus V_2 , a ‘cork’ filling the hole of V_1 . Its core curve is an arc L , part of the core curve l of V_2 . View Fig 19 (a). The second ball B^3 (Fig. 19 (b)) can be viewed as the remaining of V_2 after removing the ‘cork’ $D^1 \times D^2$:

$$B^3 = \overline{V_2 \setminus_{\vartheta} (D^1 \times D^2)}.$$

In other words the solid torus V_2 is cut into two solid cylinders, one comprising the ‘cork’ of V_1 and the other comprising the 3-ball B^3 .

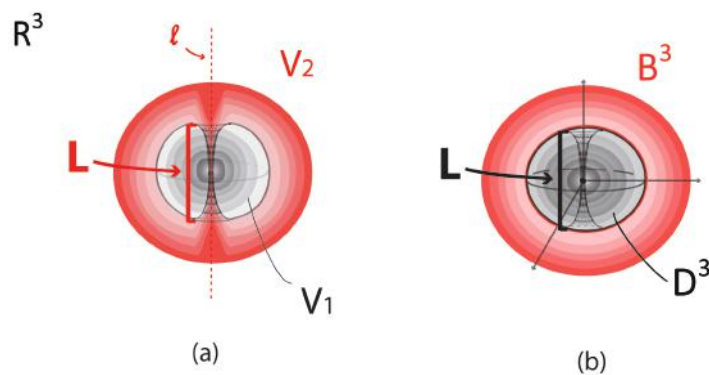


Figure 19. Passing from (a) S^3 as two solid tori to (b) S^3 as two balls.

Remark 8. If we remove a whole neighborhood B^3 of the point at infinity and focus on the remaining 3-ball D^3 , the line l of the previous picture is truncated to the arc L and the solid cylinder V_2 is truncated to the ‘cork’ of D^3 .

Remark 9. This arc L corresponds to the segment L joining the steady state points of the dynamical system of Section 7.

8.2.2 Via surgery

We can also pass from the two-ball description to the two-tori description of S^3 via solid 2-dimensional 0-surgery (with the standard embedding homeomorphism) along the arc L of D^3 , see Fig 23 and 24. As this process requires the notion of embedded surgery, it will be analyzed in Section 9.3.1. It is worth mentioning that this connection between the descriptions of S^3 and solid 2-dimensional 0-surgery is a dynamic way to visualize the connection established in Section 8.2.1.

8.3 Dynamical systems exhibiting the topology of S^3

In this section, we go back to the 3-dimensional Lotka–Volterra system (Σ) and see how its trajectories relate to the descriptions of S^3 and further present a 4-dimensional Hamiltonian system exhibiting the topology of S^3 .

8.3.1 The 3-dimensional Lotka–Volterra system

We will now pin down how the trajectories of (Σ) presented in Section 7 relate to the topology of S^3 . We start with the spherical nesting of Fig 16 (a) which can be viewed as the 3-ball D^3 shown in Fig. 18 (b) and (b’). Surgery on its central point creates the limit cycle which is the core curve c of V_1 shown in Fig. 18 (c) and (c’). If we extend the

spherical shells of Fig 16 to all of \mathbb{R}^3 and assume that the entire nest resolves to a toroidal nest, then the slow manifold L becomes the infinite line l . In the two-ball description of S^3 , l pierces all spheres, recall Fig. 18 (b'), while in the two-tori description, it is the core curve of V_2 or the 'untouched' limit circle of all tori, recall Fig. 18 (c) and (c').

8.3.2 The pair of linear harmonic oscillators

A toroidal nesting similar to the one exhibited in (Σ) and shown in Fig 16 can be found in the trajectories of the Hamiltonian system of a pair of linear harmonic oscillators, see Fig 20. Given that H is the sum of the energy functions of two harmonic oscillators with frequencies m and n and assuming that H is at least C^1 , $m > 0$ and $n > 0$, the time evolution of this system is given by the following system of four ODE of Hamilton:

$$\left\{ \begin{array}{l} \dot{x}_i(s) = \frac{\partial H}{\partial y_i} \\ \dot{y}_i(s) = -\frac{\partial H}{\partial x_i} \end{array} \right\} \text{ for } i = 1, 2 \quad (1)$$

$$H : \mathbb{R}^4 \rightarrow \mathbb{R}; H(x_1, x_2, y_1, y_2) = \frac{1}{2}m(x_1^2 + y_1^2) + \frac{1}{2}n(x_2^2 + y_2^2); \quad (2)$$

As analyzed in [7], except from H , L is also a conserved quantity or first integral: $L(x_1, x_2, y_1, y_2) = \frac{1}{2}m(x_1^2 + y_1^2) - \frac{1}{2}n(x_2^2 + y_2^2)$.

As the authors further elaborate: 'A constant energy surface $H^{-1}(h)$ of the harmonic oscillators is diffeomorphic to the three-sphere S^3 . Such a constant energy surface is the union of two critical circles $S_{h^+}^1 = \{(x_1, 0, y_1, 0) \in \mathbb{R}^4 \mid \frac{1}{2}m(x_1^2 + y_1^2) = h\}$, and $S_{h^-}^1 = \{(0, x_2, 0, y_2) \in \mathbb{R}^4 \mid \frac{1}{2}n(x_2^2 + y_2^2) = h\}$, and a one-parameter family of tori 'in between' parametrized by the values of the first integral L . This foliation of S^3 is indeed intricate; the two critical circles are linked, and concentric tori enveloping the critical circles fill the rest of S^3 .

In Figure 20, the orbits of the Hamiltonian system of a pair of linear harmonic oscillators with frequencies $m = 1$ and $n = 1$ were computed using matlab software. The system was solved for 1000 trajectories initiated on the unit 3-sphere S^3 . To make sure all of S^3 is covered, the hyperspherical coordinates (ψ, θ, ϕ) were used for $r = 1$, $\psi, \theta \in [0, \pi]$ and $\phi \in [0, 2\pi]$: $(x_1, x_2, x_3, x_4) = (r\cos(\psi), r\sin(\psi)\cos(\theta), r\sin(\psi)\sin(\theta)\cos(\phi), r\sin(\psi)\sin(\theta)\sin(\phi))$

These solutions were projected from S^3 to \mathbb{R}^3 using the stereographic projection which can be thought of as removing the point at infinity and ‘unwrapping’ S^3 into \mathbb{R}^3 . More specifically, vectors $\mathbf{x} = (x_1, x_2, x_3, x_4) \in S^3$ were projected to vectors $\mathbf{u} = (u_1, u_2, u_3) = \frac{1}{1-x_4}(x_1, x_2, x_3) \in \mathbb{R}^3$, which corresponds to a projection from the pole $(0, 0, 0, 1)$.

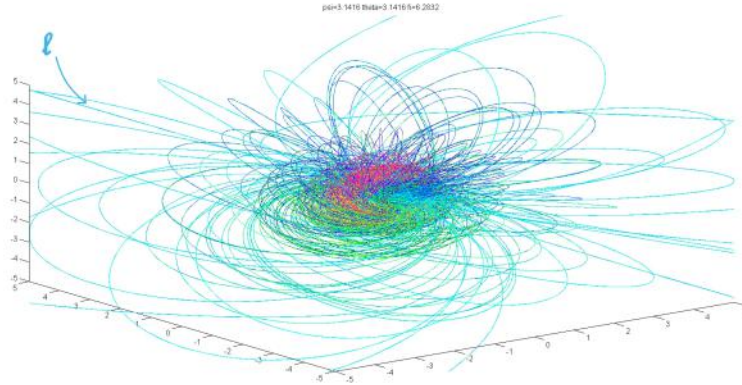


Figure 20. The decompactified view of the orbits of a pair of linear harmonic oscillators.

We will now identify the topology of S^3 in Figure 20. The two critical circle S_{h+}^1 and S_{h-}^1 mentioned above are the core curve c of V_1 and the infinite line l respectively, see Fig. 18 (c) and (c’). While l can be seen in both Figure 18 and Figure 20, the core curve c can only be seen if we visualize the trajectories of Fig. 20 step by step. Indeed, in Fig. 21 (a) we see the core curve c which is quickly covered by the other trajectories. The first three toroidal layers are shown in Fig. 21 (b),(c) and (d). Note that, comparing the trajectories of Fig. 21 with those of (Σ) shown in Fig 16 (b), a key difference is that here,

as opposed to system (Σ) , the nesting of tori does extend to infinity.

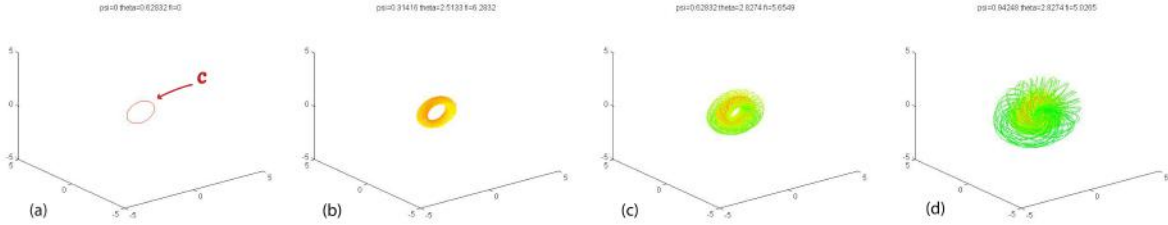


Figure 21. Nesting of orbits of a pair of linear harmonic oscillators.

To close the topological analogy, one can visualize $S^3 = V_1 \cup_{\vartheta} V_2$ by considering that V_1 is any finite number of toroidal nestings. For example V_1 could be any of the tori shown in Fig. 21 (b),(c) or (d) while, in each of these case, V_2 is naturally defined as the complement space.

9 Embedded surgery

In this section we will examine how the ambient space can be involved in the process of surgery and introduce the notion of embedded surgery in order to model such phenomena. As we will see, depending on the dimension of the manifold, the ambient space either leaves ‘room’ for the initial manifold to assume a more complicated configuration or it participates more actively in the process. Independently of dimensions, embedding surgery has the advantage that it allows us to view surgery as a process happening inside a space instead of abstractly. We define it as follows:

Definition 6. *An embedded m -dimensional n -surgery is a m -dimensional n -surgery following the process described in Definition 2 where the initial manifold is an m -embedding $e : M \hookrightarrow S^d$, $d \geq m$ of some m -manifold M , and the result is also viewed as embedded in*

S^d . Namely:

$$M' = \chi(e(M)) = \overline{e(M) \setminus h(S^n \times D^{m-n})} \cup_{h|_{S^n \times S^{m-n-1}}} D^{n+1} \times S^{m-n-1} \hookrightarrow S^d.$$

Since in this analysis we focus on phenomena exhibiting embedded 1- and 2-dimensional surgery in 3-space, from now on we fix $d = 3$ and, for our purposes, we consider S^3 or \mathbb{R}^3 as our standard 3-space.

9.1 Embedded 1-dimensional surgery

In dimension 1, the notion of embedded surgery allows the topological modeling of phenomena with more complicated initial 1-manifolds. Let us demonstrate this with the example of site-specific **DNA recombination**. In this process, the initial manifold is a (circular or linear) DNA molecule. With the help of certain enzymes, site-specific recombination performs a 1-dimensional 0-surgery on the molecule, causing possible knotting or linking of the molecule.

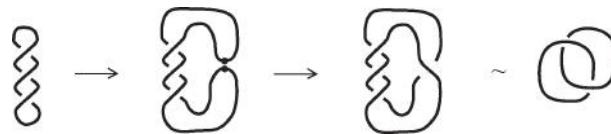


Figure 22. DNA Recombination as an example of embedded 1-dimensional 0-surgery.

The first electron microscope picture of knotted DNA was presented in [34]. In this experimental study, we see how genetically engineered circular DNA molecules can form DNA knots and links through the action of a certain recombination enzyme. A similar picture is presented in Fig. 22, where site-specific recombination of a DNA molecule produces the Hopf link. It is worth mentioning that there are infinitely many knot types

and that 1-dimensional 0-surgery on a knot may change the knot type or even result in a two-component link (as shown in Fig. 22). Since a knot is by definition an embedding of $M = S^1$ in S^3 or \mathbb{R}^3 , in this case embedded 1-dimensional surgery is the so-called *knot surgery*. A good introductory book on knot theory is [1] among many others.

We can summarize the above by stating that for $M = S^1$, embedding in S^3 allows the initial manifold to become any type of knot. More generally, in dimension 1 the ambient space which is of codimension 2 gives enough ‘room’ for the initial 1-manifold to assume a more complicated homeomorphic configuration.

Remark 10. Of course we also have, in theory, the notion of embedded solid 1-dimensional 0-surgery whereby the initial manifold is an embedding of a disc in 3-space.

9.2 Embedded 2-dimensional surgery

Passing now to 2-dimensional surgeries, let us first note that an embedding of a sphere $M = S^2$ in S^3 presents no knotting because knotting requires embeddings of codimension 2. However, in this case the ambient space plays a different role. Namely, embedding 2-dimensional surgeries *allows the complementary space of the initial manifold to participate actively in the process*. Indeed, while some natural phenomena undergoing surgery can be viewed as ‘local’, in the sense that they can be considered independently from the surrounding space, some others are intrinsically related to the surrounding space. This relation can be both *causal*, in the sense that the ambient space is involved in the triggering of the forces causing surgery, and *consequential*, in the sense that the forces causing surgery can have an impact on the ambient space in which they take place.

As mentioned in the introduction of Section 6, in most natural phenomena that exhibit 2-dimensional surgery, the initial manifold is a *solid* 3-dimensional object. Hence, in the next sections, we describe natural phenomena undergoing solid 2-dimensional surgeries

which exhibit the causal or consequential relation to the ambient space mentioned above and are therefore better described by considering them as embedded in S^3 or in \mathbb{R}^3 . In parallel, we describe how these processes are altering the whole space S^3 or \mathbb{R}^3 .

9.3 Modeling phenomena exhibiting embedded solid 2-dimensional surgery

In each of the following sections a natural phenomena undergoing embedding solid 2-dimensional surgery is analyzed. As we will see, the topological considerations of these processes also have physical implications.

9.3.1 A topological model for the density distribution in black hole formation

Let us start by considering the density distribution in **black hole** formation. Most black holes are formed from the remnants of a large star that dies in a supernova explosion. Their gravitational field is so strong that not even light can escape. In the simulation of a black hole formation in [25], the density distribution at the core of a collapsing massive star is shown. Fig. 23 (2) shows three instants of this simulation, which indicate that matter performs solid 2-dimensional 0-surgery as it collapses into a black hole. In fact, matter collapses at the center of attraction of the initial manifold $M = D^3$ creating the singularity, that is, the center of the black hole (shown as a black dot in instance (c) of Fig. 23 (2)), which is surrounded by the toroidal accretion disc (shown in white in instance (c) of Fig. 23 (2)). Let us be reminded here that an accretion disc is a rotating disc of matter formed by accretion.

Note now that the strong gravitational forces have altered the space surrounding the initial star and that the singularity is created outside the final solid torus. This means

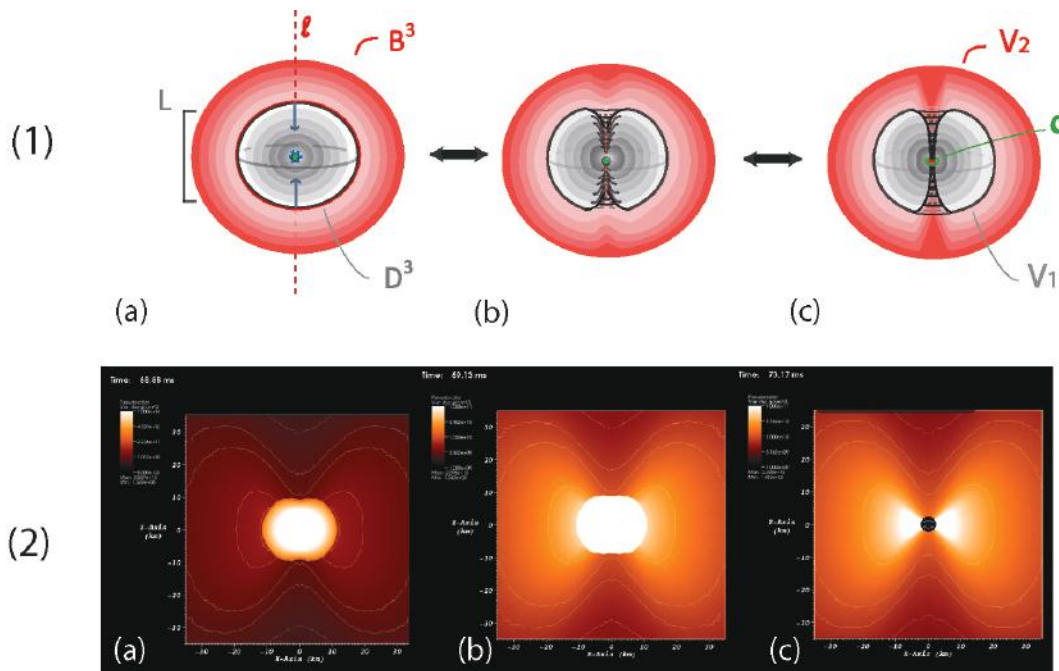


Figure 23. (1) Embedded solid 2-dimensional 0-surgery on $M = D^3$ (in \mathbb{R}^3) (2) Black hole formation

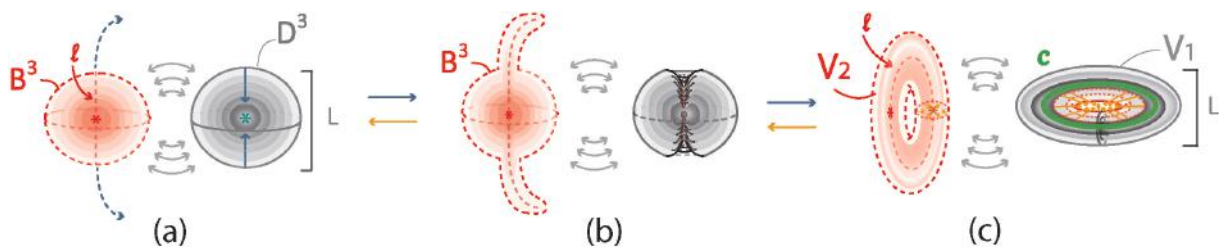


Figure 24. Embedded solid 2-dimensional 0-surgery on $M = D^3$ (in S^3)

that the process of surgery in this phenomenon has moreover altered matter outside the manifold in which it occurs. In other words, *the effect of the forces causing surgery propagates to the complement space, thus causing a more global change in 3-space*. This fact makes black hole formation a phenomenon that topologically undergoes embedded solid 2-dimensional 0-surgery.

In Fig. 23 (1), we present a model of embedded solid 2-dimensional 0-surgery on $M = D^3$.

From the descriptions of S^3 in Section 9.2, it becomes apparent that embedded solid 2-dimensional 0-surgery on one 3-ball describes the passage from the two-ball description to the two-solid tori description of S^3 . This can be seen in \mathbb{R}^3 in instances (a) to (c) of Fig. 23 (1) but is more obvious by looking at instances (a) to (c) of Fig. 24 which show the corresponding view in S^3 .

We will now detail the instances of the process of embedded solid 2-dimensional 0-surgery on $M = D^3$ by referring to both the view in S^3 and the corresponding decompactified view in \mathbb{R}^3 . Let $M = D^3$ be the solid ball having arc L as a diameter and the complement space be the other solid ball B^3 containing the point at infinity; see instances (a) of Fig. 24 and (a) of Fig. 23. Note that, in both cases B^3 represents the hole space outside D^3 which means that the spherical nesting of B^3 in instance Fig. 23 (a) extends to infinity, even though only a subset of B^3 is shown. This joining arc L is seen as part of a simple closed curve l passing by the point at infinity. In instances (b) of Fig. 24 and (b) of Fig. 23, we see the ‘drilling’ along L as a result of the attracting forces. This is exactly the same process as in Fig. 14 (b₁) if we restrict it to D^3 . But since we have embedded the process in S^3 or \mathbb{R}^3 , the complement space B^3 participates in the process and, in fact, it is also undergoing solid 2-dimensional 0-surgery. Indeed, the ‘matter’ that is being drilled out from the interior of D^3 can be viewed as ‘matter’ of the outer sphere B^3 invading D^3 . In instances (c) of Fig. 24 and (c) of Fig. 23, we can see that, as surgery transforms the solid ball D^3 into the solid torus V_1 , B^3 is transformed into V_2 . That is, the nesting of concentric spheres of D^3 (respectively of B^3) is transformed into the nesting of concentric tori in the interior of V_1 (respectively of V_2). The point at the origin (in green), which is also the attracting center, turns into the core curve c of V_1 (in green) which, by Definition 4 is 2-dimensional 0-surgery on a point. As seen in instance (c) of Fig. 24 and (c) of Fig. 23 (1), the result of surgery is the two solid tori V_1 and V_2 forming S^3 .

The described process can be viewed as a double surgery resulting from a single attracting center which is inside the first 3-ball D^3 and outside the second 3-ball B^3 . This attracting center is illustrated (in blue) in instance (a) of Fig. 23 but also in (a) of Fig. 24, where it is shown that the colinear attracting forces causing the double surgery can be viewed as acting on D^3 (the two blue arrows) and also as acting on the complement space B^3 (the two dotted blue arrows), since they are applied on the common boundary of the two 3-balls. Note that in both cases, the attracting center coincides with the limit point of the spherical layers that D^3 is made of, that is, their common center and the center of D^3 (shown in green in (a) of Fig. 23 and (a) of Fig. 24).

The reverse process of embedded solid 2-dimensional 0-surgery on D^3 is an embedded solid 2-dimensional 1-surgery on the solid torus V_2 , see instances of Fig. 24 in reverse order. This process is the embedded analog of the solid 2-dimensional 1-surgery on a solid torus $D^2 \times S^1$ defined in Definition 5 and shown in Fig. 14 (b₁) in reverse order. Here too, the process can be viewed as a double surgery resulting from one attracting center which is outside the first solid torus V_1 and inside the second solid torus V_2 . This attracting center is illustrated (in orange) in instance (c) of Fig. 24 where it is shown that the coplanar forces causing surgery are applied on the common boundary of V_1 and V_2 and can be viewed as attracting forces along a longitude when acting on V_1 and as attracting forces along a meridian when acting on the complement space V_2 .

One can now directly appreciate the correspondence of the physical phenomena (instances (a),(b),(c) of Fig. 23 (2)) with our model (instances (a),(b),(c) of Fig. 23 (1)) . Indeed, if one looks at the density distribution during the formation of a black hole and examines it as an isolated event in space, this process shows a decompactified view of the passage from a two 3-ball description of S^3 , that is, the core of the star and the surrounding space, to a two solid tori description, namely the toroidal accretion disc surrounding the

black hole (shown in white in instance (c) of Fig. 23 (2)) and the surrounding space.

Finally, it is worth pinning down the following spatial duality of embedded solid 2-dimensional 0-surgery for $M = D^3$: the attraction of two points lying on the boundary of segment L by the center of D^3 can be equivalently viewed in the complement space as the repulsion of these points by the center of B^3 (that is, the point at infinity) on the boundary of the segment $l - L$ (or the segments, if viewed in \mathbb{R}^3). Hence, the aforementioned duality tells us that the attracting forces from the attracting center that are collapsing the core of the star can be equivalently viewed as repelling forces from the point at infinity lying in the surrounding space.

9.3.2 A topological model for the formation of tornadoes

Another example of global phenomenon is the formation of **tornadoes**, recall Fig. 10 (2). As mentioned in Section 6 this phenomenon can be modelled by solid 2-dimensional 0-surgery. However, here, the initial manifold is different than D^3 . Indeed, if we consider a 3-ball around a point of the cloud and another 3-ball around a point on the ground, then the initial manifold is $M = D^3 \times S^0$ and the process followed is the one shown in Fig. 14 (b₂) (from right to left). More precisely, if certain meteorological conditions are met, an attracting force between the cloud and the earth beneath is created. This force is shown in blue in see Fig. 25 (1). Then, funnel-shaped clouds start descending toward the ground, see Fig. 25 (2). Once they reach it, they become tornadoes, see Fig. 25 (3). The only difference compared to our model is that here the attracting center is on the ground, see Fig. 25 (1), and only one of the two 3-balls (the 3-ball of cloud) is deformed by the attraction. This lack of symmetry in the process can be obviously explained by the big difference in the density of the materials.

During this process, a solid cylinder $D^2 \times S^1$ containing many layers of air is created.



Figure 25. (1) Attracting force between the cloud and the earth (2) Funnel-shaped clouds (3) Tornado

Each layer of air revolves in a helicoidal motion which is modeled using a twisting embedding as shown in Fig. 10 (1) (for an example of a twisting embedding, the reader is referred Section 3.2). Although all these layers undergo local dynamic 2-dimensional 0-surgeries which are triggered by local forces (shown in blue in Fig. 25 (1)), these local forces are not enough to explain the dynamics of the phenomenon. Indeed, the process is triggered by the difference in the conditions of the lower and upper atmosphere which create an air cycle. *This air cycle lies in the complement space of the initial manifold $M = D^3 \times S^0$ and of the solid cylinder $D^2 \times S^1$, but is also involved in the creation of the funnel-shaped clouds that will join the two initial 3-balls.* Therefore in this phenomenon, surgery is the outcome of global changes and this fact makes tornado formation an example of embedded solid 2-dimensional 0-surgery on $M = D^3 \times S^0$.

It is worth mentioning that the complement space containing the aforementioned air cycle is also undergoing solid 2-dimensional 0-surgery. The process can be seen in \mathbb{R}^3 in instances (a) to (d) of Fig. 26 while the corresponding view in S^3 is shown in instances (a') to (d') of Fig. 26.

More precisely, let us name the two initial 3-balls D_1^3 and D_2^3 , hence $M = D^3 \times S^0 = D_1^3 \amalg D_2^3$. Further, let B^3 be the complement of D_1^3 in S^3 . This setup is shown in (a')

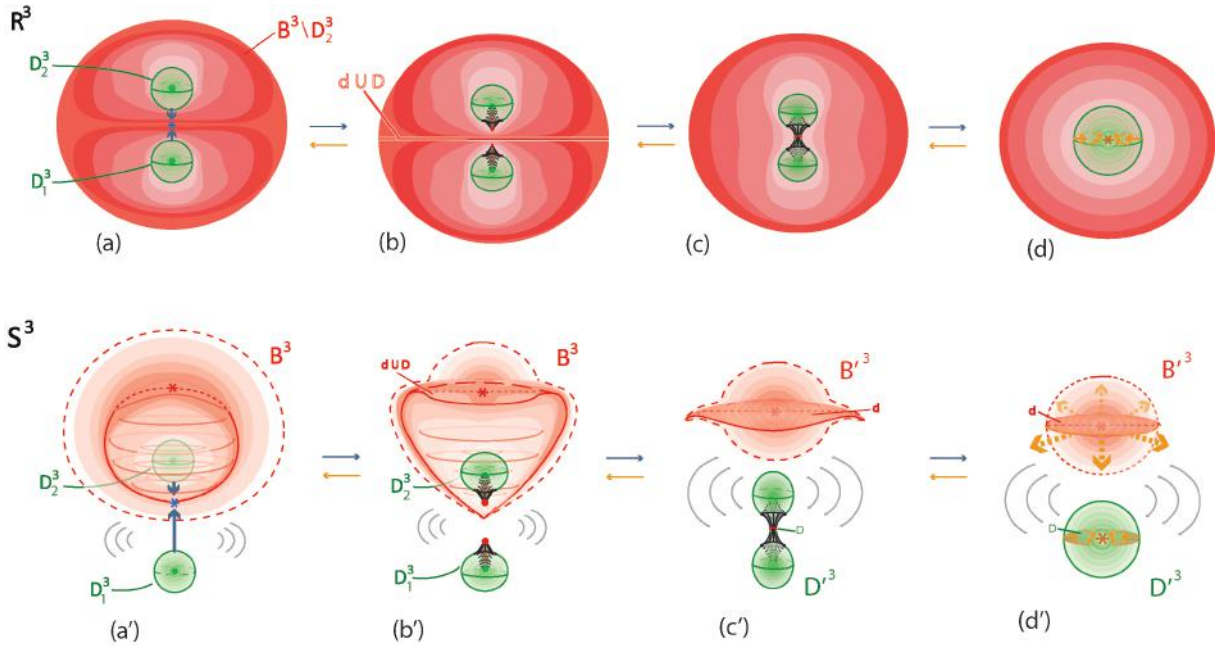


Figure 26. Embedded solid 2-dimensional 0-surgery on $D_1^3 \amalg D_2^3$ (from left to right) and embedded solid 2-dimensional 1-surgery on D'^3 (from right to left)

of Fig. 26 where S^3 is viewed as the union of the two 3-balls $D_1^3 \cup B^3$, and here too, B^3 represents everything outside D_1^3 . The complement space of the initial manifold, $S^3 \setminus M = B^3 \setminus D_2^3$, is the 3-ball B^3 where D_2^3 has been removed from its interior and its boundary consists in two spheres $S^2 \times S^0$, one bounding B^3 or, equivalently, D_1^3 (the outside sphere) and one bounding D_2^3 (the inside sphere). Next, D_1^3 and D_2^3 approach each other, see Fig. 26 (b'). In (c') of Fig. 26, D_1^3 and D_2^3 merge and become the new 3-ball D'^3 , see Fig. 26 (c') or Fig. 26 (d') for a homeomorphic representation.

At the moment of merging, the spherical boundary of D_2^3 punctures the boundary of B^3 ; see the passage from (b') to (c') of Fig. 26. As a result, the complement space is transformed from $B^3 \setminus D_2^3$ to the new deformed 3-ball B'^3 , see Fig. 26 (c') or Fig. 26 (d') for a homeomorphic representation. Note that, although the complement space undergoes a type of surgery that is different from the ones defined in Section 6 and shown in Fig. 14,

it can still be defined analogously. In short, we have a double solid 2-dimensional 0-surgery which turns $M = D_1^3 \amalg D_2^3$ into D'^3 and the complement space $S^3 \setminus (D_1^3 \amalg D_2^3)$ into B'^3 . This process is initiated by the attracting center shown (in blue) in Fig. 26 (a'). The created colinear forces can be viewed as acting on $D_1^3 \amalg D_2^3$ or, equivalently, as acting on the complement space $S^3 \setminus (D_1^3 \amalg D_2^3)$ (see the two blue arrows for both cases).

Going back to the formation of tornadoes, the above process describes what happens to the complement space and provides a topological description of the behavior of the air cycle during the formation of tornadoes. The complement space $B^3 \setminus D_2^3$ in \mathbb{R}^3 is shown in red in Fig. 26 (a) and its behavior during the process can be seen in instances (b) to (d) of Fig. 26. Note that in Fig. 26 (a), $B^3 \setminus D_2^3$ represents the hole space outside D_1^3 , which means that the red layers of Fig. 26 (a) extend to infinity and only a subset is shown.

9.3.3 Embedded solid 2-dimensional 1-surgery on $M = D^3$

We will now discuss the process of *embedded solid 2-dimensional 1-surgery* in S^3 . Taking $M = D^3$ as the initial manifold, embedded solid 2-dimensional 1-surgery is the reverse process of embedded solid 2-dimensional 0-surgery on $D^3 \times S^0$ and is illustrated in Fig. 26 from right to left. The process is initiated by the attracting center shown (in orange) in (d') of Fig. 26. The created coplanar attracting forces are applied on the circle which is the common boundary of the meridian of D'^3 and the meridian of B'^3 and they can be viewed as acting on the meridional disc D of the 3-ball D'^3 (see orange arrows) or, equivalently, in the complement space, on the meridional disc d of B'^3 (see dotted orange arrows). As a result of these forces, in Fig. 26 (c'), we see that while disc D of D'^3 is getting squeezed, disc d of B'^3 is enlarged. In Fig. 26 (b'), the central disc d of B'^3 engulfs disc D and becomes $d \cup D$, which is a separating plane in \mathbb{R}^3 , see Fig. 26 (b). At this point the initial 3-ball D^3 is split in two new 3-balls D_1^3 and D_2^3 ; see Fig. 26 (b') or Fig. 26

(a') for a homeomorphic representation. The center point of D^3 (which coincides with the orange attracting center) evolves into the two centers of D_1^3 and D_2^3 (in green) which by Definition 4, is 2-dimensional 1-surgery on a point. This is exactly the same process as in Fig. 14 (b₂) if we restrict it to D^3 , but since we are in S^3 , the complement space B^3 is also undergoing, by symmetry, solid 2-dimensional 1-surgery.

All natural phenomena undergoing embedded solid 2-dimensional 1-surgery take place in the ambient 3-space. The converse, however, is not true. For example, the phenomena exhibiting 2-dimensional 1-surgery discussed in Section 5.3 are all embedded in 3-space, but they do not exhibit the intrinsic properties of embedded 2-dimensional surgery, since they do not demonstrate the causal or consequential effects discussed in Section 9.2 involving the ambient space. Yet one could, for example, imagine taking a solid material specimen, stress it until necking occurs and then immerse it in some liquid until its pressure causes fracture to the specimen. In this case the complement space is the liquid and it triggers the process of surgery. Therefore, this is an example of embedded solid 2-dimensional 1-surgery where surgery is the outcome of global changes.

Remark 11. Note that the spatial duality described in embedded solid 2-dimensional 0-surgery, in Section 9.3.2, is also present in embedded solid 2-dimensional 1-surgery. Namely, the attracting forces from the circular boundary of the central disc D to the center of D^3 shown in (d') of Fig. 26, can be equivalently viewed in the complement space as repelling forces from the center of B^3 (that is, the point at infinity) to the boundary of the central disc d , which coincides with the boundary of D .

Remark 12. One can sum up the processes described in this section as follows. The process of embedded solid 2-dimensional 0-surgery on D^3 consists in taking a solid cylinder such that the part $S^0 \times D^2$ of its boundary lies in the boundary of D^3 , removing it from D^3 and adding it to B^3 . Similarly, the reverse process of embedded solid 2-dimensional

1-surgery on V_2 consists of taking a solid cylinder such that the part $S^1 \times D^1$ of its boundary lies in the boundary of V_2 , removing it from V_2 and adding it to V_1 . Following the same pattern, embedded solid 2-dimensional 1-surgery on $M = D^3$ consists of taking a solid cylinder in D^3 such that the part $S^1 \times D^1$ of its boundary lies in the boundary of D^3 , removing it from D^3 and adding it to B^3 . Similarly, the reverse process of embedded solid 2-dimensional 0-surgery on $S^3 \setminus (D_1^3 \amalg D_2^3)$ consists of taking a solid cylinder such that the two parts $S^0 \times D^2 = D_1^2 \amalg D_2^2$ of its boundary lie in the corresponding two parts of the boundary of $S^3 \setminus (D_1^3 \amalg D_2^3)$, removing it from $S^3 \setminus (D_1^3 \amalg D_2^3)$ and adding it to $D_1^3 \amalg D_2^3$. Note that, for clarity, in the above descriptions the attracting centers causing surgery are always inside the initial manifold. Of course a similar description starting with the complement space as an initial manifold and the attracting center outside of it would also have been correct.

10 3-dimensional surgery

In this section we present a novel way of visualizing 3-dimensional surgery as well as a phenomenon exhibiting it. In Section 10.1, we introduce the notion of decompactified 2-dimensional surgery which allows us to visualize the process of 2-dimensional surgery in \mathbb{R}^2 instead of \mathbb{R}^3 . Using this new notion and rotation, in Section 10.2, we present a way to visualize the 4-dimensional process of 3-dimensional surgery in \mathbb{R}^3 . In Section 10.3, we analyze the concept of continuity introduced in Section 4 in the case of 3-dimensional surgery by looking at the local process inside the 4-dimensional handle. Finally, in Section 10.4, we model a phenomenon exhibiting 3-dimensional surgery: the formation of black holes from cosmic strings.

10.1 Decompactified 2-dimensional surgery

We present here the notion of *decompactified 2-dimensional surgery* which allows us to visualize 2-dimensional surgery in \mathbb{R}^2 instead of \mathbb{R}^3 .

Let us first recall from Section 4 that an m -dimensional n -surgery happens inside the handle $D^{n+1} \times D^{m-n}$. In Fig. 27, the cases of dimensions 1 and 2 are shown in the first two rows where m -dimensional n -surgeries are symbolized with $[m-n]$. For example, in 2-dimensional 0-surgery, see Fig. 27 [2-0], a homeomorphic representation of S^2 is formed by gluing the two discs $S^0 \times D^2$ to the cylinder $D^1 \times S^1$. The whole time evolution of 2-dimensional 0-surgery is a way of passing from $S^0 \times D^2$ to $D^1 \times S^1$ and the frames of this evolution are included in $D^1 \times D^2$.

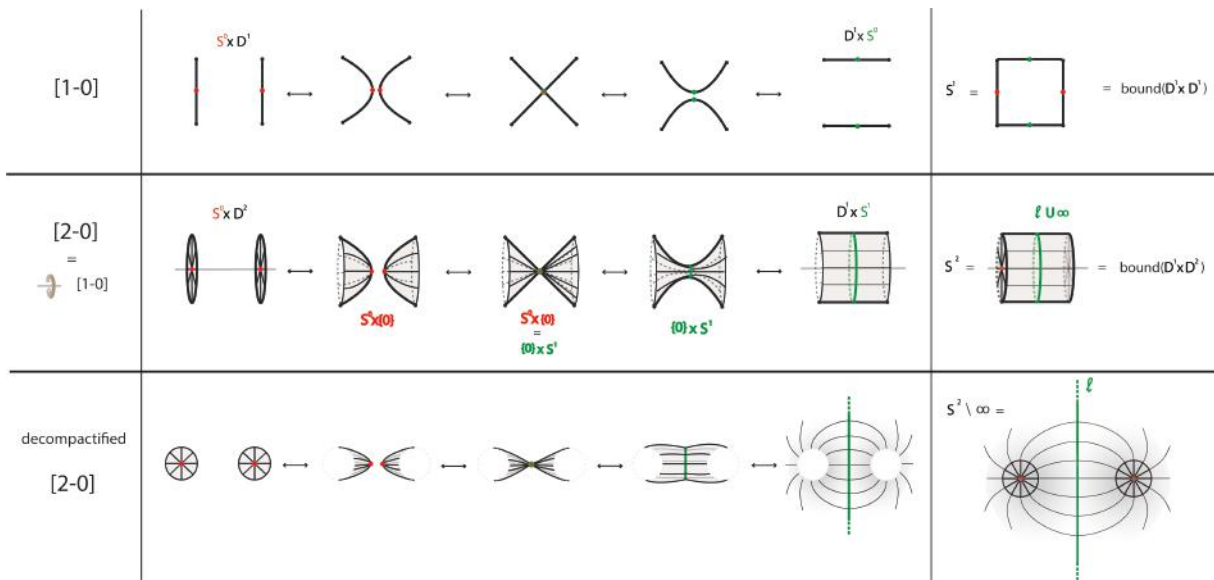


Figure 27. From top to bottom row: 1-dimensional 0-surgery, 2-dimensional 0-surgery, decompactified 2-dimensional 0-surgery.

Let us now point out that one can obtain all instances of 2-dimensional 0-surgery by rotating Fig. 27 [1-0] by 180° around a horizontal axis, see Fig. 27 [2-0]. Note that this observation is just the generalization of Remark 1, including now the intermediate instances

of surgery. From this observation it follows that 1-dimensional 0-surgery is a cross-section of 2-dimensional 0-surgery and that 2-dimensional 0-surgery can be obtained as a union of 1-dimensional 0-surgeries. While not shown here, it is also worth pointing out that, by symmetry, the instances of 2-dimensional 1-surgery can also be obtained by rotating the instances of 1-dimensional 0-surgery by 180° around a vertical axis, perpendicular to the one shown in Fig. 27 [2-0].

In analogy, for $m = 3$, 3-dimensional surgery can be viewed as a way of passing from one boundary component of $D^{n+1} \times D^{3-n} \cong D^4$ to its complement, recall Section 4 for $m = 3$. Hence, the initial and final instances of the process form $S^3 = \partial D^4$, which is a 180° rotation of the S^2 that is made of the initial and final instances of 2-dimensional surgery. To grasp this last observation, recall that S^1 is obtained by a 180° rotation of S^0 and S^2 is obtained by a 180° rotation of S^1 . Moving up one dimension, since S^2 is embedded in \mathbb{R}^3 , the S^3 created by rotation requires a fourth dimension in order to be visualized.

In order to overcome this difficulty we project stereographically S^2 in \mathbb{R}^2 , as shown in Fig. 28. Note that the two great circles $l \cup \{\infty\}$ and $l' \cup \{\infty\}$ in S^2 are projected to the two perpendicular infinite lines l and l' in \mathbb{R}^2 . With the stereographic projection of S^2 at hand, it is now easy to see that S^3 is obtained as 180° rotation of S^2 . Indeed, rotating $\mathbb{R}^2 = S^2 \setminus \{\infty\}$ in Fig. 28 around axis l by 180° we obtain $\mathbb{R}^3 = S^3 \setminus \{\infty\}$. We can now introduce the notion of decompactified 2-dimensional 0-surgery which is depicted in Fig. 27 decompactified [2-0]:

Definition 7. The process of *decompactified 2-dimensional 0-surgery* is completely analogous to 2-dimensional 0-surgery except that it is projected in \mathbb{R}^2 . It starts with two flattened discs which approach each other. The centers of the two discs touch and the discs merge into one. The resulting disc is a thickened segment $D^1 \times D^1$ which grows to infinity filling the complement space $\mathbb{R}^2 \setminus (S^0 \times D^2)$. The final thickened line $D^1 \times l$

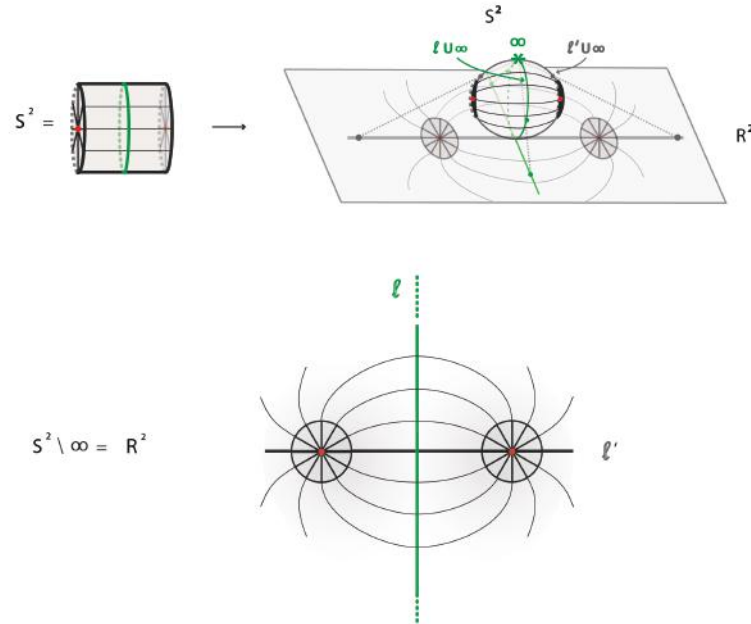


Figure 28. Stereographic projection of S^2 in \mathbb{R}^2 .

corresponds to the decompactification of the thickened circle $D^1 \times S^1 = D^1 \times (l \cup \{\infty\})$. The cores of both the thickened line and the circle are shown in green in Fig. 27 [2-0] and Fig. 27 decompactified [2-0].

Note that, in analogy to 2-dimensional 0-surgery, decompactified 2-dimensional 0-surgery can also be seen as a process caused by attracting forces and an attracting center. The forces are not shown here in order to keep the figures lighter.

In Section 10.2 we will rotate the instances of decompactified 2-dimensional 0-surgery in order to obtain our first visualization of 3-dimensional surgery in \mathbb{R}^3 .

Remark 13. The decompactified 2-dimensional 1-surgery can also be defined in analogy to the decompactified 2-dimensional 0-surgery but it is simpler to view it as its reverse process.

10.2 Visualizing 3-dimensional surgery in \mathbb{R}^3

As mentioned in Section 10.1, rotating the S^2 made of the initial and final instances of 2-dimensional surgery gives us the $S^3 = \partial D^4$ made of the initial and final instances of 3-dimensional surgery. We will now rotate the stereographic projection of S^2 in \mathbb{R}^2 , see Fig. 28, to obtain the stereographic projection of the initial and final instances of 3-dimensional surgery in \mathbb{R}^3 . We will discuss the two processes of 3-dimensional surgery, namely 3-dimensional 1-surgery and 3-dimensional 0-surgery, which were introduced in Section 3.4. Each of these processes corresponds to a different rotation, which results in a different visualization of the initial and the final stage of 3-dimensional surgery in \mathbb{R}^3 and which, in turn, corresponds to a different decomposition of S^3 . These two decompositions are presented in Section 10.2.1. Then, using these visualizations of the initial and final instances, we will visualize the intermediate steps of both processes in Section 10.2.2.

10.2.1 Initial and final steps

Let us recall the initial and final instances of our two processes of 3-dimensional surgery. For 3-dimensional 1-surgery, the initial and final instances are solid tori $S^1 \times D^2$ and $D^2 \times S^1$ while for 3-dimensional 0-surgery, we have two 3-balls $S^0 \times D^3$ and a thickened sphere $D^1 \times S^2$.

Rotating our decompactified view in \mathbb{R}^2 by 180° *vertically* gives us the initial and final instances of 3-dimensional 1-surgery in \mathbb{R}^3 . In this case the axis of rotation is line l which is at equal distance from the two flattened discs and is shown in green in Fig. 29 (a). We can directly see that this rotation transforms the two discs $S^0 \times D^2$ (the first instance of decompactified 2-dimensional 0-surgery) to the solid torus $S_1^1 \times D^2$ (the first instance of 3-dimensional 1-surgery), see Fig. 29 (b). Each of the arcs connecting the two discs $S^0 \times D^2$ generates through the rotation a 2-dimensional disc, the set of all such discs being

parametrized by the points of the line l in \mathbb{R}^3 . Therefore the complement of the solid torus $S_1^1 \times D^2$ is another solid torus $D^2 \times S_2^1$, see Fig. 29 (b), where line l in \mathbb{R}^3 is circle $S_2^1 = l \cup \{\infty\}$ in S^3 .

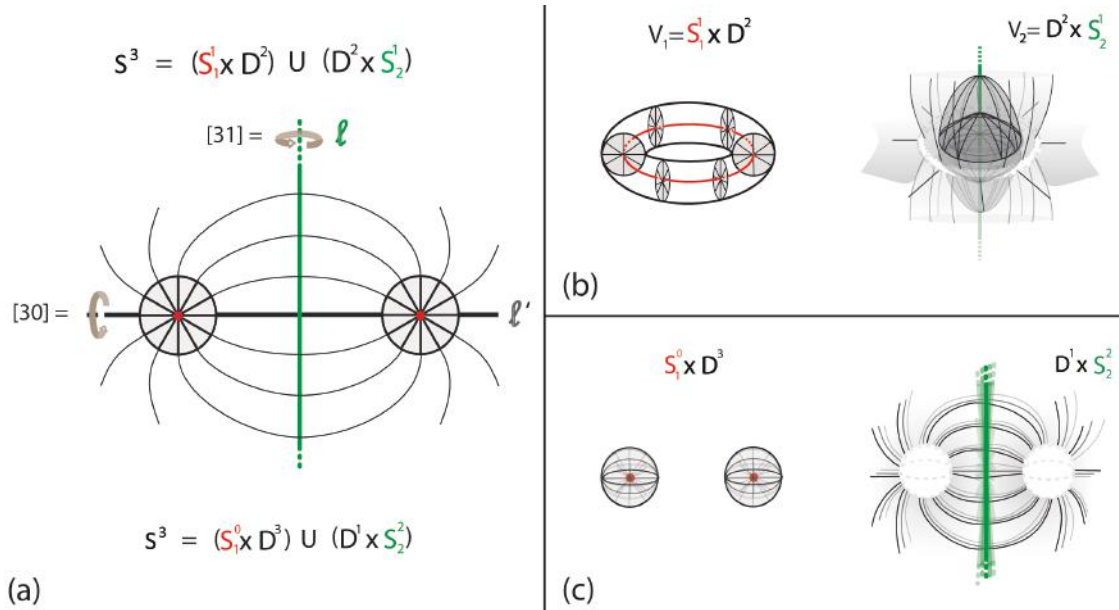


Figure 29. (a) Representations of S^3 in \mathbb{R}^3 (b) Initial and final instance of 3-dimensional 1-surgery (c) Initial and final instance of 3-dimensional 0-surgery

Note that the visualization of Fig. 29 (b) is the same as the one presented in Fig. 18 (c),(c') of Section 8 where $S^3 = V_1 \cup V_2$. Here $V_1 = S_1^1 \times D^2$ and $V_2 = D^2 \times S_2^1$, the core curve c of V_1 is S_1^1 and the core curve $l \cup \{\infty\}$ of V_2 is S_2^1 .

Similarly, rotating our decompactified view in \mathbb{R}^2 by 180° *horizontally* gives us the initial and final instances of 3-dimensional 0-surgery in \mathbb{R}^3 . The axis of rotation is line l' which pierces the two flattened discs and is shown in grey in Fig. 29 (a). We can directly see that this rotation transforms the two discs $S^0 \times D^2$ (the first instance of decompactified 2-dimensional 0-surgery) to two 3-balls $S_1^0 \times D^3$ (the first instance of 3-dimensional 0-surgery), see Fig. 29 (c). The rotation of line l along l' creates a plane that

cuts through \mathbb{R}^3 and separates the two resulting 3-balls $S_1^0 \times D^3$. This plane is thickened by the arcs connecting the two discs $S^0 \times D^2$ which have also rotated, see Fig. 29 (c). This plane is the decompactified view of sphere S_2^2 in S^3 which can be viewed as a rotation of circle $l \cup \{\infty\} = S_2^1$. Therefore the complement of the two 3-balls $S_1^0 \times D^3$ is a thickened sphere $D^1 \times S_2^2$ where the plane resulting from the rotation of line l in \mathbb{R}^3 is sphere S_2^2 in S^3 .

In both cases, in Fig. 29 (a), S^3 is represented as the result of rotating the 2 sphere $S^2 = \mathbb{R}^2 \cup \{\infty\}$. For 3-dimensional 1-surgery, S^2 is rotated about the circle $l \cup \{\infty\}$ where l is a straight horizontal line in \mathbb{R}^2 , see also Fig. 28. The resulting decomposition is $S^3 = (S_1^1 \times D^2) \cup (D^2 \times S_2^1)$. For 3-dimensional 0-surgery, S^2 is rotated about the circle $l' \cup \{\infty\}$ where l' is a straight vertical line in \mathbb{R}^2 , see also Fig. 28. The resulting decomposition is $S^3 = (S_1^0 \times D^3) \cup (D^1 \times S_2^2)$.

10.2.2 Intermediate steps

We are now ready to visualize the intermediate steps of both types of 3-dimensional surgery. By rotating the instances of decompactified 2-dimensional 0-surgery (shown in Fig. 27 decompactified [2-0]) around the axes l and l' (shown in Fig. 29 (a)) we obtain the instances of 3-dimensional 1-surgery and 3-dimensional 0-surgery respectively, see Fig. 30.

In these two processes, as in lower dimensional surgeries, the time-evolution of surgery passes through a singular point. Namely, for 3-dimensional 1-surgery we see a solid torus $S_1^1 \times D^2$ collapsing to a singularity from which emerges the complement solid torus $D^2 \times S_2^1$. This, if visualized in \mathbb{R}^3 , fills the rest of the space, see Fig. 30 (a). In this case we have used the standard (identity) embedding of $S_1^1 \times D^2$ denoted by h_s , which induces a ‘gluing’ homeomorphism along the common boundary $S^1 \times S^1$, such that the meridians of solid torus $V_1 = S_1^1 \times D^2$ are mapped to the longitudes of solid torus $V_2 = D^2 \times S_2^1$. In other

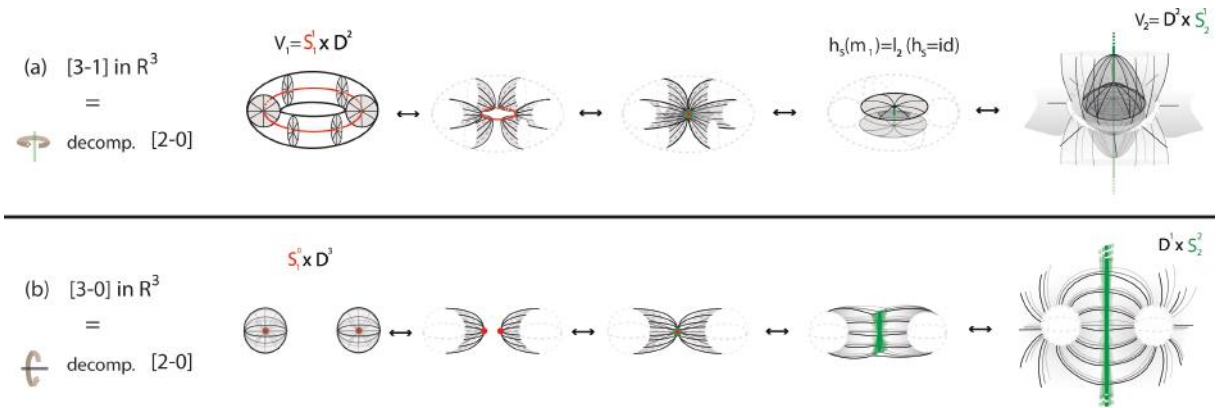


Figure 30. (a) 3-dimensional 1-surgery in \mathbb{R}^3 (b) 3-dimensional 0-surgery in \mathbb{R}^3

words, $h_s(m_1) = l_2$.

For 3-dimensional 0-surgery, we see the two 3-balls $S_1^0 \times D^3$ collapsing to a singularity from which emerges the thickened sphere $D^1 \times S_2^2$ which, if decompactified in \mathbb{R}^3 , is a thickened plane filling the rest of the space, see Fig. 30 (b).

10.3 The continuity of 3-dimensional surgery

In this section we analyze the concept of continuity for 3-dimensional surgery.

Let us first recall from Section 4 that all types of 3-dimensional surgery take place inside the 4-dimensional handle $D^{n+1} \times D^{3-n}$, $n < 3$ and that the processes of both 3-dimensional 0- and 1-surgery can be viewed as taking the boundary of the first factor D^{n+1} , thickening it, passing through the unique intersection point $D^{n+1} \cap D^{3-n}$ and then letting the thickened boundary of the second factor D^{3-n} emerge. We will first present the core view which shows how we pass from the boundary of D^{n+1} to the boundary of D^{3-n} . We will then apply the different kinds of thickenings (or framings) to the cores in order to illustrate both processes in \mathbb{R}^4 .

More precisely, 3-dimensional 1-surgery takes place inside $D_1^2 \times D_2^2$. In this case, we go

from the core $S_1^1 = \partial D_1^2$ to the core $S_2^1 = \partial D_2^2$ by passing through the unique intersection $D_1^2 \cap D_2^2$. As mentioned in Section 2.4, we consider that n -balls are centered at the origin. Hence if $D_1^2 = \{(x, y, 0, 0) : x^2 + y^2 \leq 1\}$ and $D_2^2 = \{(0, 0, z, w) : z^2 + w^2 \leq 1\}$ then $D_1^2 \cap D_2^2 = (0, 0, 0, 0)$. This process can be represented by looking at the (x, y) axes until core $S_1^1 = \partial D_1^2$ collapses to the singular point $(0, 0, 0, 0)$ and then switching to the (z, w) axes as core $S_2^1 = \partial D_2^2$ uncollapses. This is shown in Fig. 31 (a₁). We will refer to this process as the *core view of 3-dimensional 1-surgery* which will be denoted by ‘core [3-1]’.

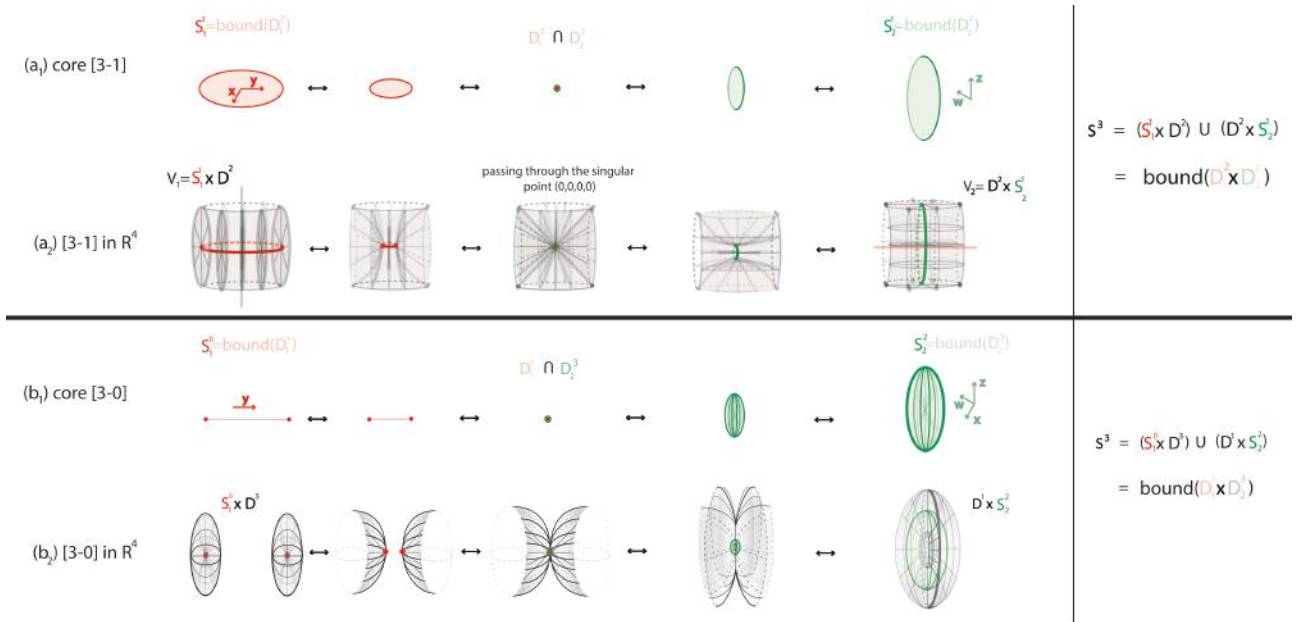


Figure 31. (a₁) Core view of [3-1] surgery (a₂) [3-1] surgery in \mathbb{R}^4 (b₁) Core view of [3-0]-surgery (b₂) [3-0] surgery in \mathbb{R}^4

On the other hand, 3-dimensional 0-surgery takes place inside $D_1^1 \times D_2^3$. In that case, we go from the core $S_1^0 = \partial D_1^1$ to the core $S_2^3 = \partial D_2^3$ by passing through the unique intersection $D_1^1 \cap D_2^3$. Hence, if $D_1^1 = \{(0, y, 0, 0) : y \in [-1, 1]\}$ and $D_2^3 = \{(x, 0, z, w) : x^2 + z^2 + w^2 \leq 1\}$, then $D_1^1 \cap D_2^3 = (0, 0, 0, 0)$. This process can be seen by looking at the y axis until core $S_1^0 = \partial D_1^1$ collapses to the singular point $(0, 0, 0, 0)$ and then, switching to the x, z, w axes,

as core $S_2^2 = \partial D_2^3$ uncollapses. This is shown in Fig. 31 (b₁). We will refer to this process as the *core view of 3-dimensional 0-surgery* which will be denoted by ‘core [3-0]’.

We will now thicken the aforementioned cores in order to present our illustrations in \mathbb{R}^4 . Let us recall that, so far, in Sections 10.2.1 and 10.2.2, the final instances of both 3-dimensional 0-surgery and 1-surgery were distorted due to decompactification. More precisely, in Fig. 29 and 30, both the solid torus $D^2 \times S_2^1$ and the thickened sphere $D^1 \times S_2^2$ were filling the rest of the space in \mathbb{R}^3 . Our goal here is to obtain the corresponding undistorted illustrations in \mathbb{R}^4 .

For 3-dimensional 1-surgery, we start by thickening our core view S_1^1 shown in Fig. 31 (a₁) with a D^2 . We collapse $S_1^1 \times D^2$ to a singularity and then need to uncollapse it in a way that produces the complement solid torus $D^2 \times S_2^1$ as a thickening of its core S_2^1 . The whole process is shown in Fig. 31 (a₂).

For 3-dimensional 0-surgery, we start by thickening our core view S_1^0 shown in Fig. 31 (b₁) with a D^3 . We collapse $S_1^0 \times D^3$ to a singularity and then we need to uncollapse it in a way that produces the $D^1 \times S_2^2$ as a thickening of its core sphere S_2^2 . The whole process is shown in Fig. 31 (b₂).

In both cases, we have combined the core with the \mathbb{R}^4 view and added the corresponding decomposition of S^3 in the end. We have used color coding in order to clarify how the notions presented in Sections 10.1,10.2 and 10.3 interplay. To complete the picture, it is worth adding that the visualizations of Fig. 30 (a) and (b) are the decompactified versions of Fig. 31 (a₂) and (b₂) respectively. In both cases the instances up to the singularity are identical while the uncollapsing is done in \mathbb{R}^3 and \mathbb{R}^4 respectively.

Remark 14. It is worth adding that the two last instances $D^2 \times S_2^1$ and $D^1 \times S_2^2$ of 3-dimensional 0- and 1-surgery in \mathbb{R}^4 shown in Fig. 31 (a₂) and (b₂) can be also obtained as different rotations of the final instance $D^1 \times S^1$ of 2-dimensional 0-surgery surgery

shown in Fig. 27 [2-0]. Indeed, starting with cylinder $D^1 \times S^1$, we first decompactify S^1 to \mathbb{R}^1 to obtain $D^1 \times \mathbb{R}^1$, see Fig. 32 (a). Then, using the same rotational axis as the one described in Section 10.2.1 and shown in green in Fig. 32 (a), we obtain the decompactified $D^2 \times \mathbb{R}^1$, where each segment D^1 has been rotated to a disc D^2 . We finally recompactify \mathbb{R}^1 to S^1 to obtain $D^2 \times S^1$. Note that the axis starts as a circle, becomes straight during decompactification and becomes a circle again when we recompactify.

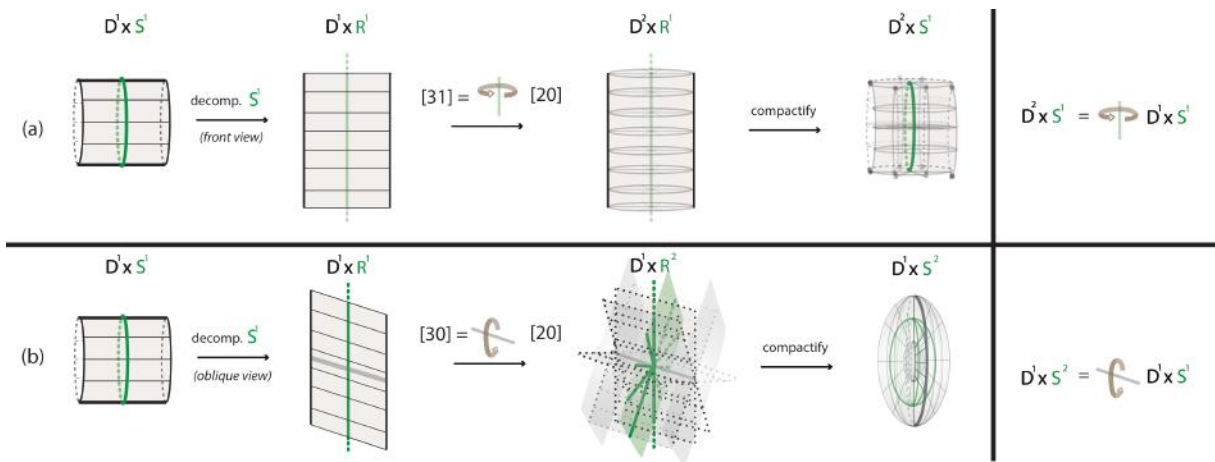


Figure 32. (a) $D^2 \times S^1$ as a rotation of $D^1 \times S^1$ (b) $D^1 \times S^2$ as a rotation of $D^1 \times S^1$

Similarly, starting again with the $D^1 \times S^1$ of 2-dimensional 0-surgery, we first decompactify S^1 to \mathbb{R}^1 to obtain $D^1 \times \mathbb{R}^1$, see Fig. 32 (b). Then, using the same rotational axis as the one described in Section 10.2.1 and shown in grey Fig. 32 (b), we obtain the decompactified $D^1 \times \mathbb{R}^2$ where each line \mathbb{R}^1 has been rotated to a plane \mathbb{R}^2 . In Fig. 32 (b), we have used an oblique view of both $D^1 \times \mathbb{R}^1$ and $D^1 \times \mathbb{R}^2$ so the effect of the rotation can be visible. We finally compactify \mathbb{R}^2 to S^2 to obtain the thickened sphere (or hollow 3-ball) $D^1 \times S^2$.

This process of decompactifying, rotating and compactifying again allowed us to visualize the final instances of 3-dimensional 1- and 0-surgery in relation with our initial

visualization of $D^1 \times S^1$ of 2-dimensional 0-surgery by following a reasoning similar to the one used in Section 10.2 for the visualizations in \mathbb{R}^3 . The difference being that in the visualizations of Section 10.2, $D^1 \times S^1$ was obtained as part of the decompactification of S^2 , hence it was inevitably deformed so that its union with $S^0 \times D^2$ would form \mathbb{R}^2 . As this constrain does not exist here, when S^1 is decompactified to \mathbb{R}^1 , its framing D^1 follows without undergoing such deformation, see the passage from the first to the second instance in Fig. 32 (a) and (b).

10.4 Modeling black hole formation from cosmic strings

In this section we will see how the formation of black holes from cosmic strings can be modeled by 3-dimensional 1-surgery.

10.4.1 Terminology

We will first explain the terms of *Schwarzschild radius*, *event horizon* and *gravitational singularity* which will be used in the following sections.

The Schwarzschild radius is the radius of a 2-sphere such that, if all the mass of an object were to be compressed within that sphere, the escape velocity from the surface of the sphere would equal the speed of light. If anything collapses to or below this radius, a black hole is formed. The event horizon is a boundary in spacetime beyond which events cannot affect an outside observer and is most commonly associated with black holes. For a nonrotating black hole, the Schwarzschild radius delimits a spherical event horizon.

In the center of a black hole, general relativity predicts the existence of a gravitational singularity (or space-time singularity), i.e a region in space in which matter takes infinite density and 0 volume (basically infinitely dense and infinitely small). The singularity cannot be seen as it is covered by the event horizon.

10.4.2 Black holes from cosmic strings

Cosmic strings are hypothetical 1-dimensional topological defects which may have formed in the early universe and are predicted by both quantum field theory and string theory models. Their existence was first contemplated by Tom Kibble in the 1970s. In [9], S.W. Hawking estimates that a fraction of cosmic string loops can collapse to a small size inside their Schwarzschild radius thus forming a black hole. As he mentions, under certain conditions, ‘one would expect an event horizon to form, and the loop to disappear into a black hole’.

Note that other estimations of the fraction of cosmic string loops which collapse to form black holes have been made in subsequent work, see [4] and [22]. While the details of the different estimations have no direct implications on this analysis, it is worth mentioning the following two statements. In [4], R.R. Caldwell and P.Casper point out that the loop ‘collapses in all three directions’ and in [22], J.H. MacGibbon, R.H. Brandenberger and U.F. Wichosk give the following example for a collapsing symmetric string loop: ‘For example, a planar circular string loop after a quarter period will collapse to a point and hence form a black hole.’

Topologically, the aforementioned loop can be considered to be a solid torus $S^1 \times D^2$ embedded in an initial manifold M . The thickening D^2 can be considered to be very small, as the diameter of a cosmic strings is of the same order of magnitude as that of a proton, i.e. ≈ 1 fm or smaller. Further, we consider M as being the 3-space S^3 or \mathbb{R}^3 or a 3-manifold corresponding to the 3-dimensional spatial section of the 4-dimensional space-time of the universe. The loop $S^1 \times D^2$ collapses to a small size inside its Schwarzschild radius thus creating a black hole the center of which contains the singularity. In this scenario, the initial 3-space M becomes a singular manifold at that point.

Physicists are undecided whether the prediction of this singularity means that it

actually exists or that current knowledge is insufficient to describe what happens at such extreme density. As we will see in the next section, we can avoid this singularity by considering that the collapsing of a cosmic string loop is followed by the uncollapsing of another cosmic string loop. In other words, we propose that the creation of a black hole is a 3-dimensional 1-surgery which changes the initial 3-dimensional space M to another 3-dimensional space $\chi(M)$ by passing through a singular point. As detailed in Section 10.3, the time evolution of this process happens locally inside the handle $D^2 \times D^2$ and requires four spatial dimensions in order to be visualized but each ‘slice’ of the process is a 3-dimensional manifold.

Note that this process is different from the global process of embedded surgery used to model the density distribution of black hole formation in Section 9.3 as it describes the local process of a cosmic string collapsing to a black hole inside the event horizon.

10.4.3 Black holes from 3-dimensional 1-surgery

We will now describe the process of 3-dimensional 1-surgery on M step by step. We start with an embedding of the loop $S^1 \times D^2$, which may also be knotted. Using an analogue which is two dimensions lower, M is shown as a line while the core S^1 of the embedding $S^1 \times D^2$ is shown as the core S^0 of embedding $S^0 \times D^1$. In Fig. 33 (initial), core S^0 is shown in red and its thickening in grey. Since the process of surgery is a local process, black hole formation can be seen independently of M . Therefore we zoom in to see this local procedure in instances (1) to (4) of Fig. 33 which happens inside $D^2 \times D^2$.

As mentioned in Section 5 and throughout this analysis, the local process of surgery is considered as a result of attracting forces. In the 3-dimensional case, we deliberately didn’t show these forces in Fig. 31 in order to keep the illustrations lighter but as explained in Section 5.5, we know that the forces of our model are applied to the core 1-embedding

$e = h|_1 : S^1 = S^1 \times \{0\} \hookrightarrow M$ of the framed n -embedding $h : S^1 \times D^2 \hookrightarrow M$.

These forces are added in blue in Fig. 33 (1), where we see the same process as Fig. 31 (a₂) but with a knotted embedding of the core S^1 . Note that these local forces of our model correspond to the string tension, which collapses the cosmic string (see [9] for details). In instance (2) of Fig. 33 the cosmic string shrinks to a radius smaller than its Schwarzschild radius, thus the event horizon is formed. We are not showing the black hole inside the event horizon as we want to focus on the topological change. Further, instance Fig. 33 (3) shows the loop shrinking to a point in the 3-dimensional space where this point is the singular point mentioned in Section 10.3.

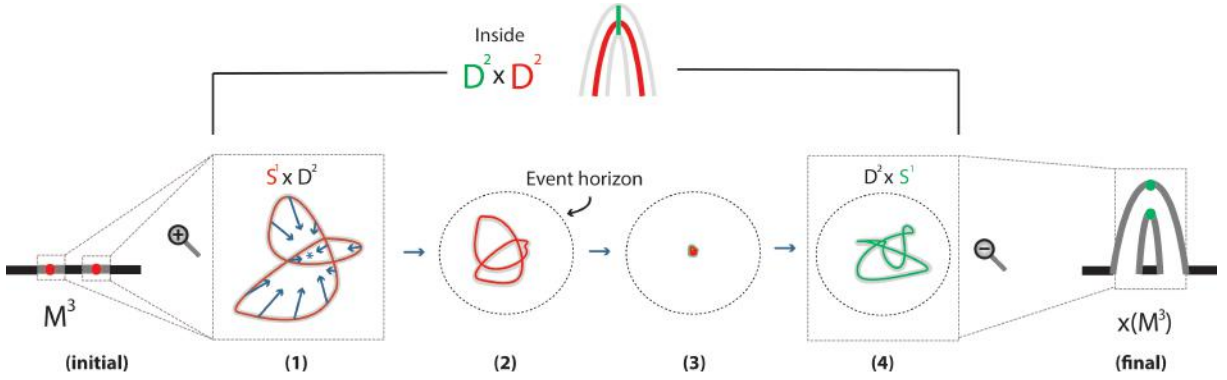


Figure 33. 3-dimensional 1-surgery inside the event horizon

According to our model, after the collapsing the process doesn't stop, but another manifold $D^2 \times S^1$, which corresponds to another cosmic string loop, grows from the singular point of instance Fig. 33 (3), and this is the added value of our model. In Fig. 33 (4) we show the uncollapsing of cosmic string $D^2 \times S^1$ which transforms the initial manifold M to $\chi(M) = \overline{M \setminus h(S^1 \times D^2)} \cup_h (D^2 \times S^1)$, see Fig. 33 (final). Note that instances Fig. 33 (1),(2),(3),(4) are analogous to the instances of Fig. 31 (a₂).

It is worth mentioning that Fig. 33 (final) is also shown two dimensions lower. Namely, as in Fig. 33 (initial), the core S^1 of the cosmic string loop $D^2 \times S^1$ is represented by the

core S^0 of $D^1 \times S^0$. In Fig. 33 (final), core S^0 is shown in green and its thickening in grey. The whole process occurs inside the handle $D^1 \times D^1$ illustrated in the upper part of Fig. 33 which, following this analogy, stands for $D^2 \times D^2$. The global 4-dimensional visualization of 3-dimensional 1-surgery on an initial 3-manifold such as S^3 following the line of thought of Sections 10.2.2 and 10.3 is an intriguing subject and will be the subject of future work. However, for the purpose of this analysis we do not need to visualize the initial and final manifold but rather the idea behind the local process illustrated in instances Fig. 33 (1),(2),(3),(4).

Summarizing the above, modeling the collapsing of a cosmic string loop with a 3-dimensional 1-surgery allows us to go through the singular point of the black hole without having a singular manifold in the end. Instead, we end up in the same universe with a local topology change from the 3-dimensional space M to the 3-dimensional space $\chi(M)$ and, as seen in Fig. 33 (2),(3),(4), this topology change happens within the event horizon.

11 Conclusions

In this thesis we explained many natural processes via topological surgery. Examples comprise chromosomal crossover, magnetic reconnection, mitosis, gene transfer, the creation of Falaco solitons, the formation of tornadoes and the formation of black holes. To do this we first enhanced the usual static description of topological surgery by introducing dynamics, by means of continuity and attracting forces. In order to model more phenomena, we then filled in the interior space by introducing the notion of solid surgery. Further, we introduced the notion of embedded surgery, which leaves room for the initial manifold to assume a more complicated configuration and describes how the complementary space of the initial manifold participates in the process. Thus, instead of considering surgery as

a formal and static process, our new model and definitions can be used to analyze the topological changes occurring in natural phenomena.

Apart from the examples studied in this thesis, there are several other phenomena exhibiting surgery. Our topological model indicates where to look for the forces causing surgery and what deformations should be observed in the local submanifolds involved and these predictions may prove significant for the study of these phenomena. Also, it would be worth applying our modeling of the changes occurring in the complement space during embedded surgery in more natural processes as it provides a ‘global’ explanation of the phenomenon, which can also be of great physical value.

Equally important, all these new notions resulted in pinning down the connection of solid 2-dimensional 0-surgery with a dynamical system. This connection gives us on the one hand a mathematical model for 2-dimensional surgery and, on the other hand, a dynamical system modeling natural phenomena exhibiting 2-dimensional topological surgery through a ‘hole-drilling’ process. The provided dynamical system presents significant common features with solid 2-dimensional 0-surgery, in the sense that eigenvectors act as the attracting forces, trajectories lie on the boundaries of the manifolds undergoing surgery and surgery on the steady state point creates a limit cycle thus coinciding with our definition of solid surgery. A possible future research direction would be to search for other dynamical systems realizing surgery and use these dynamical systems as a base for establishing a more general theoretical connection between topological surgery and bifurcation theory.

Moreover, we presented a visualization of the 4-dimensional process of 3-dimensional surgery in \mathbb{R}^3 by introducing the notion of decompactified 2-dimensional surgery. This notion could be used to visualize 3-dimensional lens spaces occurring from 3-dimensional surgery on the 3-sphere and other 4-dimensional processes.

Finally, we also modeled the formation of black holes from cosmic strings using 3-dimensional 1-surgery. As our model suggests that a black hole does not necessarily result in a spatial singularity, it would be very interesting to collaborate with physicists in order to investigate the physical implications of the proposed topological change.

We hope that through this study, topology and dynamics of natural phenomena, as well as topological surgery itself, will be better understood and that our connections will serve as ground for many more insightful observations and new physical implications.

A Appendix: Definitions

Manifolds

1. A Hausdorff space M^n with countable base is said to be an n -dimensional *topological manifold* if any point $x \in M^n$ has a neighborhood homeomorphic to \mathbb{R}^n or to \mathbb{R}_+^n , where $\mathbb{R}_+^n = \{(x_1, \dots, x_n) \mid x_i \in \mathbb{R}, x_1 \geq 0\}$. For example, a surface is a 2-dimensional manifold.
2. The set of all points $x \in M^n$ that have no neighbourhoods homeomorphic to \mathbb{R}^n is called the *boundary* of the manifold M^n and is denoted by ∂M^n . When $\partial M^n = \emptyset$, we say that M^n is a *manifold without boundary*. It is easy to verify that if the boundary of a manifold M^n is nonempty, then it is an $(n - 1)$ -dimensional manifold.

Topologies

3. If (X, τ) is a topological space, a *base* of the space X is a subfamily $\tau' \subset \tau$ such that any element of τ can be represented as the union of elements of τ' . In other words, τ' is a family of open sets such that any open set of X can be represented as the union of sets from this family. In the case when at least one base of X is countable, we say that X is a space with *countable base*.
4. To define the topology τ , it suffices to indicate a base of the space. For example, in the space $\mathbb{R}^n = \{(x_1, \dots, x_n) \mid x_i \in \mathbb{R}\}$, the standard topology is given by the base $U_{a,\epsilon} = \{x \in \mathbb{R}^n \mid |x - a| < \epsilon\}$, where $a \in \mathbb{R}^n$ and $\epsilon > 0$. We can additionally require that all the coordinates of the point a , as well as the number ϵ , be rational; in this case we obtain a countable base.
5. To the set \mathbb{R}^n let us add the element ∞ and introduce in $\mathbb{R}^n \cup \{\infty\}$ the topology whose base is the base of \mathbb{R}^n to which we have added the family of sets $U_{\infty,R} = \{x \in$

$\mathbb{R}^n \mid |x| > R\} \cup \{\infty\}$. The topological space thus obtained is called the *one-point compactification* of \mathbb{R}^n ; it can be shown that this space is homeomorphic to the n -dimensional sphere $S^n = \{x \in \mathbb{R}^{n+1} \mid |x| = 1\}$.

Topological spaces

6. A *topological space* is a set X with a distinguished family τ of subsets possessing the following properties:

- the empty set and the whole set X belong to τ
- the intersection of a finite number of elements of τ belongs to τ
- the union of any subfamily of elements of τ belongs to τ

The family τ is said to be the *topology* on X . Any set belonging to τ is called *open*. A *neighborhood* of a point $x \in X$ is any open set containing x . Any set whose complement is open is called *closed*. The minimal closed set (with respect to inclusion) containing a given set $A \subset X$ is called the *closure* of A and is denoted by \bar{A} . The maximal open set contained in a given set $A \subset X$ is called the *interior* of A and is denoted by $Int(A)$.

7. The map of one topological space into another is called *continuous* if the preimage of any open set is open. A map $f : X \rightarrow Y$ is said to be a *homeomorphism* if it is bijective and both f and f^{-1} are continuous; the spaces X and Y are then called *homeomorphic* or *topologically equivalent*.

8. A topological space is said to be a *Hausdorff space* if any two distinct points of the space have nonintersecting neighborhoods.

9. Suppose X and Y are topological spaces without common elements, A is a subset of X , and $f : X \rightarrow Y$ is a continuous map. In the set $X \cup Y$, let us introduce the relation $a \sim f(a)$. The resulting quotient space $(X \cup Y) / \sim$ is denoted by $X \cup_f Y$; the procedure of constructing this space is called *gluing* or *attaching* Y to X along the map f .
10. If $X \times Y$ is the Cartesian product of the topological spaces X and Y (regarded as sets), then $X \times Y$ becomes a topological space (called the *product* of the spaces X and Y) if we declare open all the products of open sets in X and in Y and all possible unions of these products.
11. An injective continuous map between topological spaces $f : X \hookrightarrow Y$ is called an *embedding* if f is a homeomorphism between X and $f(X)$.

For further reading, excellent references on the subject are [26, 28, 29].

References

1. Adams C.: The Knot Book, An Elementary Introduction to the Mathematical Theory of Knots. American Mathematical Society (2004).
2. Antoniou S., Lambropoulou S.: Topological Surgery in Nature. Book ‘Algebraic Modeling of Topological and Computational Structures and Applications’, Springer Proceedings in Mathematics and Statistics (accepted) (2017).
3. Antoniou S., Lambropoulou S.: Extending Topological Surgery to Natural Processes and Dynamical Systems. PLOS ONE. DOI: 10.1371/journal.pone.0183993 (2017).
4. Caldwell R.R., Casper P.: Formation of Black Holes from Collapsed Cosmic String Loops, Phys.Rev. D53. DOI: 10.1103/PhysRevD.53.3002 (1996).
5. Dahlburg R.B., Antiochos S.K.: Reconnection of antiparallel magnetic flux tubes. J Geophys Res 100, No. A9: 16991–16998. DOI: 10.1029/95JA01613 (1995).
6. Glatzmaier G.A., Roberts P.H.: A three-dimensional self-consistent computer simulation of a geomagnetic field reversal, Nature 377 (6546); 203–209. DOI:10.1038/377203a0 (1995).
7. Hale J.K, Kocak H.: Dynamic and bifucation. Springer-Verlag, Chapter 18:00 Dimension Four (1996).
8. Hartwell L.H., Hood L., Goldberg M.L., Reynolds A.E., Silver L.M., Veres R.C.: Genetics, from genes to genomes. McGraw Hill. pp. 486 (2000).
9. Hawking S.W.: Black Holes from cosmic strings, Physics Letters B 231 No. 237 DOI:10.1016/0370-2693(89)90206-2 (1989).

10. Johnson N.: A visualization of the Hopf fibration. Available from: <http://nilesjohnson.net/hopf.html>.
11. Johnson A.B., Lewis J. et al: Molecular Biology of the Cell. Garland Science (2002). Available from: <http://www.ncbi.nlm.nih.gov/books/NBK26845/>.
12. Keeton W.T., McFadden C.H.: Elements of biological science. W.W. Norton & Company Inc; pp. 395 (1983).
13. Kerr R.M.: Fully developed hydrodynamic turbulence from a chain reaction of reconnection events. Procedia IUTAM. No. 9:00 57–68. DOI: 10.1016/j.piutam.2013.09.006 (2013). Available from: <http://www.sciencedirect.com/science/article/pii/S2210983813001284>.
14. Kiehn R.M.: Non-equilibrium systems and irreversible processes - Adventures in applied topology vol. 1 - Non equilibrium thermodynamics, pp. 147, 150 University of Houston Copyright CSDC Inc (2013).
15. Kiehn R.M.: Falaco Solitons, Cosmic Strings in a Swimming Pool. Preprint (2001). Available from: <http://arxiv.org/pdf/gr-qc/0101098v1>.
16. Kondrashov D., Feynman J., Liewer P.C., Ruzmaikin A.: Three-dimensional Magnetohydrodynamic Simulations of the Interaction of Magnetic Flux Tubes. The Astrophysical Journal 519; 884–898. DOI: 10.1086/307383 (1999).
17. Laing C.E., Ricca R.L., Sumners D.: Conservation of writhe helicity under anti-parallel reconnection. Scientific Reports 5, No 9224. DOI: 10.1038/srep09224 (2014).
18. Lambropoulou S., Samardzija N., Diamantis I., Antoniou S.: Topological Surgery and Dynamics, Mathematisches Forschungsinstitut Oberwolfach Report

- No. 26/2014, Workshop: Algebraic Structures in Low-Dimensional Topology. DOI: 10.4171/OWR/2014/26 (2014).
19. Lambropoulou S., Antoniou S.: Topological Surgery, Dynamics and Applications to Natural Processes. *Journal of Knot Theory and its Ramifications*. DOI: 10.1142/S0218216517430027 (2016).
 20. Langford L.D.: A review of interactions of Hopf and steady-state bifurcations, Non-linear dynamics and turbulence, G.I. Barrenblatt, G.Iooss, D.D Joseph, Pitman, Boston; 215-237 (1983).
 21. Lotka A.J.: Undamped Oscillations Derived from the Law of Mass Action, *J. American Chem. Soc*; No. 42:00:00 1595–1599 (1920).
 22. MacGibbon J.H, Brandenberger R.H., Wichoski U.F.: Limits on Black Hole Formation from Cosmic String Loops, *Phys.Rev. D57 -1998* 2158-2165. DOI: 10.1103/PhysRevD.57.2158 (1998).
 23. Matsuda T.: Primordial black holes from cosmic necklaces, *Journal of High Energy Physics*, *JHEP04(2006)017*. DOI: 10.1088/1126-6708/2006/04/017 (2006).
 24. Milnor J.: *Morse Theory*. Princeton University Press (1963).
 25. Ott C.D., et al: Dynamics and Gravitational Wave Signature of Collapsar Formation. *Phys Rev Lett* 106, 161103 DOI: 10.1103/PhysRevLett.106.161103 (2011).
 26. Prasolov V.V., Sossinsky, A.B.: *Knots, links, braids and 3-manifolds*. AMS Translations of Mathematical Monographs 154 (1997).
 27. Pujari S.: Useful Notes on the Mechanism of Crossing Over. *Your Article Library* (2015). Available from: <http://www.yourarticlelibrary.com/biology/>

useful-notes-on-the-mechanism-of-crossing-over-biology-810-words/
6634/.

28. Ranicki A.: Algebraic and Geometric Surgery. Oxford Mathematical Monographs, Clarendon Press (2002).
29. Rolfsen D.: Knots and links. Publish or Perish Inc. AMS Chelsea Publishing (2003).
30. Samardzija N., Greller L.: Explosive route to chaos through a fractal torus in a generalized Lotka-Volterra model. Bull Math Biol 50, No. 5:00 465–491. DOI: 10.1007/BF02458847 (1988).
31. Samardzija N., Greller L.: Nested tori in a 3-variable mass action model. Proc R Soc Lond A Math Phys Sci 439, No. 1907:00:00 637–647. DOI: 10.1098/rspa.1992.0173 (1992).
32. Sumners D.: Lifting the Curtain: Using Topology to Probe the Hidden Action of Enzymes. Not Am Math Soc 42 No. 5:00 528–537 (1995). Available from: <http://www.ams.org/notices/199505/sumners.pdf>.
33. Volterra V.: Leçons sur la Théorie Mathématique de la lutte pour la vie, Paris, Gauthier-Villars. Gabay, J.; DOI: 10.1090/S0002-9904-1936-06292-0 (1931, reissued 1990).
34. Wasserman S.A., Dungan J.M., Cozzarelli N.R.: Discovery of a predicted DNA knot substantiates a model for site-specific recombination. Science 229, 171–174 (1985).
35. Zhigilei L.V.: Lecture notes, Chapter 8: Failure - University of Virginia, Department of Materials Science (2010). Available from: <http://people.virginia.edu/~lz2n/mse209/Chapter8.pdf>.

Index

- 4-dimensional space, 11, 78, 90, 91
- bifurcation, 49, 57, 58
- black hole, 12, 31, 69, 78, 89
- chromosomal crossover, 30, 31
- cosmic strings, 12, 78, 89, 90
- DNA recombination, 27, 30, 67
- dynamical system, 48, 49, 57–59, 63
- embedded topological surgery , 58, 66, 67,
69, 70, 74, 76
- Falaco solitons, 31, 35, 45, 57
- fractal torus, 54, 56
- fracture, 34, 47
- gene transfer, 31, 35, 45
- gluing homeomorphism, 18, 20, 21, 30,
33, 46, 60, 84, 97
- Lotka-Volterra, 49, 63
- magnetic reconnection, 27, 29
- meiosis, 27
- mitosis, 31, 47
- nested spheres, 44, 54, 61
- nested tori, 41, 43, 61
- numerical analysis, 48, 51, 65
- recoupling, 27, 31, 33
- slow manifold, 53, 54, 57, 64
- solid topological surgery, 35, 37, 38, 40,
48
- splicing, 27
- three-sphere, 64, 67–69, 74, 76, 80
- topological thread, 35, 46
- tornadoes, 31, 33, 37, 57, 73